Continuous Foliar Cover of Plant Species and Aggregates in North American Beringia

Map User Guide and Accuracy Assessment

Version 1.0 (May 2021)

Timm W. Nawrocki, Alaska Center for Conservation Science, University of Alaska Anchorage

Matthew L. Carlson, Alaska Center for Conservation Science, University of Alaska Anchorage

Aaron F. Wells, ABR, Inc.—Environmental Research & Services

Matthew J. Macander, ABR, Inc.—Environmental Research & Services

E. Jamie Trammell, Department of Environmental Science & Policy, Southern Oregon University

Frank D.W. Witmer, Department of Computer Science & Engineering, University of Alaska Anchorage

Carl. A. Roland, Central Alaska Network Inventory, U.S. National Park Service

Kathryn Baer, Pacific Northwest Research Station, U.S. Forest Service

David K. Swanson, Arctic Network, U.S. National Park Service

Please cite as:

Nawrocki, T.W., M.L. Carlson, A.F. Wells, M.J. Macander, E. Jamie Trammell, F.D.W. Witmer, C.A. Roland, K. Baer, and D.K. Swanson. 2021. Continuous Foliar Cover of Plant Species and Aggregates in North American Beringia. Map User Guide and Accuracy Assessment. Version 1.0 (May 2021). Available: https://doi.org/10.5281/zenodo.3897482

Abstract

Research, conservation, and effective natural resource management often depend on maps that characterize patterns of vegetation composition. Quantitative and ecologically specific representations of plant proportional abundance have several advantages: they are theoretically consistent with plant community ecology, avoid arbitrary and subjective thresholds or categorizations, and minimize information loss relative to field observations and covariates. They also avoid a human interpretational bias not necessarily shared by or important to plants or wildlife. We developed quantitative continuous foliar cover maps for 15 plant species or ecologically narrow aggregates in Arctic and boreal Alaska and adjacent Yukon (North American Beringia). We integrated new and existing ground and aerial vegetation observations for Arctic and boreal Alaska from three vegetation plots databases. To map patterns of foliar cover, we statistically associated observations of vegetation foliar cover with environmental, multi-season spectral, and surface texture covariates using hierarchical statistical learning models. To provide context to the performance of our continuous foliar cover maps, we compared our results to the performances of three categorical vegetation maps that cover Arctic and boreal Alaska: the National Land Cover Database and the coarse and fine classes of the Alaska Vegetation and Wetland Composite. Our maps predicted 40% to 62% of the observed variation in foliar cover per species or aggregate at the site scale. A multi-scale accuracy assessment showed that the maps generally captured patterns of plant abundance accurately at landscape and regional scales. All continuous foliar cover maps performed substantially better than the existing categorical vegetation maps. The vegetation database and scripted workflow that we developed to create the continuous foliar cover maps will allow consistent future updates to include new observations of plant abundance patterns and new or updated covariates. Our scripted workflow also allows the application of our methods to areas beyond North American Beringia. The continuous foliar cover maps that we developed improve representation of vegetation composition patterns relevant to plant communities and wildlife habitats in North American Beringia.

Contents

Figures

Tables

Acknowledgements

Bureau of Land Management and National Park Service provided funding for the Alaska Vegetation Plots Database (AKVEG), enabling the data standardization and infrastructure necessary to a large regional mapping effort. Alaska Department of Fish and Game and Bureau of Land Management provided funding to develop continuous foliar cover maps of plant species and aggregates. We thank Kassidy Colson, Dr. Jeffrey Stetz, Parker Martyn, Scott Guyer, and Aliza Segal for their support of this work. Numerous vegetation ecologists, botanists, and soil scientists collected the ground and aerial observations of vegetation patterns that provided the train and test data for development of foliar cover maps. Although too numerous to list by name, this work was only possible through their collective efforts across two decades. Dr. Aaron Wells provided Ecological Land Survey and other data collected during the past 20 years by ABR, Inc.—Environmental Research & Services. Carl Roland and Dr. David Swanson provided National Park Service Central Alaska Network and Arctic Network Inventory and Monitoring data for use in the maps of *Picea glauca* - × *lutzii* and *Picea mariana*.

1. Introduction

Plant communities are organized by the establishment, survival, and reproduction of individuals of constituent species based on tolerance to environmental conditions, interactions between species with geographic (dispersal) access to the same physical space, and stochastic events (Gleason 1926, Whittaker 1967, Nicholson and McIntosh 2002, Lortie et al. 2004, Cushman et al. 2010, Feilhauer et al. 2020). Problems involving complex ecological systems can benefit from spatial representations of vegetation that are quantitative and consistent with ecological theory, similar to the ordination statistics used to describe patterns of plant community composition along environmental and biotic gradients. One effective option is the map proportional abundance of individual species or ecologically narrow aggregates of species (Nawrocki et al. 2020; see Feilhauer et al. 2020 for alternative approaches). Proportional abundance maps of species and aggregates are ideal for subsequent modeling or analyses because they capture ecological complexity, represent both gradual and abrupt transitions or changes, allow unique data associations to drive individual maps for minimal information loss, include map-specific estimates of error, and remain interpretable in subsequent modeling outputs.

The distribution and abundance of plant species impacts all aspects of terrestrial ecosystems in Arctic and boreal Alaska and adjacent Yukon (hereafter referred to as "North American Beringia"). Consistent and quantitative spatial descriptions of ecologically specific abundance patterns from site to sub-continental scales will help researchers, natural resource managers, conservationists, local communities, and industries understand the interactions between plant community composition and structure, environmental characteristics and heterogeneity, wildlife nutritional input and habitat, and biophysical processes. The goals of this mapping effort were to: 1) map proportional abundance (as foliar cover) of 15 widespread and frequently dominant plant species or aggregates (Table 1) within North American Beringia, and 2) develop a repeatable mapping workflow that will enable regular updates and extension to other regions.

1.1. Data Access

All provided urls will automatically refer to updated versions as available.

1. Continuous foliar cover maps for 15 species and aggregates representative of the 20-year period from 2000-2019 for North American Beringia are available at:
    a. Data archive in Zenodo: https://doi.org/10.5281/zenodo.3897482
    b. Data archive in ACCS Data Catalog: https://accscatalog.uaa.alaska.edu/dataset/continuous-foliar-cover-vegetation-north-american-beringia
2. The Alaska Vegetation Plots Database (AKVEG; Nawrocki 2021), which supported the statistical analyses, is available for public use:
    a. A public web portal: https://akveg.uaa.alaska.edu
    b. Git repository enabling local replication: https://github.com/accs-uaa/vegetation-plots-database
3. The scripted analytical workflow used to produce the maps is available at:
    a. Git repository: https://github.com/accs-uaa/beringian-vegetation

Table 1. Suite of widespread species and aggregates selected for mapping based on prevalence in combined vegetation plot data for North American Beringia.

Species or Aggregate	Lifeform	Rationale
Picea glauca – × *lutzii*	Coniferous Tree	forest structure, fuels for fire, hydrography, wildlife physical habitat
Picea mariana	Coniferous Tree	forest structure, fuels for fire, wildlife physical habitat
Betula Trees	Deciduous Tree	forest structure, post-fire succession, wildlife habitat and forage
Deciduous Trees	Deciduous Tree	forest structure, post-fire succession, wildlife habitat and forage
Alnus Shrubs	Low-tall Shrub	shrub expansion, snow retention, hydrography
Salix Low-tall Shrubs	Low-tall Shrub	shrub expansion, snow retention, hydrography, wildlife habitat and forage (e.g., for moose, caribou, muskox, and snowshoe hare)
Betula Shrubs	Low-tall Shrub	shrub expansion, snow retention
Rhododendron Shrubs	Low-tall Shrub	associational herbivore resistance, ethnobotanical uses, post-fire succession
Vaccinium uliginosum	Low-Dwarf Shrub	subsistence, wildlife habitat and forage
Dryas Shrubs	Dwarf Shrub	alpine and Arctic plant communities
Vaccinium vitis-idaea	Dwarf Shrub	subsistence, wildlife habitat and forage (e.g., for voles, lemmings, sparrows, bears, and caribou in winter)
Empetrum nigrum	Dwarf Shrub	subsistence, wildlife habitat and forage, Alaska Peninsula and Yukon-Kuskokwim Delta plant communities
Eriophorum vaginatum	Graminoid	tussock formation, soil ice dynamics (e.g., high- and flat-centered polygons)
Wetland Sedges	Graminoid	wetland indicator, soil-ice dynamics (e.g., troughs, low-centered polygons, drained thaw lakes), wildlife habitat and forage
Sphagnum	Bryophyte	wetland indicator, carbon sequestration, soil thermal regulation

2. Methods

Four components enabled quantifying continuous foliar cover patterns in North American Beringia: 1) direct observations of vegetation composition and abundance at scales relevant to the spatial resolution of the analyses; 2) a standardized database with observations reconciled to a common taxonomy and schema; 3) remotely sensed spectral, textural, topographic, and climatic covariates that represent gradients of environmental and biotic variation consistently across the study region; and 4) a statistical learning method capable of predicting complex patterns of binary and continuous responses from numerous, potentially weak correlations in samples that are small relative to the size of the mapped area. Hereafter, we refer to the mapped species and aggregates as "map groups".

2.1. Software and Reproducibility

Data acquisition, analyses, and map post-processing were coded so that the entire mapping workflow can be repeated at regular intervals or adapted to regions outside of North American Beringia. We conducted spatial processing in ArcGIS Pro 2.7.2 with Python 3.7.9; spectral and textural data acquisition with Google Earth Engine (Gorelick et al. 2017) and the Anaconda 2020.11 distribution of Python 3.8.5 with Google API Python Client 1.8.3 and PyDrive 1.3.1; data formatting using using R 4.0.4, RStudio 1.4.1106, and RStudio Server 1.4.1106 with dplyr 1.0.2, lubridate 1.7.9, readr 1.4.0, RPostgres 1.2.1, readxl 1.3.1, stringr 1.4.0, tibble 3.0.4, and tidyr 1.1.2; statistical modeling in the Anaconda 2020.11 distribution of Python 3.8.5 with LightGBM 3.2.0 (Ke et al. 2017), Scikit-learn 0.24.1 (Pedregosa et al. 2011), GPy 1.9.9 (GPy 2014), and GPyOpt 1.2.6 (González et al. 2014); and prediction post-processing using R 4.0.4 and RStudio Server 1.4.1106 with sp 1.4-1 (Pebesma and Bivand 2005), raster 3.1-5 (Hijmans 2017), and rgdal 1.4-8 (Bivand et al. 2018). Because the training and prediction of the hierarchical statistical learning models requires computational power beyond that of traditional computing, we deployed models and data processing and on virtual machines requisitioned in Google Cloud Compute Engine with the Linux Ubuntu 20.04 LTS operating system. Our script repository includes routines for the replication of cloud machines for both statistical modeling and geospatial processing.

2.2. Study Area

We defined North American Beringia (referred to in this document as "the study area") to include boreal and Arctic Alaska and adjacent Yukon based on a combination of the Circumarctic Vegetation Map (Walker et al. 2005), the Alaska-Yukon Region of the Circumboreal Vegetation Map (Jorgeson and Meidinger 2015), and the Unified Ecoregions of Alaska (Nowacki et al. 2001; hereafter referred to as "ecoregions"). A manually altered, smoothed, and buffered eastern boundary of the ecoregions defined the eastern boundary of the study area. The western edge of the Kenai Mountains and the northern edge of the Chugach and St. Elias Mountains defined the southern boundary of the study area. Because of the abrupt transition to alpine rock and ice that separates North American Beringia from southern coastal Temperate Alaska and because of the substantial abrupt floristic and climatic differences between the two, the Temperate region of Alaska is not included in these maps. The resulting boundary (Figure 1) has the advantage over the Alaska state boundary of containing the entirety of the ecoregions (excluding the Temperate region), which extend into Yukon, while the cartographic modifications present a relatively clean and generalized edge. In Version 1.x of the maps (the current version), we removed all islands from the study area, including the Aleutian and Bering Sea Islands. Further data integration and collection must be accomplished prior to incorporating the Aleutian and Bering Sea Islands into a future version of the maps.

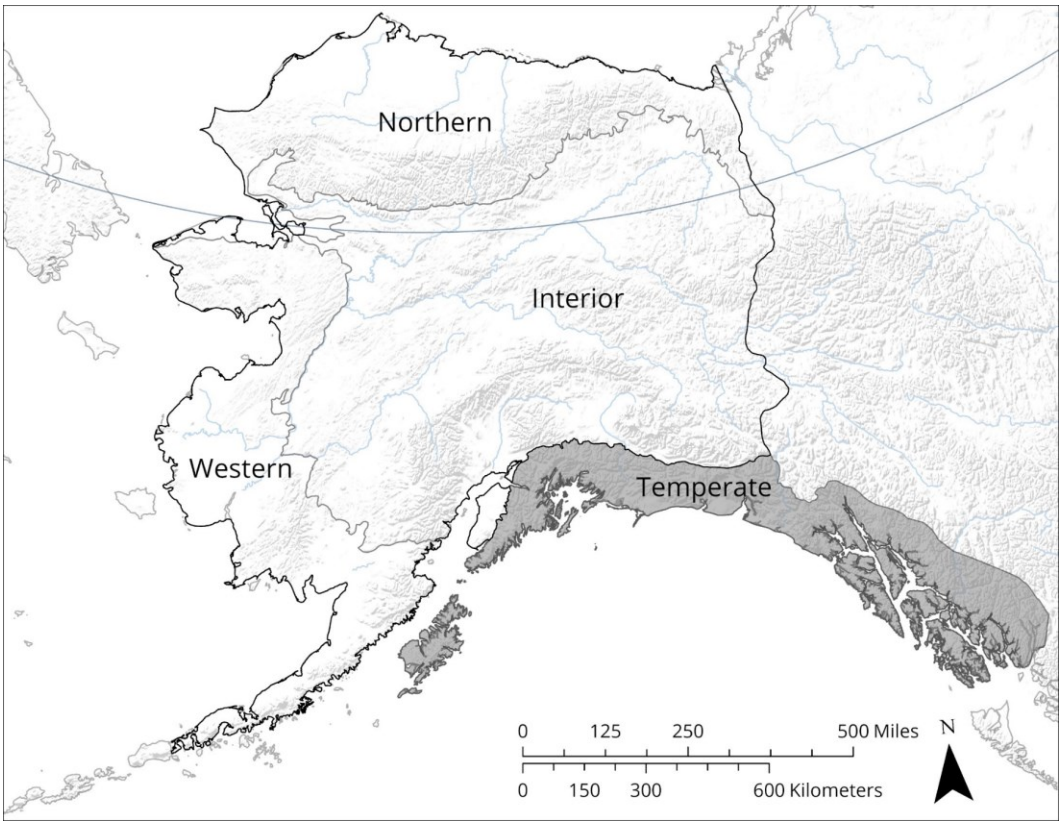

Figure 1. North American Beringia consists of the continental portions of Arctic and Boreal Alaska and adjacent Yukon. For the purpose of accuracy assessment, we further subdivided the study area into western, interior, and northern subregions.

Environmental and ecological transitions in Alaska between the Arctic (sensu Circumarctic Vegetation Map; Walker et al. 2005) and boreal (sensu Alaska-Yukon Region of the Circumboreal Vegetation Map; Jorgenson and Meidinger 2015) are gradual and dynamic. The lack of well-defined climatic, environmental, or biotic breaks between Arctic and Boreal Alaska have led to well-justified differences of opinion on where to divide the biomes. However, for the sole purpose of providing geographic nuance to our accuracy assessments, we divided North American Beringia into western, interior, and northern subregions based on ecoregions (Figure 1). The boundaries between the subregions should be viewed as heuristic divisions rather than abruptly different ecological zones.

The interior subregion is boreal as defined by both Nowacki et al. (2001) and Jorgenson and Meidinger (2015). Boreal Alaska is dominated by both coniferous and deciduous trees because of widespread and frequent fire. Treeless tundra, wetland, subalpine, and alpine communities are also frequent. The difference between summer and winter temperatures in boreal Alaska is high: summers are warm despite the short snow-free season while winters are cold. The boreal biome in Alaska receives moderate to low amounts of precipitation, except for high mountain areas such as the Alaska Range, and permafrost is absent or discontinuous (Jorgenson and Meidinger 2015).

A general lack of trees is characteristic of Arctic Alaska as defined by the Circumarctic Vegetation Map (Bioclimatic Subzones C-E; Elvabakk 1999, Walker et al. 2005), which includes all of the northern subregion. Trees in the northern subregion are common only in the gradual transition to boreal Alaska south of the ridge crest of the Brooks Range (Nowacki et al. 2001). Isolated stands of *Populus*

balsamifera also occur at perennial springs and sheltered areas along rivers and south-facing slopes north of the ridge crest of the Brooks Range (Breen 2014). Low shrub-, dwarf shrub-, and graminoid-dominated communities are common in Arctic Alaska; tall shrub-dominated communities occur along large floodplains, such as the Colville River (Walker et al. 2005). Despite the low annual precipitation, soils in the northern subregion are generally hydric to mesic because the continuous permafrost impedes drainage. Thus, Arctic Alaska north of the Brooks Range includes large wetland complexes. Summers are cool and short while winters are cold. Snow cover dominates the annual cycle (Nowacki et al. 2001).

The western subregion is a transitional zone that includes portions of the Arctic as defined by Walker et al. (2005; Bioclimatic Subzone E) and the boreal as defined by Jorgenson and Meidinger (2015). In the western subregion, tree-dominated communities occur on well drained hills and uplands, floodplains, and lake shores. Shrub- and graminoid-dominated tundra communities are common and frequently intermixed with tree-dominated communities. Permafrost is discontinuous but widespread in certain areas, such as the Yukon-Kuskokwim Delta (Whitley et al. 2018). The close proximity to the Bering Sea moderates the difference between summer and winter temperatures such that summers are cool and winters are cold with moderate amounts of precipitation (Jorgenson and Meidinger 2015).

2.3. Environmental Covariates

We developed a suite of 14 environmental covariates to represent climatic, topographic, and hydrographic conditions across North American Beringia (Table 2). We created 16-year averages for total annual precipitation, summer warmth index, and minimum January temperature using Climate Research Unit Time Series (CRU TS) 4.0 historic data from Scenarios Network for Alaska and Arctic Planning (SNAP 2020), which included years 2000 to 2015. In addition to the air temperature-based summer warmth index, we also developed a land surface temperature-based summer warmth index from MODIS land surface temperature data collected from 2010 to 2019. Topographic covariates included or originated from a mosaic of multi-resolution IFSAR Digital Elevation Models (DEMs) available through the USGS 3D Elevation Program (3DEP). The collection of IFSAR data at 5 × 5 m resolution began in Alaska in 2010 and was available for most of continental Alaska at the time of processing. Adjacent Yukon was covered mostly by 30 × 30 m data. In a few included areas, the best resolution available was 60 × 60 m. We merged elevation data sources prioritized by highest resolution and resampled the elevation composite to 10 × 10 m. Calculations for topographic and hydrographic metrics followed Evans et al. (2014). High resolution geospatial data representing soils characteristics, including permafrost, must be considered critical data gaps at the time of publication.

Table 2. Fourteen environmental covariates derived from SNAP CRU TS 4.0 historic climate data, MODIS land surface temperature, and a composite 10 × 10 m DEM represented climatic, topographic, and hydrographic patterns.

Covariate	Data Source and Resolution	Data Reference
MODIS Land Surface Temperature Summer Warmth Index 2010-2019	MODIS LST; 250 × 250 m	Wan 2013
Air Temperature Summer Warmth Index 2000–2015	SNAP CRU TS 4.0; 2 × 2 km	SNAP 2020

Covariate	Data Source and Resolution	Data Reference
Total Annual Precipitation 2000–2015	SNAP CRU TS 4.0; 2 × 2 km	SNAP 2020
Minimum January Temperature	SNAP CRU TS 4.0; 2 × 2 km	SNAP 2020
Elevation	USGS 3DEP Composite; 10 × 10 m	USGS 3DEP
Linear Aspect	USGS 3DEP Composite; 10 × 10 m	Evans et al. 2014
Mean Slope	USGS 3DEP Composite; 10 × 10 m	Evans et al. 2014
Roughness	USGS 3DEP Composite; 10 × 10 m	Blaszczynski 1997, Riley et al. 1999
Site Exposure	USGS 3DEP Composite; 10 × 10 m	Evans et al. 2014
Surface Area Ratio	USGS 3DEP Composite; 10 × 10 m	Berry 2002
Surface Relief Ratio	USGS 3DEP Composite; 10 × 10 m	Pike and Wilson 1971
Topographic Position	USGS 3DEP Composite; 10 × 10 m	Evans et al. 2014
Topographic Radiation	USGS 3DEP Composite; 10 × 10 m	Evans et al. 2014
Topographic Wetness	USGS 3DEP Composite; 10 × 10 m	Moore et al. 1993, Gessler et al. 1995

2.4. Textural and Spectral Covariates

To match the requirements of our target map resolution of 10 × 10 m, which in turn was driven by the need to reconcile different plot sizes at scales smaller than individual Landsat pixels, we incorporated spectral and textural composite data from the Sentinel-1 and -2 satellite systems (Table 3). Data collection from both Sentinel-1 and -2 is relatively high resolution (10 to 20 m), but data are only available since 2015. We sacrificed full temporal coverage of the same timespan encompassed by the selected vegetation observations for high spatial resolution. For the Sentinel-1 Synthetic Aperture Radar (SAR), we calculated composite vv and vh for the months of June through August 2015 through 2020. Multiple studies have demonstrated the importance of representing multiple parts of the growing season for vegetation mapping in northern systems rather than relying on single scenes or composites (Langford et al. 2016, Macander et al. 2017, Nawrocki et al. 2020). Thus, we generated spectral representations of early, middle, and late growing season 2015 through 2020 from the Top-Of-Atmosphere (TOA) Reflectance Sentinel-2 image collection: a median composite of May through July, a maximum Normalized Difference Vegetation Index (NDVI) composite of July, and a median composite of August and September. We included bands 2-8a and 11-12 plus Enhanced Vegetation Index-2 (EVI2; see Jiang et al. 2008), Normalized Burn Ratio (NBR; see Key and Benson 1999), Normalized Difference Moisture Index (NDMI; see Jin and Sader 2005), Normalized Difference Snow Index (NDSI; see Hall et al. 1995), Normalized Difference Vegetation Index (NDVI; see Tucker 1979), and Normalized Difference Water Index (NDWI; see Gao 1996). We selected Top-Of-Atmosphere Reflectance rather than Surface Reflectance because not enough Surface Reflectance data were available in Google Earth Engine to create complete and relatively anomaly-free composites. We did not perform any additional atmospheric corrections to the TOA Reflectance data.

Table 3. Fifty textural and spectral covariates derived from Sentinel-1 and -2 represented biotic and environmental patterns.

Covariate (May-September)	Data Source and Resolution
vv	Sentinel-1; 10 × 10 m
vh	Sentinel-1; 10 × 10 m
Band 2: Blue (blue)	Sentinel-2; 10 × 10 m
Band 3: Green (green)	Sentinel-2; 10 × 10 m
Band 4: Red (red)	Sentinel-2; 10 × 10 m
Band 5: Red Edge 1 (redge1)	Sentinel-2; 20 × 20 m
Band 6: Red Edge 2 (redge2)	Sentinel-2; 20 × 20 m
Band 7: Red Edge 3 (redge3)	Sentinel-2; 20 × 20 m
Band 8: Near Infrared (nearIR)	Sentinel-2; 10 × 10 m
Band 8a: Red Edge 4 (redge 3)	Sentinel-2; 20 × 20 m
Band 11: Shortwave Infrared 1 (SI1)	Sentinel-2; 20 × 20 m
Band 12: Shortwave Infrared 2 (SI2)	Sentinel-2; 20 × 20 m
Metric 1: Enhanced Vegetation Index-2 (EVI2)	Sentinel-2; 10 × 10 m
Metric 2: Normalized Burn Ratio (NBR)	Sentinel-2; 20 × 20 m
Metric 3: Normalized Difference Moisture Index (NDMI)	Sentinel-2; 20 × 20 m
Metric 4: Normalized Difference Snow Index (NDSI)	Sentinel-2; 20 × 20 m
Metric 5: Normalized Difference Vegetation Index (NDVI)	Sentinel-2; 10 × 10 m
Metric 6: Normalized Difference Water Index (NDWI)	Sentinel-2; 10 × 10 m

2.5. Range Map Development

For *Picea glauca* - × *lutzii*, *Picea mariana*, and *Betula* trees, we mapped realized ranges generalized to a sub-continental scale to provide additional context to the mapped distributions and to enable the generation of pseudo-absences beyond the range of each species or aggregate within the Western Alaska subregion, for which mostly aerial data were available. We integrated three data sources to develop range maps. First, we aggregated observed sites from vegetation plots databases and herbarium specimens. Second, we generated random points within digitized range maps from Little (1971). Third, we manually interpreted high resolution Maxar 0.5 × 0.5 m imagery available from Alaska Department of Natural Resources (ADNR) by searching for identifiable occurrences of the species or aggregate along visible landforms at the edges of the documented occurrences. Once occurrence points were assembled, we generated concave bounding polygons using an automated method (see Carlson et al. 2018, Nawrocki 2018). *Picea glauca* and *Picea mariana* are difficult to distinguish from imagery alone. We therefore merged the ranges of *Picea glauca* - × *lutzii* and *Picea mariana* prior to generating pseudo-absences. We generated a random set of 250 absences for *Betula* trees and 150 absences for *Picea* trees in the Western Alaska subregion outside of lakes and glaciers. The pseudo-

absence sets augmented the observed absences in the models for *Picea glauca* - × *lutzii*, *Picea mariana*, and *Betula* trees.

2.6. Vegetation Data Compilation

Predictions of plant species or aggregate foliar cover require extensive observations that cover the maximum logistically feasible amount of environmental variation present across a region. Because North American Beringia is a large region that includes much ecological diversity, we relied on the integration of 28 past vegetation survey and monitoring projects as well as limited new data collection (Appendix 1). Four databases provided the vegetation observation data necessary to develop the maps: 1) the Alaska Vegetation Plots Database (AKVEG; Nawrocki 2021) maintained by Alaska Center for Conservation Science (ACCS) at University of Alaska Anchorage (UAA), 2) a database of Ecological Land Survey field data maintained by ABR, Inc.—Environmental Research & Services (ABR), and 3) Inventory and Monitoring (I&M) databases maintained by the Central Alaska Network (CAKN) and Arctic Network (ARCN) of the National Park Service (NPS; for *Picea glauca* - × *lutzii* and *P. mariana* only). We included observations made during the 20-year period of 2000-2019 as a balance between location accuracy, temporal specificity, and data availability to cover such a large study area.

To develop species- and aggregate-specific training and validation datasets, we queried data from AKVEG and combined it with data exports from the ABR and NPS I&M databases, which we standardized to the AKVEG taxonomic standard (https://akveg.uaa.alaska.edu/#taxonomic-standard). Because our intent was to map continuous total foliar cover (i.e., the foliar cover across all canopy layers), we selected only observations made by quantitative point-intercept and semi-quantitative visual estimate methods. No observations recorded as classified abundances, such as according to the Braun-Blanquet methodology, contributed to the train and test data. Aerial observations are available only as top foliar cover (i.e., the foliar cover of only the uppermost canopy layer), which is often inconsistent with total foliar cover. However, we included aerial observations of top foliar cover because they provided the only available data across much of the study area. Because top foliar cover does not account for all canopy layers, it is not reliable for determining the presence or absence of species within communities, except for those species that usually contribute to the uppermost canopy when present. For trees and *Alnus*, we used all aerial observation data, including absences because those groups usually occur in the uppermost canopy when present. For all other map groups, we included the aerial data only for presences above 10% foliar cover to avoid including false absence data while also removing the presences most likely to be confused with absences. Trace cover of dominant or widespread species is often linked to the occurrence of micro-habitats that cannot be well represented at the 10 × 10 m mapped resolution. In addition to true absences, we considered observations of the species at less than 0.5% cover, including values of "trace", to be absences in both the input data and the output predictions.

The 20-year interval of observations introduced the possibility that some plots have burned subsequent to observation. To control for discrepancies between field data and imagery related to fire, we removed all plots that were within burn polygons mapped by the Alaska Interagency Coordination Center where the burn year was greater than the observation year. We retained any plots that burned prior to observation. The target map resolution of 10 × 10 m enabled reconciliation of plots of different sizes between minimum and maximum dimensional limits. For ground plots, we removed all plot sizes smaller than 8 × 8 m, greater than 30 m radius, or that differed in one dimension by more than 50%. We assumed a 20 m radius size for the irregular polygon aerial plots. For all plots, we calculated area-weighted means for all covariates per plot. After controlling for fire and plot sizes,

the AKVEG and ABR databases provided observation data from 6,901 plots for all map groups, and the NPS ARCN and CAKN I&M databases provided an additional 2,320 plots for the two *Picea* species (Figure 2).

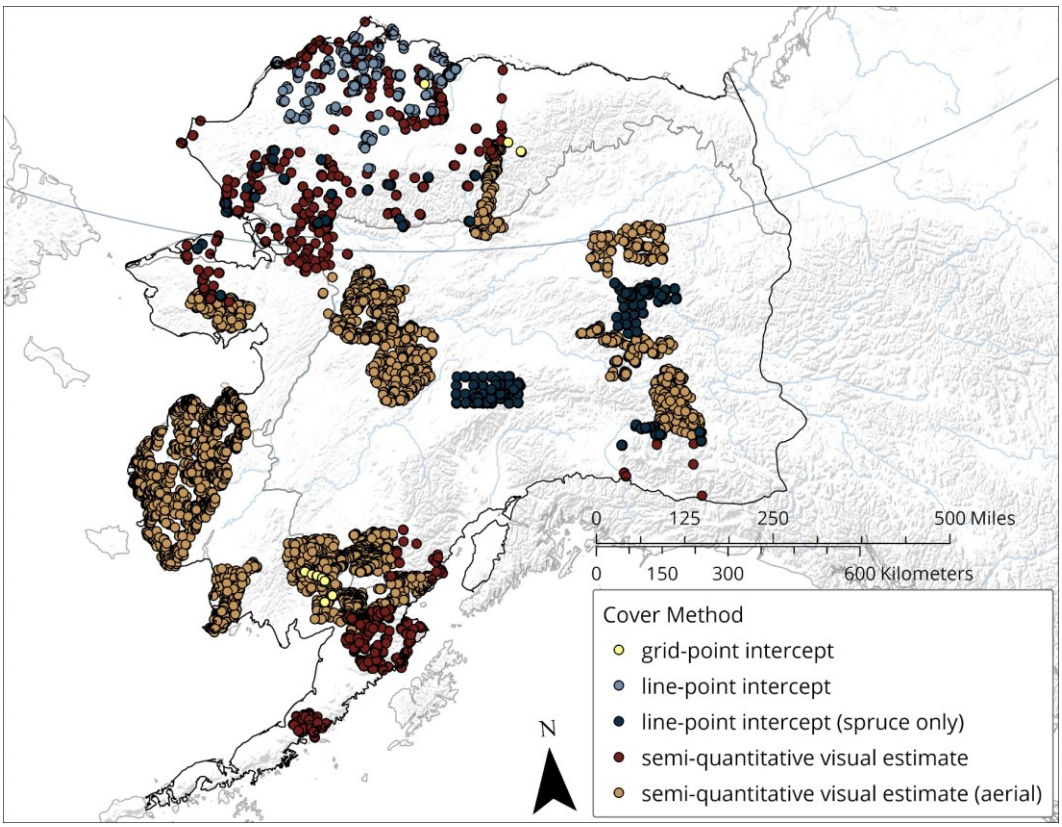

Figure 2. Locations of grid-point intercept, line-point intercept, and semi-quantitative visual estimate vegetation composition observations integrated from the AKVEG, ABR, and NPS I&M vegetation plots databases and selected into the train and test data for at least one species or aggregate.

2.7. Statistical Modeling

At the species or aggregate level, foliar cover data are zero-inflated. Thus, we viewed mapping foliar cover at ecologically specific levels as a hierarchical problem consisting of distribution (or occupancy) and abundance. To produce raster maps of predicted total foliar cover across the study area, we statistically associated vegetation observations with environmental, multi-season spectral, and surface texture covariates using a hierarchical statistical learning approach with a distribution and an abundance component. We predicted distribution of species or aggregates using a probabilistic classifier and, within predicted presences, we predicted total foliar cover using a regressor. A simple rule-based algorithm combined the predictions of the two model components into a single output.

Modeling distribution and abundance of species or aggregates requires a statistical method capable of distinguishing poorly separated samples, which represent similar species or aggregates (e.g., *Picea glauca* and *Picea mariana*) or similar environmental or spectral characteristics (e.g., species absence versus presence at low abundance). We selected stochastic gradient boosting ensembles, implemented in LightGBM (Ke et al. 2017), as the most appropriate modeling algorithm for both classifiers and regressors. Stochastic gradient boosting ensembles combine iterative weak learners,

where each weak learner performs slightly better than random, to sequentially fit the gradient remaining from combined previous weak learners to minimize a loss function (Hastie et al. 2009, Kuhn and Johnson 2013, Ke et al. 2017). Stochastic gradient boosting using decision trees as the weak learners has the following advantages that make it optimal for modeling the distribution and abundance of species or aggregates: 1) creates splits from numerous weakly informative and/or collinear relationships; 2) incorporates multivariate interactions and non-linearities among covariates and responses; 3) resistant to outliers, and 4) internally selects for the most informative covariates (Friedman 2002, Hastie et al. 2009). We included random selections of observations and covariates in each iteration and split to prevent overfitting (Friedman 2002).

Tuning model hyperparameters to the individual structure of each data problem maximizes predictive generalizability and prevents overfitting (Hastie et al. 2009, Cawley and Talbot 2010). We optimized ten hyperparameters for each model in a Bayesian statistical framework using a Gaussian process generative model implemented in GPyOpt (González et al. 2014). For the distribution component, we also optimized the probabilistic threshold for conversion to binary presence and absence by empirically determining the threshold that minimized the absolute value difference between sensitivity and specificity (Liu et al. 2005, Jiménez-Valverde and Lobo 2007). To ensure the statistical independence of our model optimizations and performance tests, we conducted a nested inner cross validation within an outer cross validation (see Hastie et al. 2009, Cawley and Talbot 2010). We split our available data into an outer 10-fold cross validation to provide train and test partitions, where test partitions provided independent data to test model performance. Within the outer train partitions, we split the data into an inner 10-fold cross validation to provide train and optimization partitions, where the optimization partitions provided data to validate the optimization of hyperparameters and conversion thresholds without bias. Thus, the outer cross-validation divided our available data into 10 train-test partitions, and the inner cross-validation subdivided each outer train partition into 10 train-optimize partitions. The merged test partitions of the outer cross-validation were used only a single time to evaluate the performance of the composite model, wherein each observation was predicted exactly once. Final spatial predictions were calculated from classifiers and regressors trained on all available data, using the same inner cross-validation scheme for optimization of hyperparameters and conversion thresholds as described above, to ensure the best possible models.

2.8. Site-scale Accuracy Assessment

We evaluated overall model performance at the site scale by calculating metrics suited to continuous data: R^2, mean absolute error (MAE), and root mean squared error (RMSE). In the context of predictive models, R^2 is the proportion of variation explained by a simple linear model for observed values as a function of predicted values where the intercept is 0 and the slope coefficient is 1. Additionally, we summarized mean and median cover values for the observed presences of each map group to provide necessary context to MAE and RMSE. Because our modeling method minimized the absolute value difference between specificity and sensitivity, the prediction accuracy for presences and absences were approximately the same. We therefore summarized the distributional accuracy of the models by a percentage accuracy (% ACC) of the binary distribution predictions compared to observations. In addition to the % ACC, we calculated the area under the receiver operating characteristic curve (AUC) to provide additional context to the performance of the distribution component. All performance metrics were calculated across the test partitions of the integrated vegetation observations with each site considered as the sampling unit.

2.9. Scaled Accuracy Assessment

Accuracy assessments at multiple scales can help users determine the appropriate scale at which to interpret or analyze maps for particular applications (Riemann et al. 2010). In addition to the site scale accuracy assessment, we assessed the accuracy of the models for landscape (using 10 × 10 km grids) to regional (using ecoregions) scale vegetation patterns. To assess landscape scale accuracy, we divided the study area into a regular grid with cells sized at 10 × 10 km and assigned observation sites to each grid. For all grids containing three or more sites, we calculated R^2, MAE, and RMSE of the mean predicted cover compared to the mean observed foliar cover with the grid as the sampling unit. To assess regional scale accuracy, we assigned observed sites to ecoregions and calculated R^2, MAE, and RMSE of the mean predicted cover compared to the mean observed foliar cover with the ecoregion as the sampling unit. As with the site scale accuracy assessment, regional and landscape mean predicted cover were calculated only from the independent test partitions of the integrated vegetation observations.

2.10. Covariate Importances

Gradient boosting models are intended to maximize the accuracy of the response predictions rather than describe the strength and direction of correlations between covariates and the response for the purpose of testing hypotheses. However, because each split results in a reduction in squared error, it is possible to calculate a relative and non-directional size-weighted contribution of each covariate (Kuhn and Johnson 2013), hereafter referred to as "importance." We calculated importance for each covariate per response per map group. Each model differed in optimized hyperparameters and distribution of the input data; therefore, the importance values should not be compared numerically among models. We provide covariate importance plots with the data because they reveal important patterns between responses and among species.

2.11. Comparison to Categorical Vegetation Maps

To provide context to the performance of the continuous foliar cover maps, we also calculated the R^2, MAE, and RMSE of existing categorical vegetation maps that cover most of the study area for each map group using the same set of data as used to develop the foliar cover maps. We selected three vegetation maps that cover Arctic and boreal Alaska: the National Land Cover Database (NLCD) and the coarse and fine classes of the Alaska Vegetation and Wetland Composite (AKVWC), all of which have a 30 × 30 m resolution and are primarily derived from Landsat data. For each species or aggregate, we estimated the discrete mean foliar cover for each vegetation class using ordinary least squares linear regression models with the vegetation classes as the independent variables and foliar cover as the dependent variable. We calculated the site scale performance of the linear regressors, and thus of the mapped vegetation classes, from the merged test partitions of a single iteration of 10-fold cross validation, such that each observation was predicted exactly once. The R^2, MAE, and RMSE calculated for the categorical vegetation maps are directly comparable to those calculated for the continuous foliar cover maps at the site scale because we estimated performance for discrete mean foliar cover as a function of vegetation class using the same set of observation data and the same cross-validation framework.

3. Results

We modeled the distribution-abundance of 15 map groups across North American Beringia. Site scale predictions (i.e., individual pixels) represented 40% to 62% of observed variation. Although there was substantial noise in the predictions at the site scale, predictions at the landscape and regional scales were more accurate, meaning that pixel level errors were not consistent in magnitude or direction. Site scale errors tended to result from generalizations; thus, the maps accurately represent landscape to regional patterns. Continuous foliar cover maps better represented observed patterns for all map groups than did categorical maps at the site scale.

3.1. Accuracy Assessment

The accuracy of the map products varied by both region and scale. To capture broad regional patterns in map accuracy, we report accuracy per map group for the entire study area (the regional accuracy) and also partition the accuracies by subregions. We report R^2, MAE, RMSE, AUC, and % ACC to quantify the overall map performances at three scales: site, landscape (10 × 10 km grid), and ecoregion.

Table 4. Regional accuracy at the site scale for R^2, MAE, RMSE, AUC, and % ACC from the merged test partitions of the outer 10-fold cross validation. The mean and median cover of each species or aggregate where present provide context to MAE and RMSE.

Map Group	Continuous Foliar Cover Performance					Cover %	
	R^2	MAE	RMSE	AUC	% ACC	Mean	Median
Alnus Shrubs	0.58	4.1	10.5	0.91	84	26.7	15.0
Betula Shrubs	0.50	5.3	9.3	0.95	88	17.3	15.0
Betula Trees	0.62	2.2	7.8	0.94	87	26.8	15.0
Deciduous Trees	0.59	3.4	10.0	0.94	87	30.4	20.0
Dryas Dwarf Shrubs	0.41	2.6	6.9	0.90	83	16.5	12.0
Empetrum nigrum	0.43	3.6	7.9	0.91	83	13.7	10.0
Eriophorum vaginatum	0.53	3.3	8.2	0.95	88	19.5	15.0
Picea glauca – × *lutzii*	0.54	2.1	5.7	0.94	86	14.7	10.0
Picea mariana	0.50	2.0	6.1	0.95	88	18.6	15.0
Rhododendron Shrubs	0.55	3.4	6.3	0.95	88	13.5	10.0
Salix Low-Tall Shrubs	0.40	9.4	16.3	0.88	80	22.7	15.0
Sphagnum	0.52	6.3	13.6	0.92	83	25.5	16.0
Vaccinium uliginosum	0.49	3.8	7.1	0.91	83	12.8	10.0
Vaccinium vitis-idaea	0.40	2.5	5.7	0.93	85	10.1	7.0
Wetland Sedges	0.45	7.1	14.9	0.91	83	25.6	17.7

Table 5. Landscape and ecoregion accuracy for R^2, MAE, and RMSE from the merged test partitions of the outer 10-fold cross validation.

Map Group	Landscape Scale			Ecoregion Scale		
	R^2	MAE	RMSE	R^2	MAE	RMSE
Alnus Shrubs	0.69	2.8	4.9	0.89	1.0	1.4
Betula Shrubs	0.77	3.2	4.9	0.89	1.7	2.2
Betula Trees	0.82	1.6	3.5	0.94	0.6	0.9
Deciduous Trees	0.81	2.1	4.5	0.94	0.9	1.3
Dryas Dwarf Shrubs	0.65	1.7	3.3	0.82	2.1	3.4
Empetrum nigrum	0.74	2.0	3.5	0.89	1.1	2.1
Eriophorum vaginatum	0.70	2.2	4.2	0.89	2.3	3.6
Picea glauca – × lutzii	0.71	1.3	2.7	0.95	0.4	0.6
Picea mariana	0.70	1.4	3.3	0.88	0.8	1.2
Rhododendron Shrubs	0.75	2.0	3.4	0.95	1.0	1.2
Salix Low-Tall Shrubs	0.57	5.4	7.9	0.90	2.1	2.5
Sphagnum	0.64	3.9	6.8	0.94	1.5	2.0
Vaccinium uliginosum	0.77	2.2	3.7	0.90	1.6	2.1
Vaccinium vitis-idaea	0.58	1.6	2.7	0.91	0.7	1.0
Wetland Sedges	0.71	4.1	6.9	0.92	1.9	2.5

Table 6. Performance of the NLCD, AKVWC Coarse Classes, and AKVWC Fine Classes at the site scale show the relative improvement of the continuous foliar cover maps over existing statewide categorical vegetation maps.

Map Group	NLCD			AKVWC Coarse			AKVWC Fine		
	R^2	MAE	RMSE	R^2	MAE	RMSE	R^2	MAE	RMSE
Alnus Shrubs	0.08	8.3	15.5	0.18	7.6	14.7	0.20	7.1	14.5
Betula Shrubs	0.09	9.1	12.5	0.16	8.5	12.0	0.26	7.4	11.3
Betula Trees	0.26	4.0	10.8	0.31	3.7	10.5	0.39	3.4	9.9
Deciduous Trees	0.31	5.7	13.1	0.34	5.4	12.7	0.36	5.2	12.5
Dryas Dwarf Shrubs	0.03	4.8	8.8	0.07	4.4	8.6	0.16	3.9	8.2
Empetrum nigrum	0.07	6.3	10.1	0.14	5.8	9.7	0.26	4.8	9.0
Eriophorum vaginatum	0.04	7.0	11.8	0.17	6.1	10.9	0.34	4.9	9.8
Picea glauca – × lutzii	0.21	3.7	7.5	0.23	3.5	7.4	0.23	3.5	7.3
Picea mariana	0.17	3.6	7.9	0.21	3.3	7.7	0.23	3.2	7.6
Rhododendron Shrubs	0.08	6.8	9.0	0.18	6.1	8.6	0.3	5.0	7.9
Salix Low-Tall Shrubs	0.09	14.6	20.1	0.11	14.3	19.8	0.18	13.2	19.1
Sphagnum	0.08	12.0	18.8	0.08	11.7	18.7	0.19	10	17.5

Map Group	NLCD			AKVWC Coarse			AKVWC Fine		
	R^2	MAE	RMSE	R^2	MAE	RMSE	R^2	MAE	RMSE
Vaccinium uliginosum	0.11	6.4	9.3	0.14	6.2	9.2	0.27	5.2	8.5
Vaccinium vitis-idaea	0.03	4.5	7.2	0.11	4.1	6.9	0.11	4.0	6.9
Wetland Sedges	0.14	11.7	18.6	0.17	11.5	18.3	0.18	10.9	18.2

3.2. Appropriate Interpretation

A primary strength of the continuous foliar cover maps presented here is the ability to represent vegetation as a stack of overlapping gradient patterns, especially in subsequent statistical analyses or models. We strongly recommend against the application of arbitrary thresholds in interpreting the continuous map products for three reasons: 1) thresholds defeat the purpose of maps intentionally designed to avoid representing artificial breaks in plant communities; 2) with the exception of presence-absence, the accuracy assessments will not be valid after the application of thresholds, preventing the user from understanding the error structure; and 3) the predicted distributions are not the same as the observed distributions, meaning that any threshold based on the observed distributions will be biased when applied to the predicted distributions.

For all map groups, the landscape and regional scale accuracies of the predictions were higher than the site scale accuracies. Users should therefore prefer applications of the maps that integrate the results of multiple pixel-level predictions over individual pixel-level predictions. For example, users applying the foliar cover map products for wildlife movement or resource selection modeling should design path selection functions rather than step selection functions. Similarly, comparisons of foliar cover summarized over landforms (e.g., floodplain *Salix* versus non-montane upland *Salix*) will be more informative than a comparison between individual pixels (e.g., an individual pixel representing *Salix* cover on a floodplain versus an individual pixel representing *Salix* cover on an adjacent upland).

Interpretations of the foliar cover predictions at any scale should be based on the MAE or RMSE specific to the map group and appropriate to the scale. For example, predicted differences between two pixels should be considered significant if the difference is greater than the RMSE or two times the MAE for the site scale. Whereas, predicted differences between two animal paths or landform summaries should be considered significant if the difference is greater than the RMSE or two times the MAE for the landscape scale. If the distribution of the map group is of primary interest, then the percentage accuracy should be interpreted rather than the MAE or RMSE. However, the user should keep in mind that for non-tree, non-*Alnus* map groups, certain regions were informed primarily by presence-only aerial data and thus predictions are likely biased towards presences.

3.3. Sources of Error

The continuous foliar cover models presented here have multiple sources of error relating to field measurements. First, all vegetation measurements and estimations are approximations of reality. Field measurement methods include error such that multiple measurement attempts at the same plot and at the same time will yield different results varying by observation method, observer, transect orientation and randomness for transect-based plots, etc. The composition data from vegetation plots should not be regarded as accurate. A second type of error relating to field measurement is the discrepancy between total cover collected from the ground, which is the target response variable for

our maps, and top cover collected from aerial platforms, which is the only available type of data for much of North American Beringia. Although top cover is less ecologically relevant to plant community composition and structure and wildlife habitat, we included top cover data because the number of plots with total cover data is prohibitively small relative to the large geographic size of the study area and the complexity of the models. Finally, some vegetation plots are imperfectly geolocated. Geolocation errors include positional inaccuracies measured by GPS and alignment problems for some aerial plots. All aerial plots were actually measured within irregular polygons but were generalized to 20 m radius plots from the polygon centroids for better consistency with the scale of the maps. Errors from field measurement were integrated within the model error metrics calculated from the outer cross-validation. Future efforts that prioritize ground data collection by quantitative and repeatable methods, which allow calculation of both total and top cover, over aerial data collection and visual estimation will contribute to more reliable foliar cover maps.

Discrepancies between available remotely sensed data or other environmental data and the vegetation observations also contributed to model error. The Sentinel-1 and -2 composites that informed the modeling effort are derived from discrete times that do not necessarily match the date of vegetation observation. Sentinel data are available from 2015 on, a smaller range of time than the 20-year interval of vegetation observations selected as train and test data. The model did not account for vegetation change between observation date and imagery dates; thus, any vegetation change that actually occurred was included in the model error metrics calculated from the outer cross-validation. We controlled for fire using generalized fire perimeters. In uncommon cases, plots that burned subsequent to observation may not have been within the mapped fire perimeters and may have been erroneously retained in our train and test data. We did not attempt to control for insect and disease damage subsequent to plot observation because of incomplete annual insect and disease survey paths and lack of uniform application of observed damage across all map groups. However, insect and disease damage may have resulted in discrepancies between vegetation observations and radiometry at some plots.

3.4. Data Gaps

Ground-based survey effort for total cover data in the study area has focused primarily on National Petroleum Reserve Alaska (NPR-A) and lands managed by NPS (Figure 2). The lack of total cover data across the entire study area imposes a major limitation on absence data for species that do not consistently occur within the top canopy. Absence data is critical to modeling unbiased distributions and distinguishing presence at low abundances. Even with the inclusion of aerial survey data, much of the study area has not received substantial survey effort. However, we refrain from performing a formal statistical assessment of the spatial coverage of vegetation observations until additional existing datasets are integrated into the AKVEG database. Coordinated survey efforts across land management jurisdictions would likely ensure better spatial coverage across the entire study area than jurisdiction-specific efforts.

Soils and permafrost are two critical environmental properties that lack representations at appropriate scales within the study area. Although the Geophysical Institute Permafrost Lab (GIPL) at University of Alaska Fairbanks (UAF) has produced an active layer depth model that covers the Alaska portion of the study area, it does not cover adjacent Yukon and Northwest Territories. The lack of data for adjacent Canada prevented integration of the GIPL model with the foliar cover models. Additionally, the GIPL active layer depth model contains two types of zero that cannot be reconciled across large geographies wherein both occur. A high-resolution active layer depth model with full

coverage of the study are could be informative to distinguish some species patterns. Similarly, high-resolution data for soil pH, rooting substrate, and organic layer depth would be valuable whereas current representations for the entire study area are available only at extremely coarse resolution.

Available climate models with a 2 × 2 km resolution from Scenarios Network for Alaska and Arctic Planning (SNAP) at UAF are informative to foliar cover models only for broad biogeographic patterns. The discrepancy between mapped resolutions for climate and foliar cover was problematic for some map groups for which aerial data were included as presence only data. Without absences, the models could in some cases predict distribution successfully by only predicting presences within 2 × 2 km cells based on climate. To avoid this problem, we limited the inclusion of some climate metrics for some map groups. We removed: january minimum temperature from the models for *Betula* Shrubs, *Empetrum nigrum*, and *Vaccinium uliginosum*; summer warmth index from the models for *Eriophorum vaginatum*; and both january minimum temperature and total annual precipitation from the models for *Dryas* Dwarf Shrubs. The 2 × 2 km resolution downscaled climate data cover Alaska and adjacent Yukon, but not the Northwest Territories. The study area included a small portion of Arctic Northwest Territories to the Mackenzie River Delta. We performed a simple imputation by geographic nearest neighbors for the missing data. Future models could benefit from higher resolution climate and weather data, such as derived from MERRA-2 reanalysis data. In addition to the climate covariates selected here, partnership with a climate and weather modeler in the future would enable inclusion of other potentially important covariates at an appropriate scale, such as date of snow melt and maximum snow depth.

3.5. Future Needs

The continuous foliar cover maps presented here are outputs of a repeatable scripted workflow. Future iterations of the map will be produced as funding allows to update the maps with new field and remotely sensed data and incorporate technical improvements. For changes already integrated into the maps, refer to Appendix 2 (Change Log). The following is a list of planned improvements for the next major version (2.0). Minor version improvements of the maps or this user guide may appear in the interim.

1. Incorporate additional data into the AKVEG database, especially ground data that can provide true absences to all map groups.
2. Generate early and late growing season image composites from Sentinel-2 as date-specific synthetic images using the Continuous Change Detection and Classification algorithm (CCDC; Zhu and Woodcock 2014).
3. Predict distribution maps for non-vegetation components to provide mask layers to be used in subsequent analyses: water, barren, and developed.
4. Expand study area to include Aleutian and Bering Sea Islands.
5. Statistically assess spatial coverage of vegetation observations relative to suite of mapping covariates across the study area.

Picea glauca – ×*lutzii*

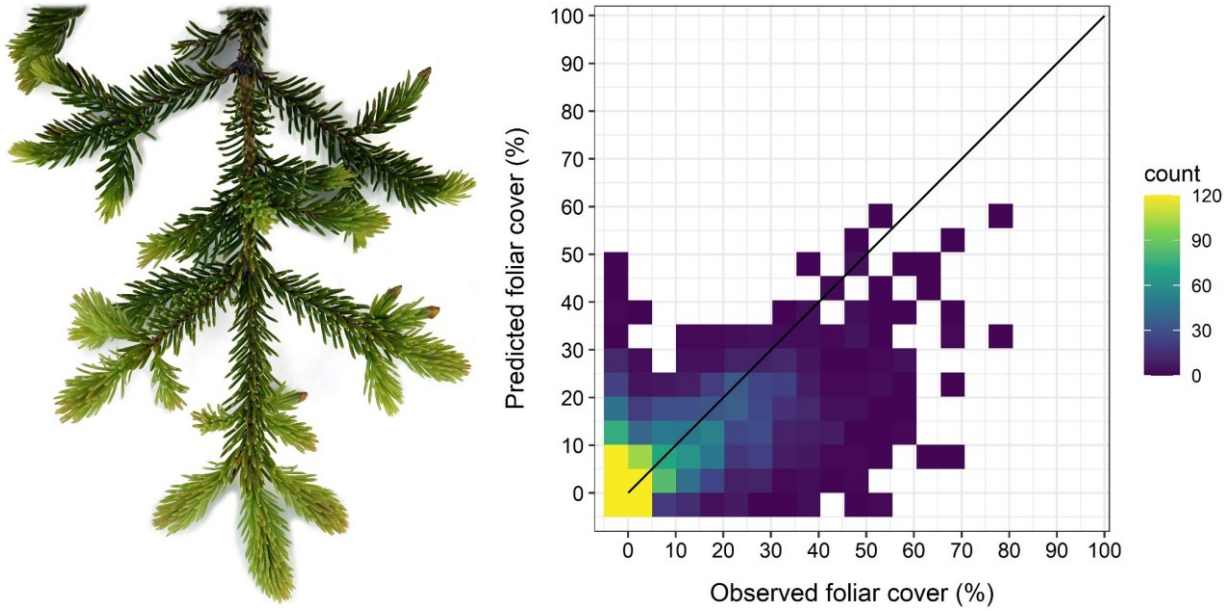

Figure 3. Observed foliar cover compared to predicted foliar cover for *Picea glauca* – × *lutzii* from the merged test partitions of 10-fold cross-validation, wherein each observation was predicted exactly once. R^2 values were calculated relative to the theoretical 1:1 ratio between observed and predicted foliar cover (solid black line). *Picea glauca* shown at left.

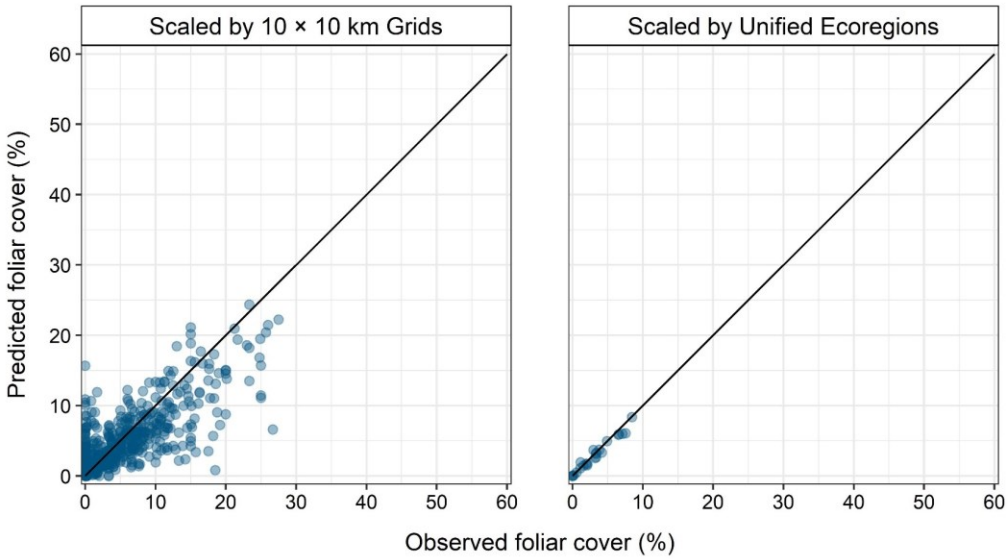

Figure 4. Mean observed foliar cover compared to mean predicted foliar cover for *Picea glauca* – × *lutzii* summarized by 10 × 10 km grids (right) and by ecoregions (left) from the merged test partitions of 10-fold cross-validation.

Table 7. Accuracy of *Picea glauca* - ×*lutzii* by region and subregion at the site scale.

Subregion	Continuous Foliar Cover Performance					Cover	
	R^2	MAE	RMSE	AUC	% ACC	Mean	Median
All	0.54	2.1	5.7	0.94	86	14.7	10.0
Northern	0.53	0.6	3.2	0.98	97	14.6	12.5
Western	0.67	1.3	4.1	0.95	91	15.3	15.0
Interior	0.47	3.4	7.4	0.89	77	14.5	10.0

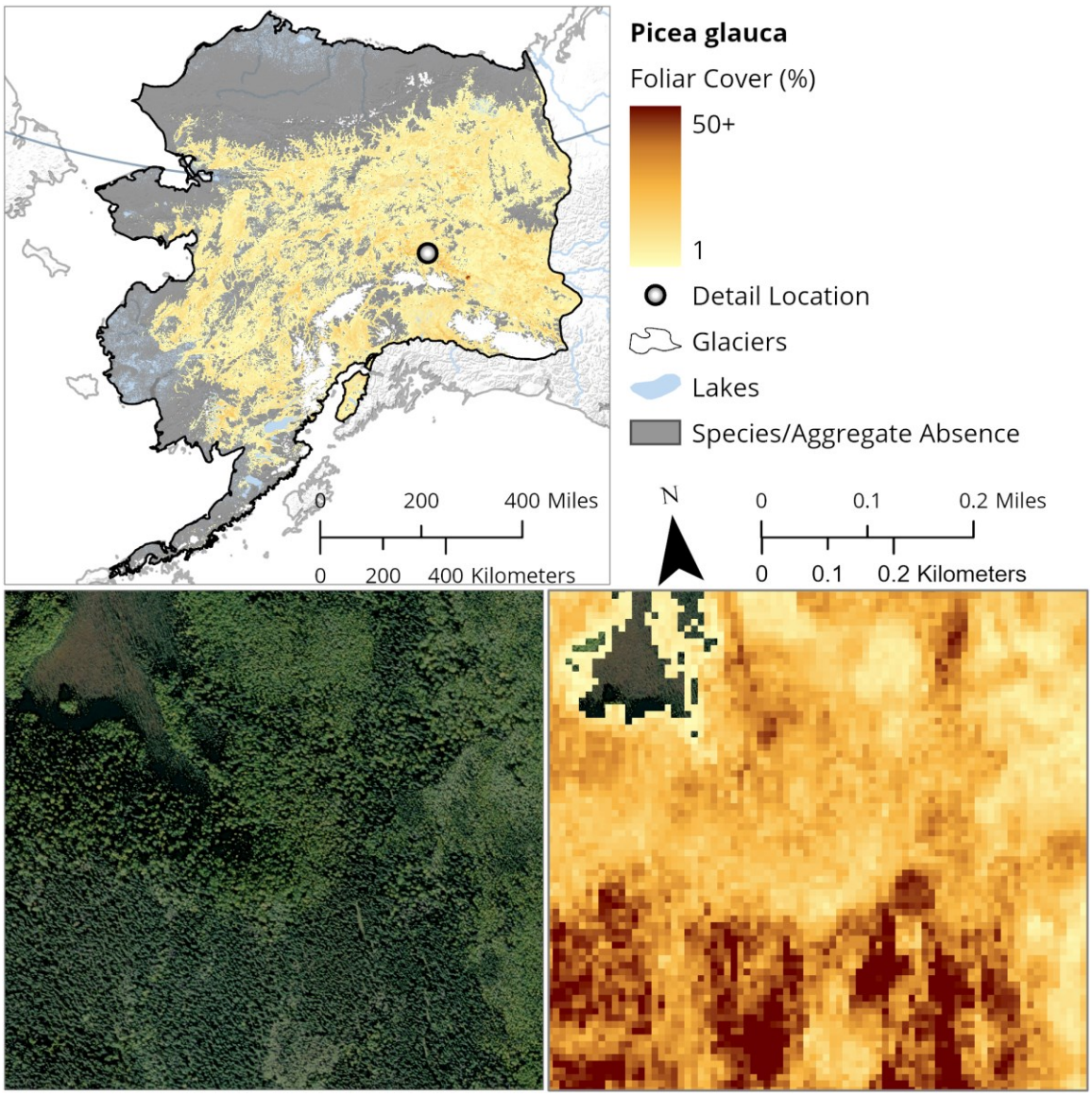

Figure 5. Map of *Picea glauca* in North American Beringia (top) and comparison between high resolution Maxar satellite imagery (bottom left) and predicted map (bottom right) at 1:10,000 scale.

Components

The *Picea glauca* – ×*lutzii* map group consists of *Picea glauca* (Moench) Voss and *Picea* ×*lutzii* Little, a fertile hybrid between *Picea glauca* and *Picea sitchensis* (Bong.) Carrière. *Picea glauca* is common and widespread throughout the forested parts of the study area. *Picea* ×*lutzii* is common in the Kenai Mountains outside of the study area. Within the study area, *Picea* ×*lutzii* is known from several locations in Lake Clark National Park in Southwest Alaska. We merged *Picea* ×*lutzii* with *Picea glauca* because our models were not able to distinguish the two.

Figure 6. An isolated stand of *Picea glauca* near treeline in the eastern Alaska Range (left). High abundance of *Picea glauca* in mesic low hills along the Copper River (right).

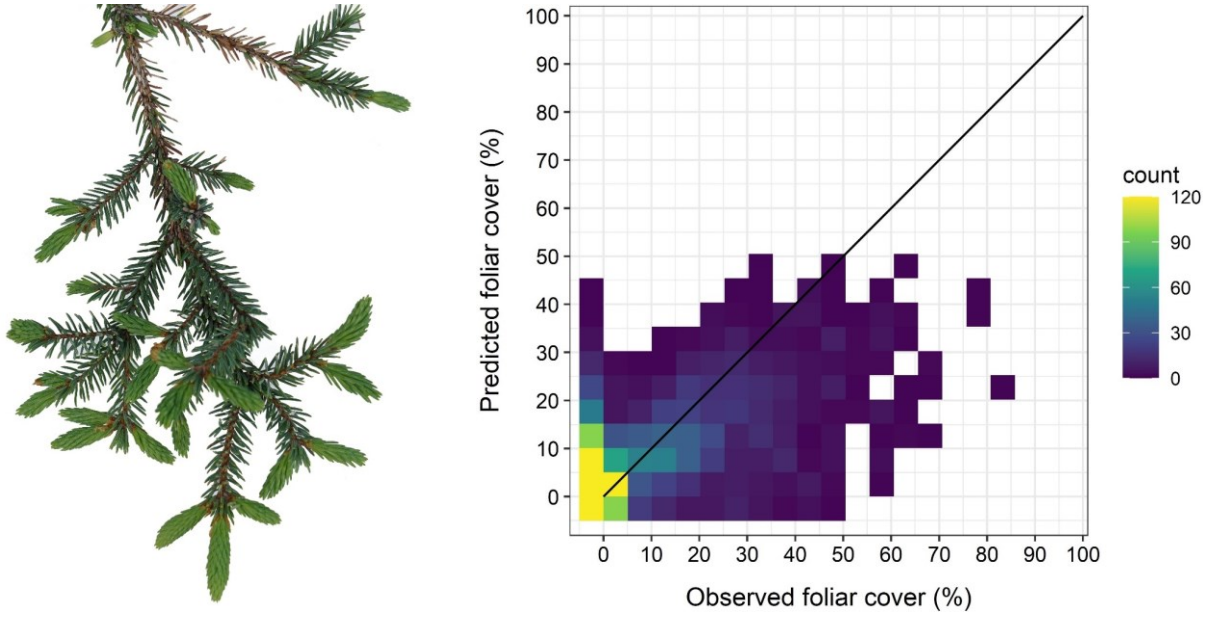

Figure 7. Observed foliar cover compared to predicted foliar cover for *Picea mariana* from the merged test partitions of 10-fold cross-validation, wherein each observation was predicted exactly once. R^2 values were calculated relative to the theoretical 1:1 ratio between observed and predicted foliar cover (solid black line). *Picea mariana* shown at left.

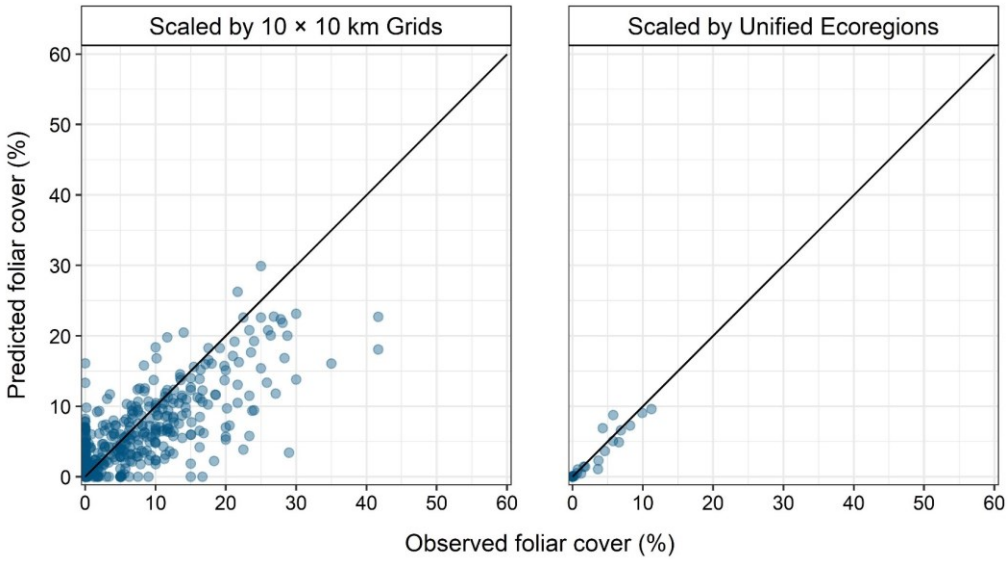

Figure 8. Mean observed foliar cover compared to mean predicted foliar cover for *Picea mariana* summarized by 10 × 10 km grids (right) and by ecoregions (left) from the merged test partitions of 10-fold cross-validation.

Table 8. Accuracy of *Picea mariana* by region and subregion at the site scale.

Subregion	Continuous Foliar Cover Performance					Cover	
	R^2	MAE	RMSE	AUC	% ACC	Mean	Median
All	0.50	2.0	6.1	0.95	88	18.6	15.0
Northern	0.31	0.3	2.2	0.98	97	16.2	12.0
Western	0.42	0.4	2.8	0.93	98	19.6	20.0
Interior	0.47	4.2	8.7	0.90	76	18.6	15.0

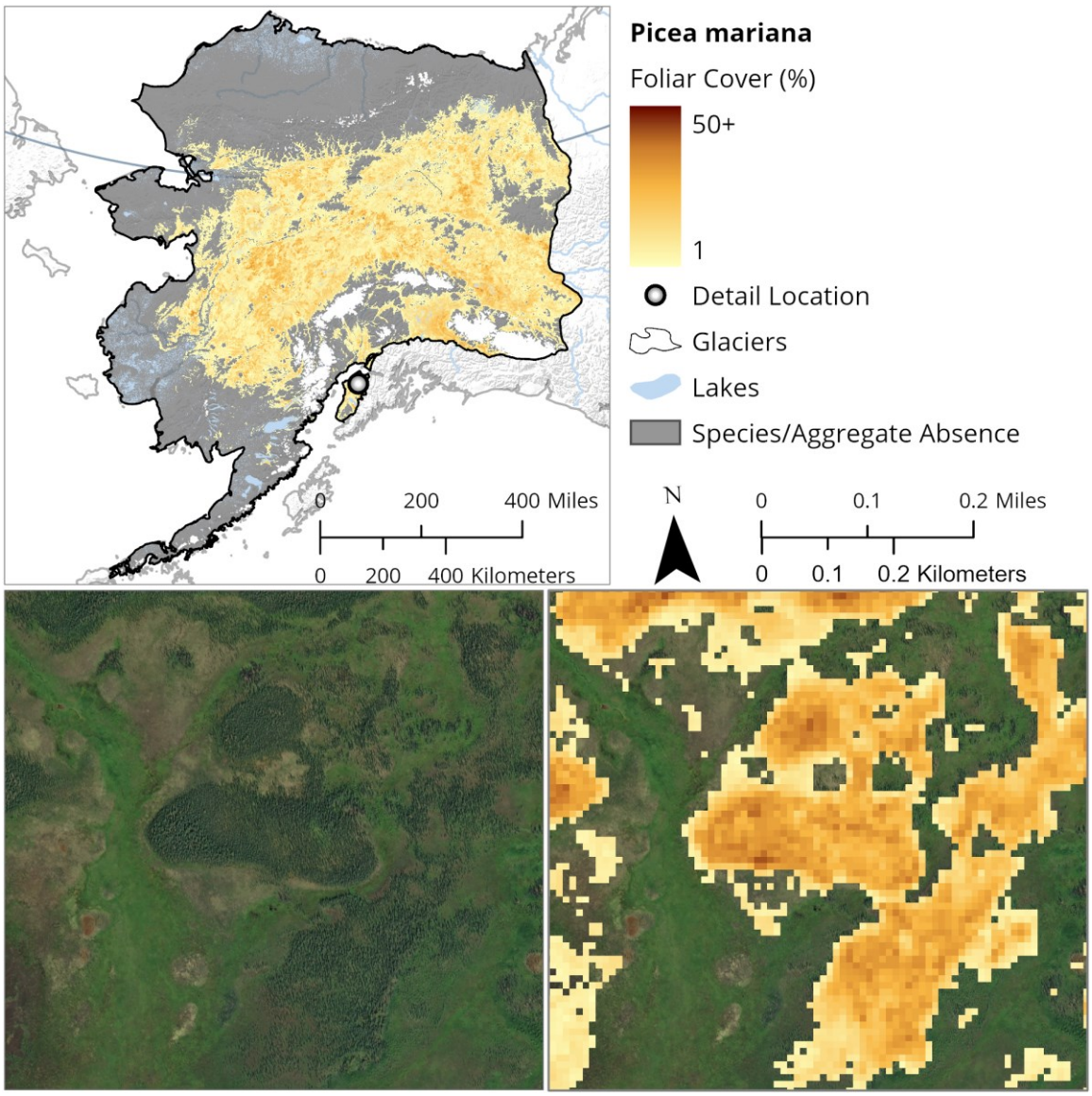

Figure 9. Map of *Picea mariana* in North American Beringia (top) and comparison between high resolution Maxar satellite imagery (bottom left) and predicted map (bottom right) at 1:10,000 scale.

Components

The *Picea mariana* map group consists only of *Picea mariana* (Mill.) Britton, Sterns, & Poggenb.

Figure 10. *Picea mariana* growing in stunted form near the elevational treeline in the southern Brooks Range (left). In warm, mesic soils in lowland areas, such as in the western Kenai Peninsula, *Picea mariana* can form dense and tall stands (right).

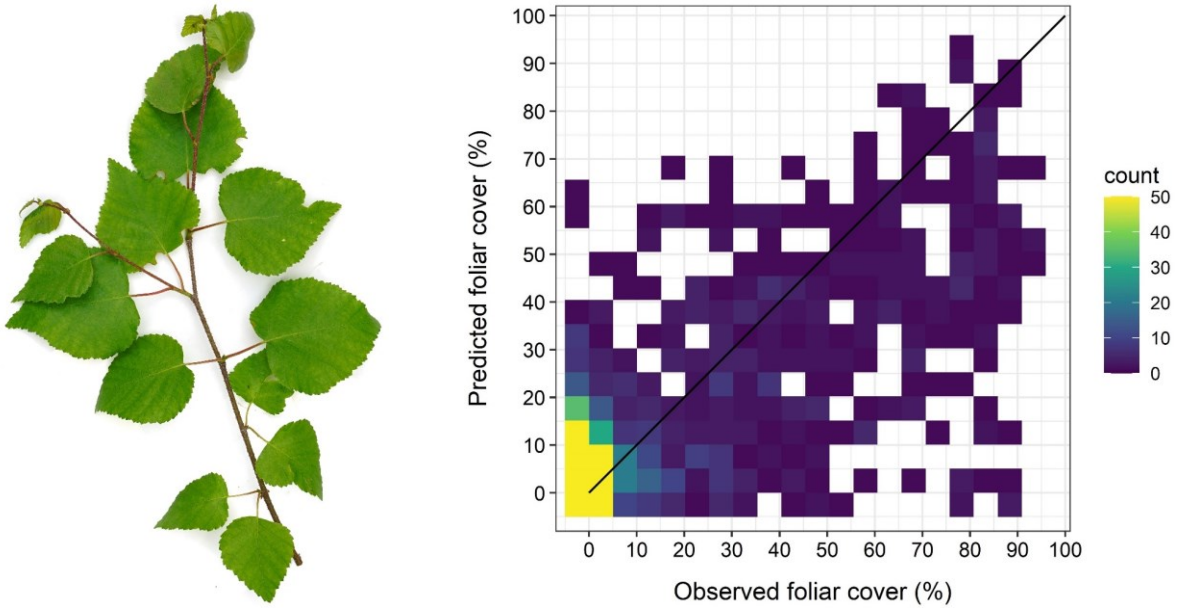

Figure 11. Observed foliar cover compared to predicted foliar cover for *Betula* Trees from the merged test partitions of 10-fold cross-validation, wherein each observation was predicted exactly once. R^2 values were calculated relative to the theoretical 1:1 ratio between observed and predicted foliar cover (solid black line). *Betula neoalaskana* shown at left.

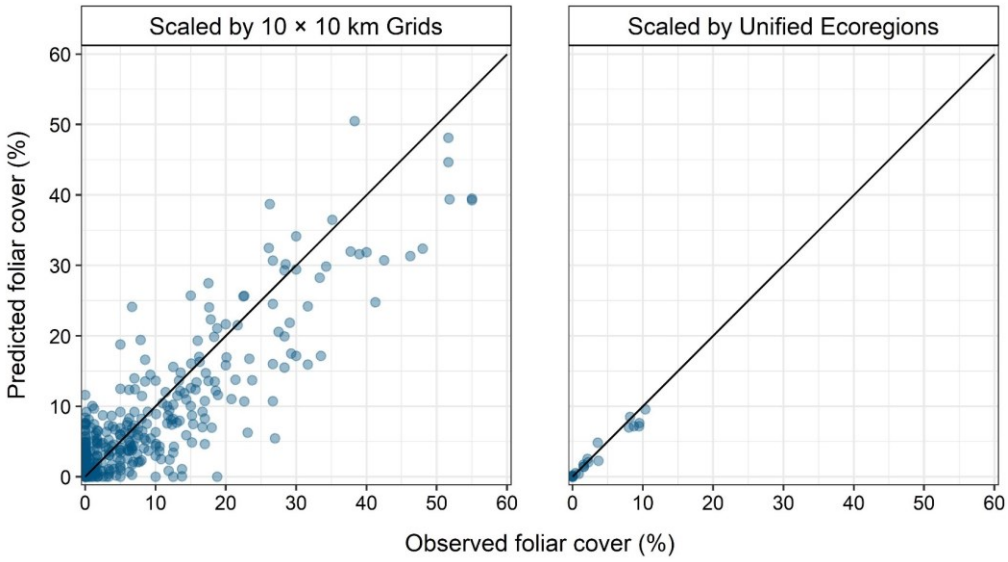

Figure 12. Mean observed foliar cover compared to mean predicted foliar cover for *Betula* Trees summarized by 10 × 10 km grids (right) and by ecoregions (left) from the merged test partitions of 10-fold cross-validation.

Table 9. Accuracy of *Betula* Trees by region and subregion at the site scale.

Subregion	Continuous Foliar Cover Performance					Cover	
	R^2	MAE	RMSE	AUC	% ACC	Mean	Median
All	0.62	2.2	7.8	0.94	87	26.8	15.0
Northern	0.44	0.3	3.1	0.96	99	35.0	25.0
Western	0.59	1.7	6.7	0.96	92	29.4	25.0
Interior	0.62	4.6	11.1	0.87	72	25.4	10.0

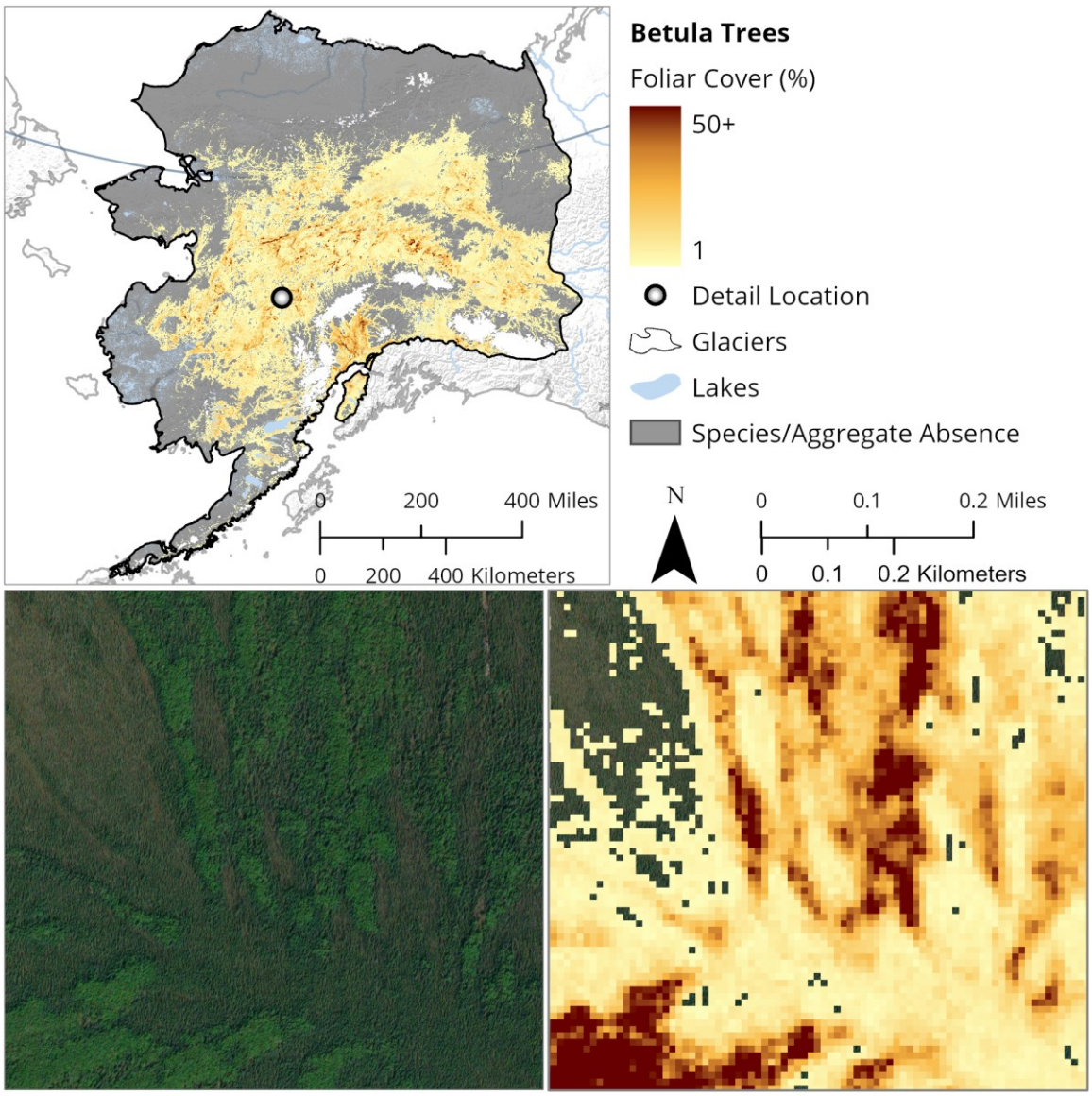

Figure 13. Map of *Betula* Trees in North American Beringia (top) and comparison between high resolution Maxar satellite imagery (bottom left) and predicted map (bottom right) at 1:10,000 scale.

Components

The *Betula* Trees map group consists of *Betula neoalaskana* Sarg. and *Betula kenaica* W.H. Evans. *Betula papyrifera* Marshall occurs in Alaska only outside of the study area in the vicinity of Haines. In the past, *Betula neoalaskana* and *Betula kenaica* have commonly been considered as belonging within a broad *Betula papyrifera* (see synonymy). Thus, all of the observations within the study area of *Betula papyrifera* refer to *Betula neoalaskana* or *Betula kenaica*. *Betula kenaica* is common near the coast in the southern part of the study area, primarily in Southwest Alaska and the western Kenai Peninsula. *Betula neoalaskana* is common in most forested parts of the study area.

Figure 14. The high return interval of fire in the Yukon-Tanana Uplands maintains areas of high abundance of *Betula neoalaskana* (left). *Betula neoalaskana* growing on the lower slope of a mountain near its northern limit in the Brooks Range (right).

Deciduous Trees

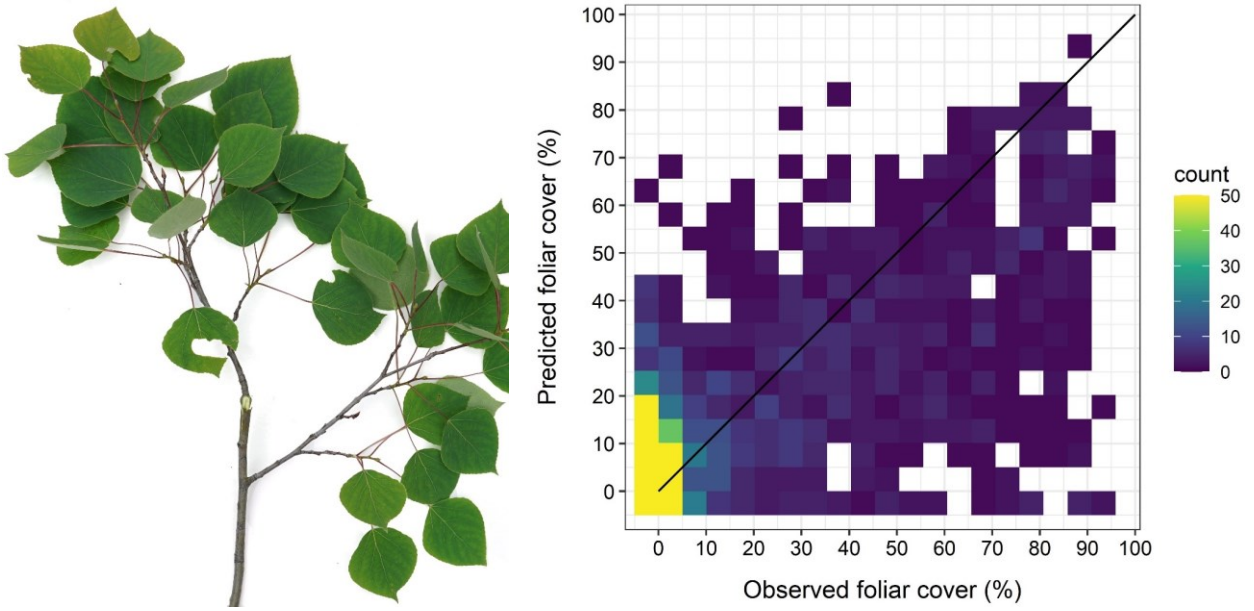

Figure 15. Observed foliar cover compared to predicted foliar cover for Deciduous Trees from the merged test partitions of 10-fold cross-validation, wherein each observation was predicted exactly once. R^2 values were calculated relative to the theoretical 1:1 ratio between observed and predicted foliar cover (solid black line). *Populus tremuloides* shown at left.

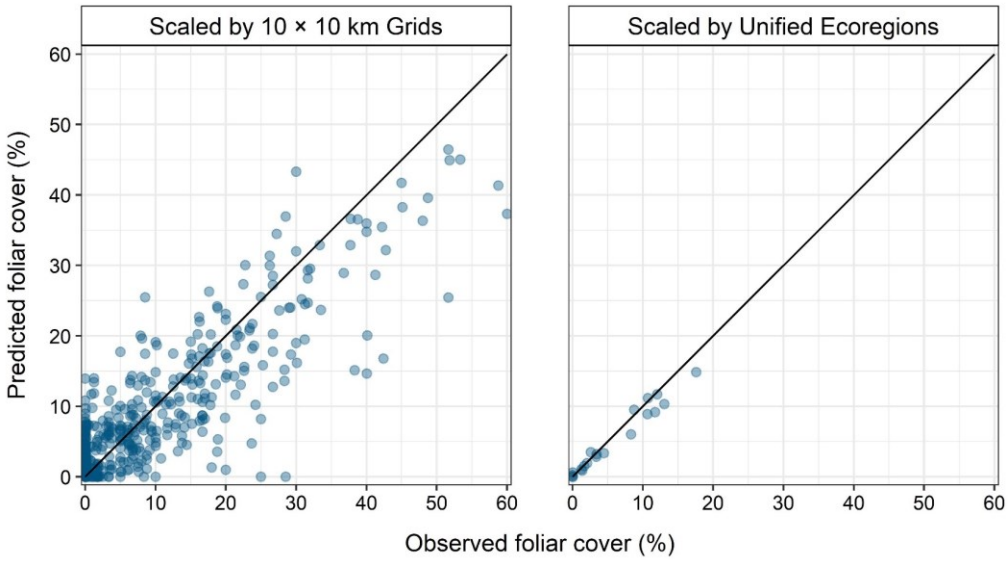

Figure 16. Mean observed foliar cover compared to mean predicted foliar cover for Deciduous Trees summarized by 10 × 10 km grids (right) and by ecoregions (left) from the merged test partitions of 10-fold cross-validation.

Table 10. Accuracy of Deciduous Trees by region and subregion at the site scale.

Subregion	Continuous Foliar Cover Performance					Cover	
	R^2	MAE	RMSE	AUC	% ACC	Mean	Median
All	0.59	3.4	10.0	0.94	87	30.4	20.0
Northern	0.54	0.4	3.1	0.95	98	25.3	15.0
Western	0.61	2.4	8.3	0.95	90	32.5	30.0
Interior	0.55	6.8	14.5	0.87	74	29.6	15.5

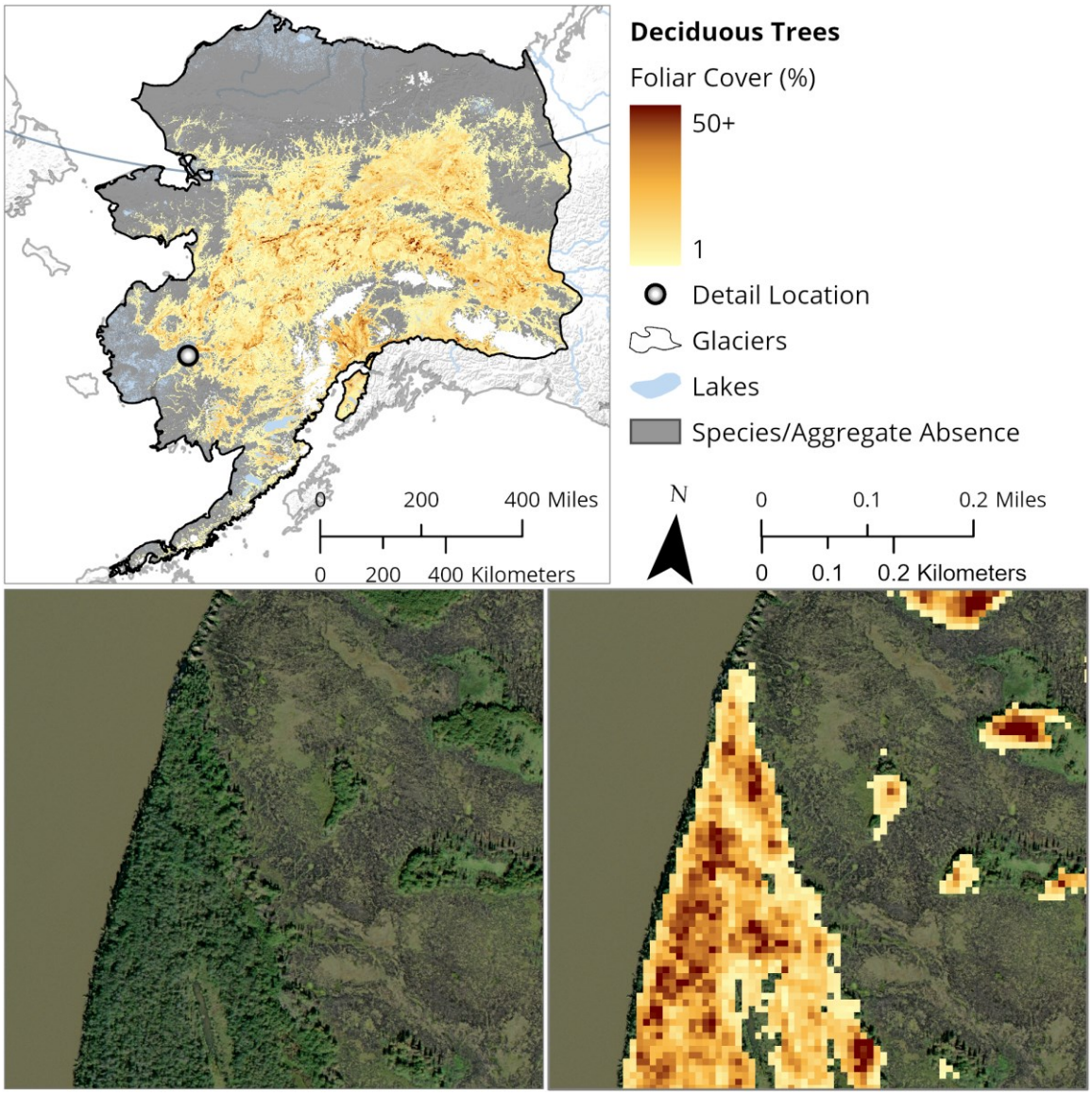

Figure 17. Map of Deciduous Trees in North American Beringia (top) and comparison between high resolution Maxar satellite imagery (bottom left) and predicted map (bottom right) at 1:10,000 scale.

Components

The Deciduous Trees map group is composed of *Betula neoalaskana* Sarg., *Betula kenaica* W.H. Evans, *Populus tremuloides* Michx., *Populus trichocarpa* Torr. & A. Gray ex Hook., and *Populus balsamifera* L.. *Betula papyrifera* Marshall is excluded for the reasons described above. Although *Larix laricina* (Du Roi) K. Koch is technically a deciduous tree, we excluded it from the map group because it belongs within the Class *Pinopsida*, rather than in *Magnoliopsida* with *Betulaceae* and *Salicaceae*, and because of its affinity for poorly drained, hygric soils.

Populus balsamifera is common throughout the study area, except in southern coastal lowland forests and floodplains where it is replaced by *Populus trichocarpa*. *Populus balsamifera* and *Populus trichocarpa* form hybrids where their ranges overlap in southern coastal Alaska (Viereck and Little 2007). *Populus balsamifera* is not uncommon along sheltered river drainages and perennial springs in the northern Brooks Range and Brooks Foothills (Breen 2014), making it the only widespread tree on the North Slope. *Populus balsamifera* also extends past the ranges of other tree species in Western Alaska and at the elevational limits on mountain slopes in Interior Alaska. *Populus tremuloides* is common in Interior Alaska but also occurs in isolated stands within forested parts of Western Alaska and in the southern Brooks Range of Northern Alaska.

Figure 18. *Populus tremuloides* occurs in isolated stands in Southwest Alaska, such as along the Nuyakuk River in Bristol Bay (left). High abundance of *Populus balsamifera* on a frequently disturbed floodplain of the Mulchatna River (right).

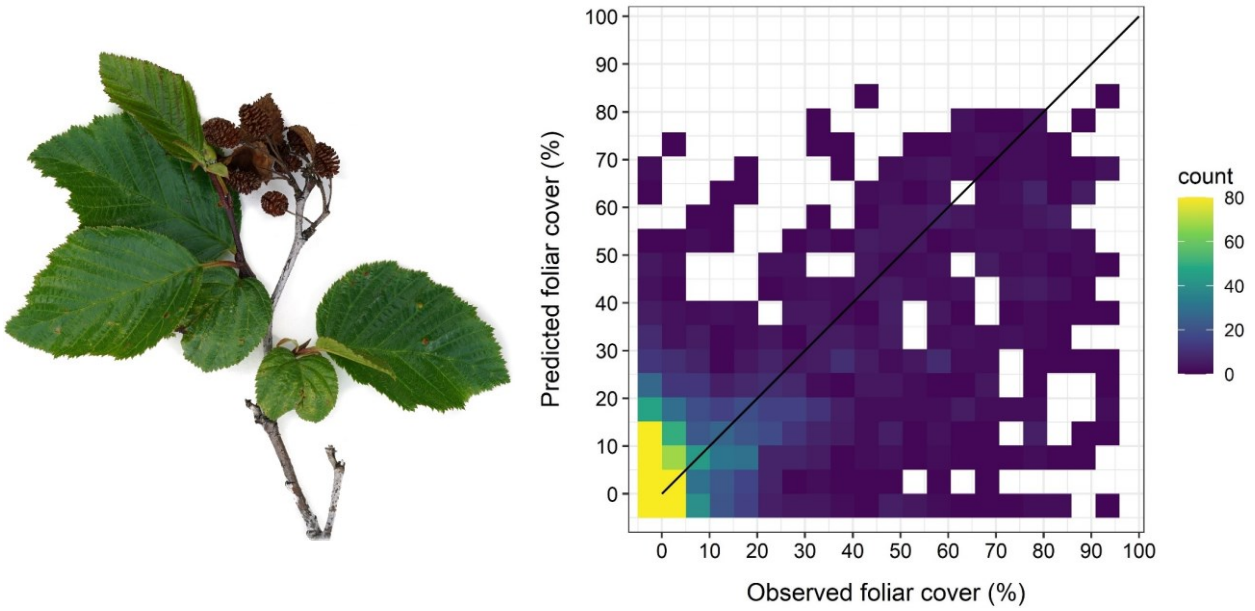

Figure 19. Observed foliar cover compared to predicted foliar cover for *Alnus* Shrubs from the merged test partitions of 10-fold cross-validation, wherein each observation was predicted exactly once. R^2 values were calculated relative to the theoretical 1:1 ratio between observed and predicted foliar cover (solid black line). *Alnus alnobetula* ssp. *sinuata* shown at left.

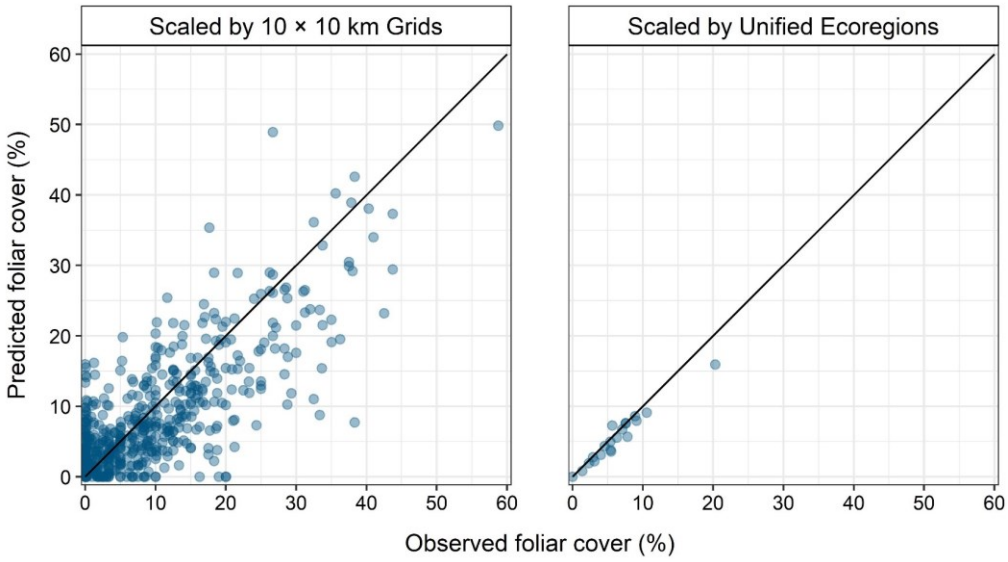

Figure 20. Mean observed foliar cover compared to mean predicted foliar cover for *Alnus* Shrubs summarized by 10 × 10 km grids (right) and by ecoregions (left) from the merged test partitions of 10-fold cross-validation.

Table 11. Accuracy of *Alnus* Shrubs by region and subregion at the site scale.

Subregion	Continuous Foliar Cover Performance					Cover	
	R^2	MAE	RMSE	AUC	% ACC	Mean	Median
All	0.58	4.1	10.5	0.91	84	26.7	15.0
Northern	0.56	2.2	7.6	0.95	90	22.2	15.0
Western	0.61	4.1	11.5	0.91	87	36.5	25.0
Interior	0.51	5.4	11.0	0.87	75	21.6	15.0

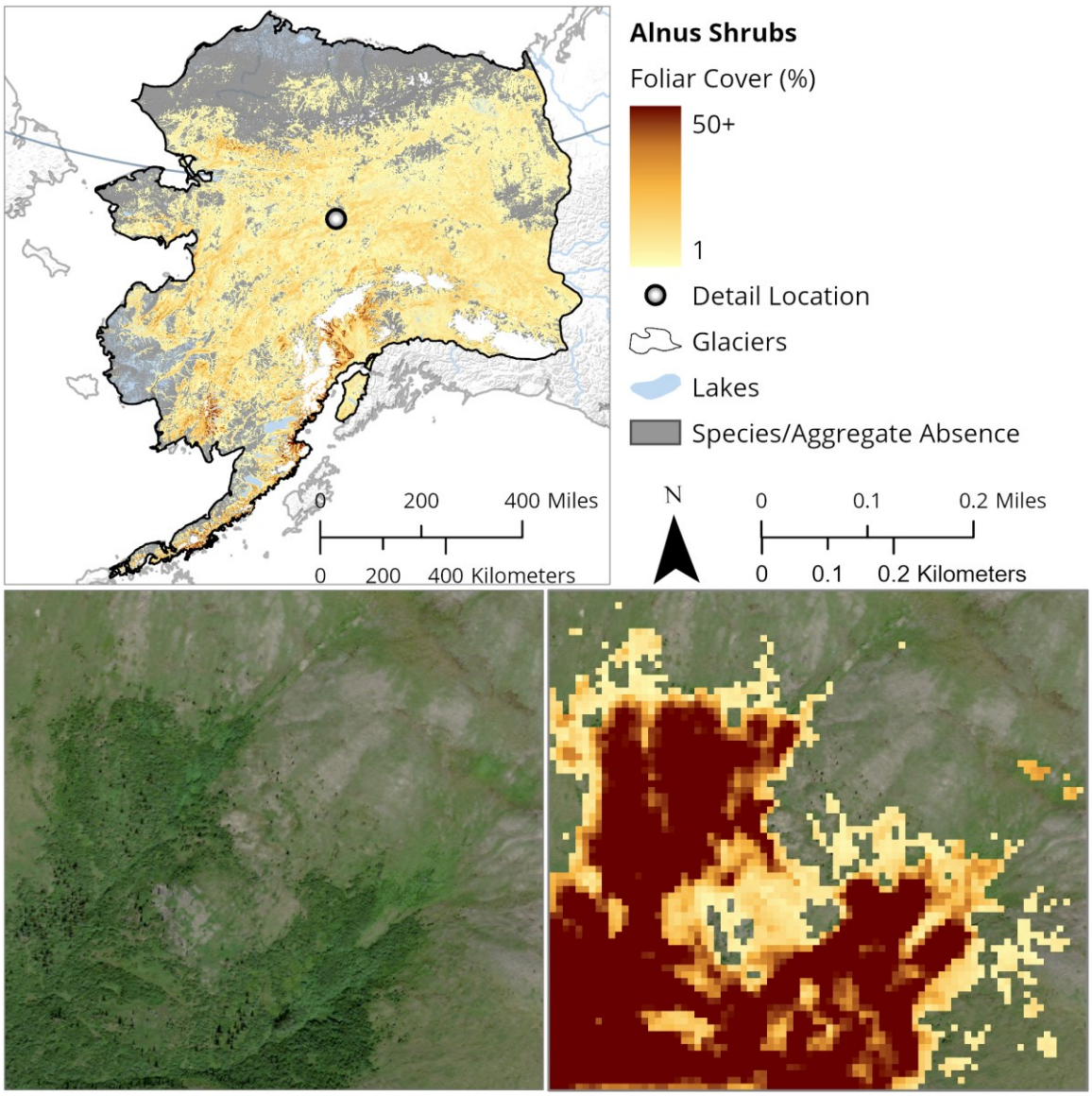

Figure 21. Map of *Alnus* Shrubs in North American Beringia (top) and comparison between high resolution Maxar satellite imagery (bottom left) and predicted map (bottom right) at 1:10,000 scale.

Components

The *Alnus* Shrubs map group consists of *Alnus incana* ssp. *tenuifolia* (Nutt.) Breitung, *Alnus alnobetula* ssp. *fruticosa* (Rupr.) Raus., and *Alnus alnobetula* ssp. *sinuata* (Regel) Raus. In the past, *Alnus alnobetula* subspecies have commonly been known as combinations within *Alnus viridis* (Chaix) DC. However, the name "*alnobetula*" has priority over "*viridis*" (Greuter and von Raab-Straube 2011). The name *Alnus crispa* (Dryl. ex Aiton) Pursh has also been frequently misapplied within Alaska for *Alnus alnobetula* ssp. *fruticosa*.

Figure 22. *Alnus incana* ssp. *tenuifolia* growing underneath *Picea glauca* on a floodplain of the Nuyakuk River in Southwest Alaska (left). *Alnus alnobetula* ssp. *fruticosa* is widespread and abundant in parts of the North Slope, such as in vicinity of the Colville River in the Brooks Foothills (right).

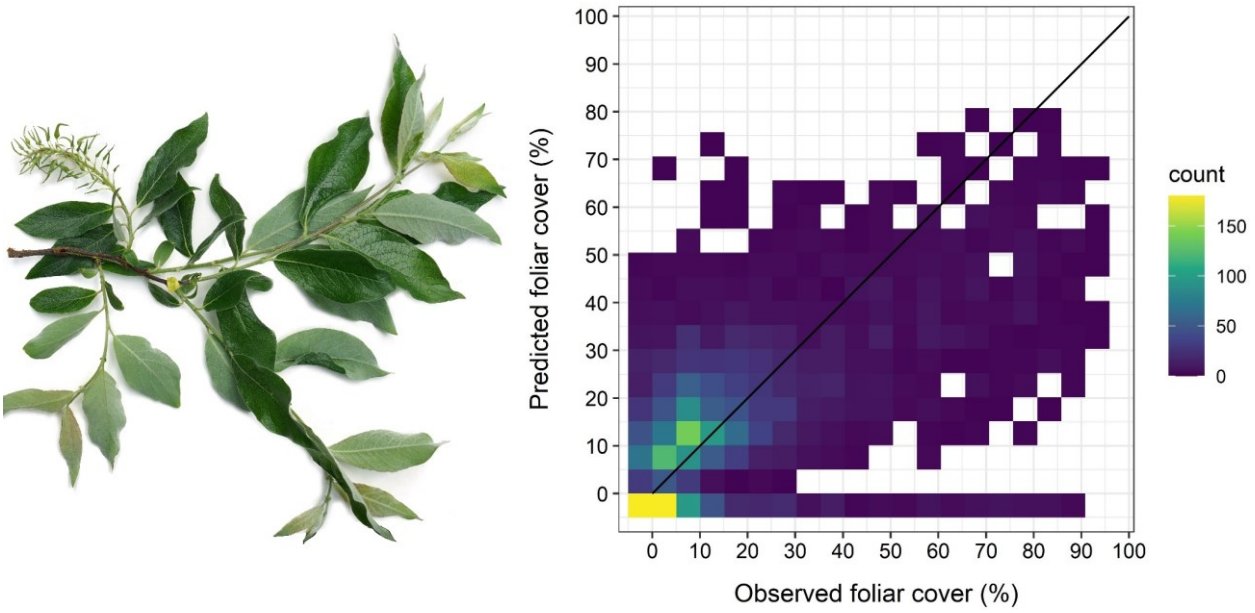

Figure 23. Observed foliar cover compared to predicted foliar cover for *Salix* Low-Tall Shrubs from the merged test partitions of 10-fold cross-validation, wherein each observation was predicted exactly once. R^2 values were calculated relative to the theoretical 1:1 ratio between observed and predicted foliar cover (solid black line). *Salix bebbiana* shown at left.

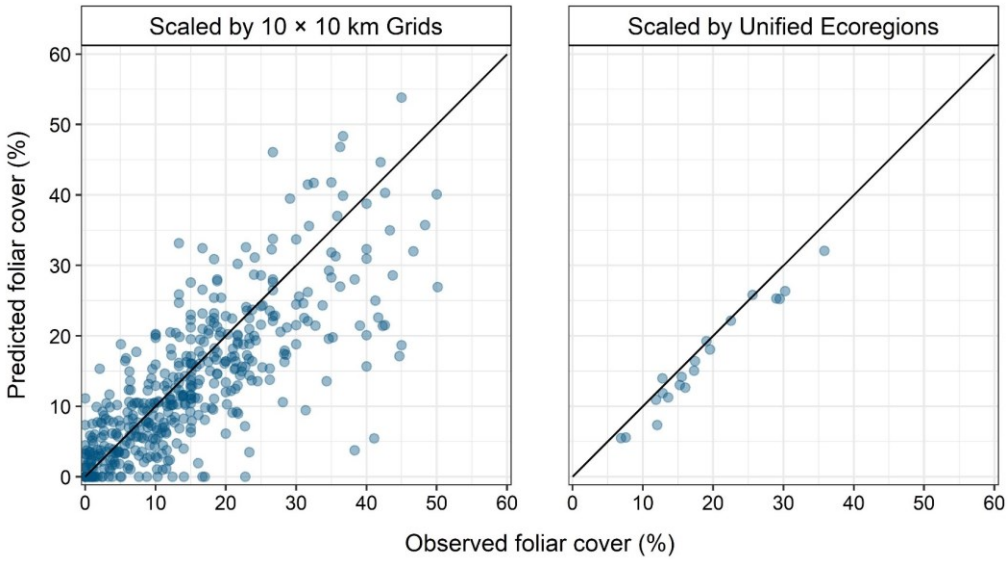

Figure 24. Mean observed foliar cover compared to mean predicted foliar cover for *Salix* Low-Tall Shrubs summarized by 10 × 10 km grids (right) and by ecoregions (left) from the merged test partitions of 10-fold cross-validation.

Table 12. Accuracy of *Salix* Low-tall Shrubs by region and subregion at the site scale.

Subregion	Continuous Foliar Cover Performance					Cover	
	R^2	MAE	RMSE	AUC	% ACC	Mean	Median
All	0.40	9.4	16.3	0.88	80	22.7	15.0
Northern	0.41	8.0	14.6	0.85	76	19.1	10.0
Western	0.37	10.7	18.6	0.88	79	26.4	18.0
Interior	0.39	9.9	14.9	0.90	87	21.9	15.0

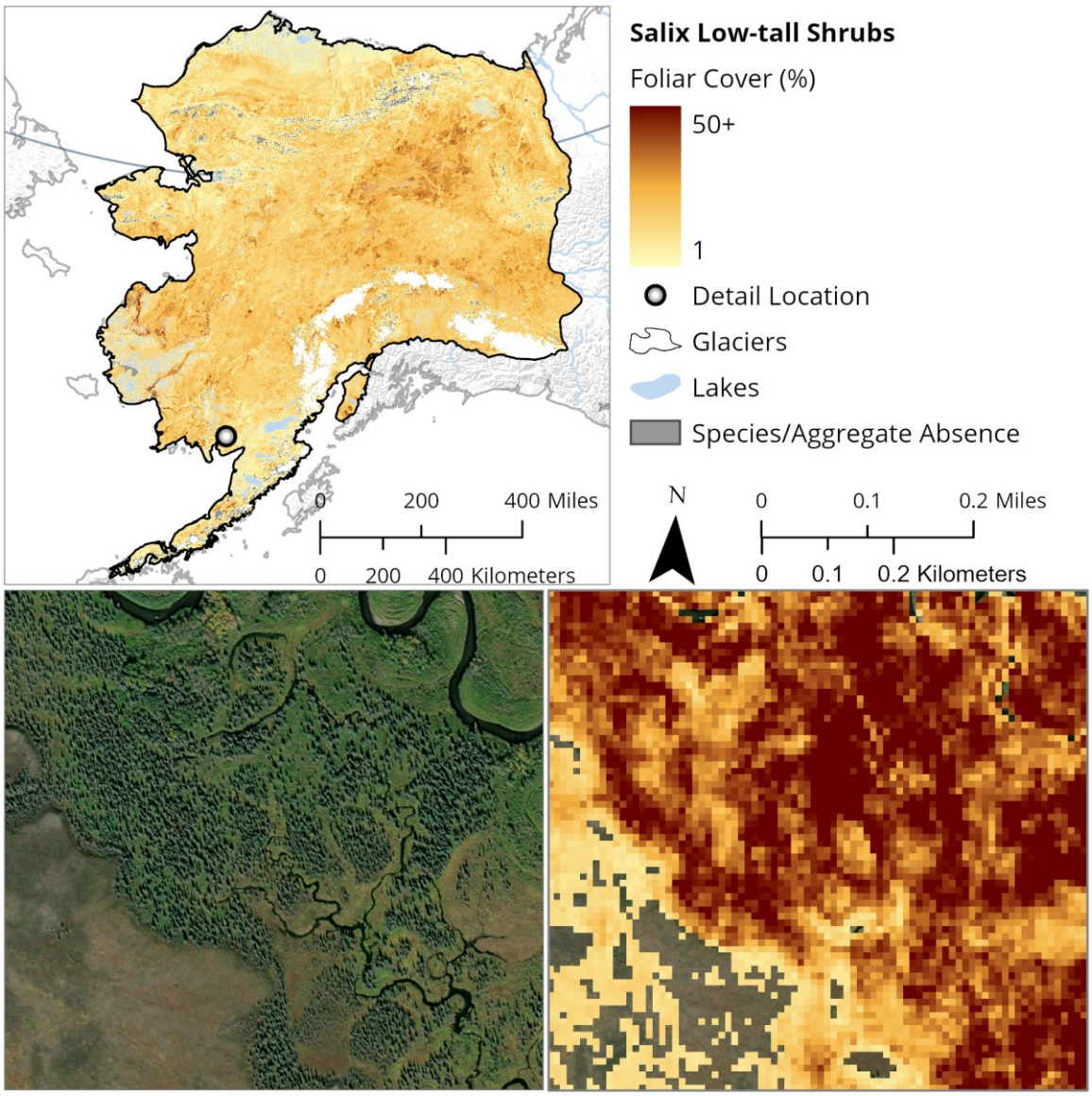

Figure 25. Map of *Salix* Low-tall Shrubs in North American Beringia (top) and comparison between high resolution Maxar satellite imagery (bottom left) and predicted map (bottom right) at 1:10,000 scale.

Components

The *Salix* Low-tall Shrub map group includes the *Salix* species listed in Table 13 that commonly or typically grow as tall shrubs or upright low shrubs, where tall shrubs are greater than 1.5 m in height and low shrubs are less than 1.5 m in height. We follow Argus (2004) in adopting a minimum height for low upright *Salix* shrubs around 20 cm. Thus, we excluded from this class all *Salix* species that commonly or typically grow as dwarf shrubs or prostrate low shrubs. The included species vary in their geographic patterns, but the map group as a whole is ubiquitous throughout the study area. Species include those that are relatively widespread and common throughout the entire study area (e.g., *Salix pulchra*), those that are geographically restricted within the study area (e.g., *Salix pseudomonticola*), those that extend into the study area from primary ranges that include the Temperate Northern Pacific region (e.g., *Salix sitchensis*), and those that are rare in Alaska (e.g., *Salix athabascensis*). Although species can be loosely generalized to height classes listed in Table 13, *Salix* are highly polymorphic in height and form depending on environment.

Figure 26. *Salix pulchra* (foreground) and *Salix alaxensis* (background) growing tall and at high abundance on a floodplain of the Nushagak River in Bristol Bay (left). *Salix pulchra* growing short and at moderate abundance with *Eriophorum vaginatum* and *Betula nana* ssp. *exilis* in the vicinity of the Colville River in the Brooks Foothills (right).

Table 13. Species included in the *Salix* Low-tall Shrub aggregate.

Species	Typical Size
Salix alaxensis var. *alaxensis* (Andersson) Coville	Tall (occasionally tree)
Salix alaxensis var. *longistylus* (Rydb.) C.K. Schneid.	Tall (occasionally tree)
Salix arbusculoides Andersson	Tall (occasionally tree)
Salix athabascensis Raup	Low
Salix barclayi Andersson	Low-tall
Salix barrattiana Hook.	Low
Salix bebbiana Sarg.	Tall (occasionally tree)
Salix candida Flueggé ex Willd.	Tall
Salix commutata Bebb	Low-tall
Salix glauca ssp. *acutifolia* (Hook.) Hultén	Low-tall
Salix glauca ssp. *stipulifera* (Flod. ex Häyrén) Hiitonen	Low-tall
Salix hastata L.	Low-tall
Salix hookeriana Barratt ex Hook.	Tall (occasionally tree)
Salix interior Rowlee	Tall
Salix lasiandra var. *caudata* (Nutt.) Sudw.	Tall (occasionally tree)
Salix lasiandra var. *lasiandra* Benth.	Tall (occasionally tree)
Salix myrtillifolia Andersson	Low
Salix niphoclada Rydb.	Low
Salix planifolia Pursh	Excluded: not in study area
Salix pseudomonticola C.R. Ball	Tall
Salix pseudomyrsinites Andersson	Tall
Salix pulchra Cham.	Low-tall
Salix richardsonii Hook.	Low-tall
Salix scouleriana Barratt ex Hook.	Tall (occasionally tree)
Salix sitchensis Sanson ex Bong.	Tall (occasionally tree)

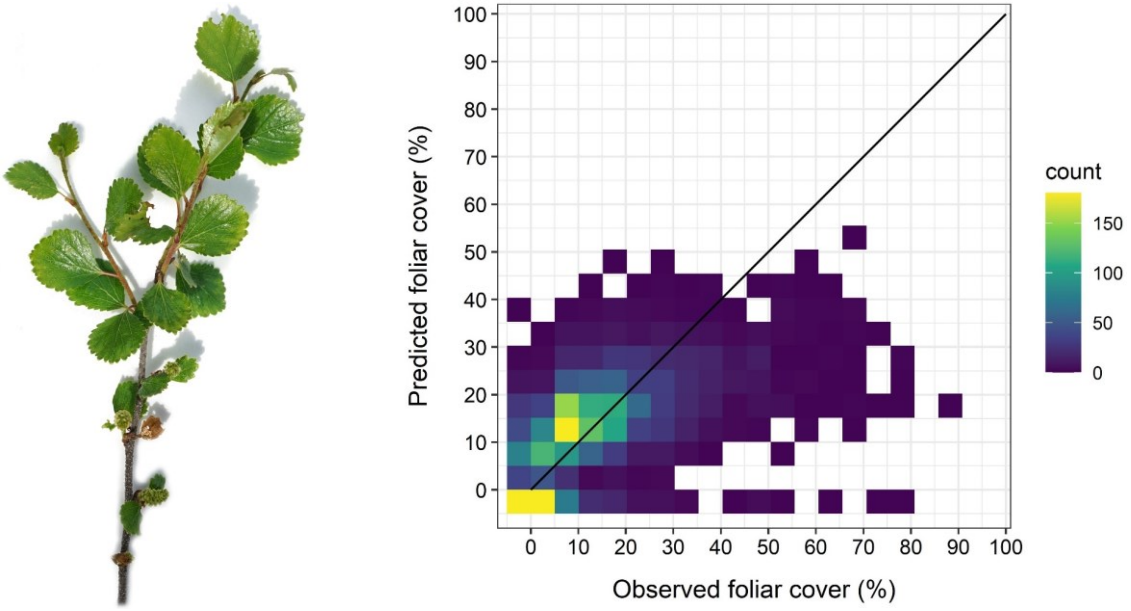

Figure 27. Observed foliar cover compared to predicted foliar cover for *Betula* Shrubs from the merged test partitions of 10-fold cross-validation, wherein each observation was predicted exactly once. R^2 values were calculated relative to the theoretical 1:1 ratio between observed and predicted foliar cover (solid black line). *Betula glandulosa* shown at left.

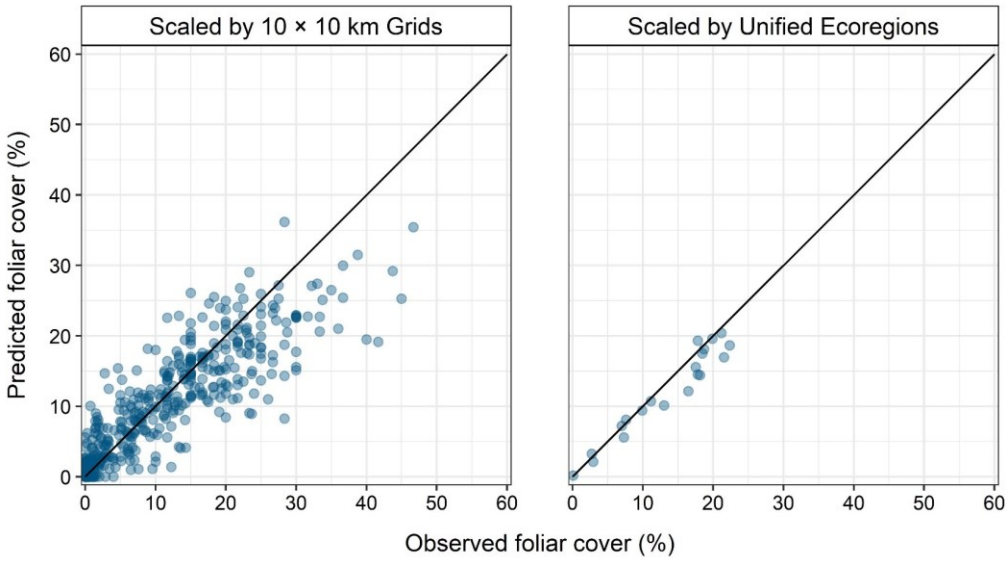

Figure 28. Mean observed foliar cover compared to mean predicted foliar cover for *Betula* Shrubs summarized by 10 × 10 km grids (right) and by ecoregions (left) from the merged test partitions of 10-fold cross-validation.

Table 14. Accuracy of *Betula* Shrubs by region and subregion at the site scale.

Subregion	Continuous Foliar Cover Performance					Cover	
	R^2	MAE	RMSE	AUC	% ACC	Mean	Median
All	0.50	5.3	9.3	0.95	88	17.3	15.0
Northern	0.44	4.6	9.6	0.93	85	15.0	10.0
Western	0.56	4.6	7.7	0.96	89	16.7	15.0
Interior	0.38	7.2	11.0	0.96	91	19.9	15.0

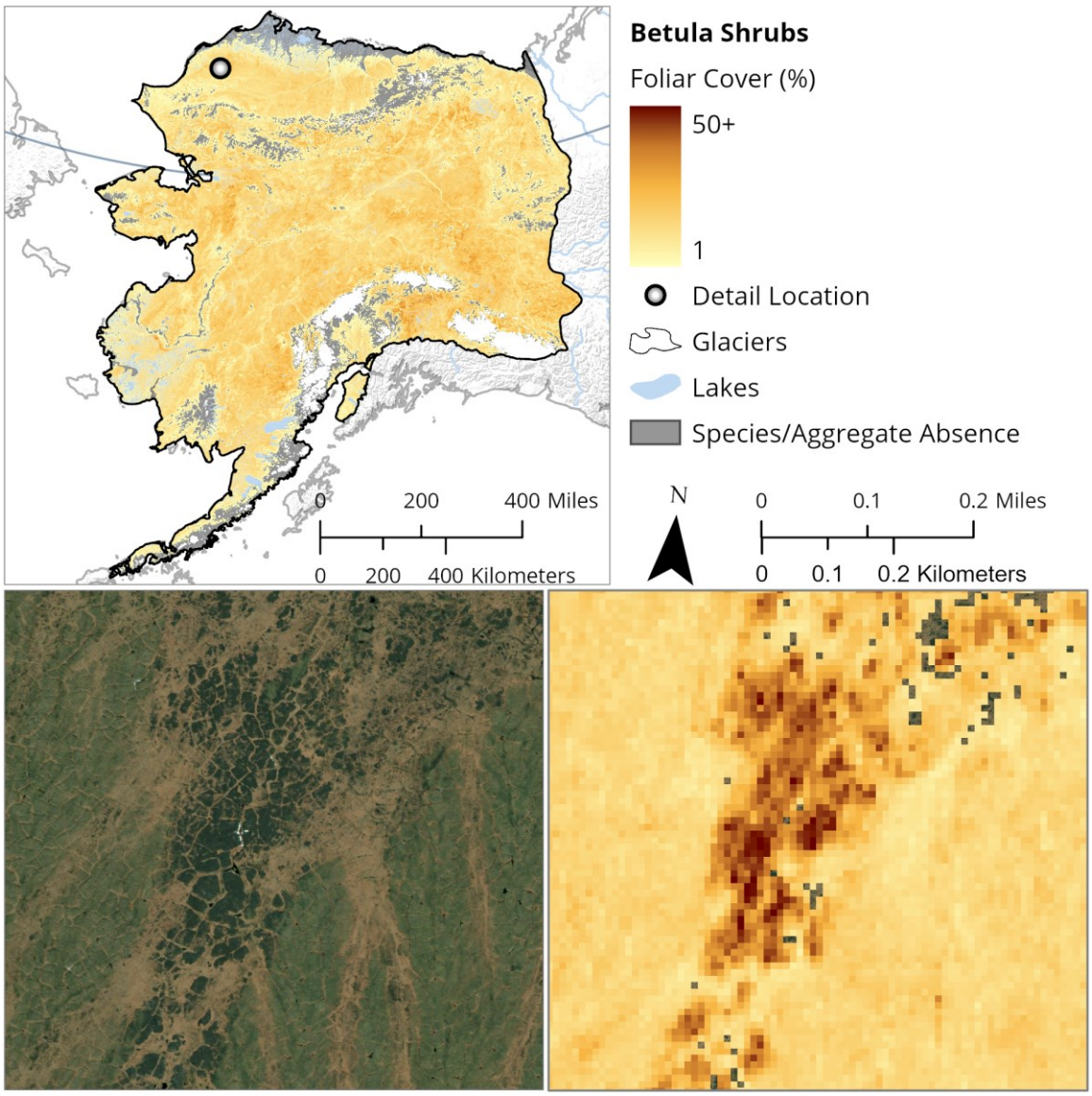

Figure 29. Map of *Betula* Shrubs in North American Beringia (top) and comparison between high resolution Maxar satellite imagery (bottom left) and predicted map (bottom right) at 1:10,000 scale.

Components

The *Betula* Shrubs map group consists of *Betula nana* ssp. *exilis* (Sukaczev) Hultén and *Betula glandulosa* Michx. These species frequently hybridize with each other and often cannot be clearly separated (Furlow 1997). *Betula glandulosa* also frequently hybridizes with *Betula neoalaskana* Sarg. to form a tall shrub birch hybrid: *Betula neoalaskana* × *glandulosa*, which has been described as *Betula* ×*dugleana* Lepage. We excluded *Betula neoalaskana* × *glandulosa* from the *Betula* Shrubs map group because it tends to grow in sporadic clusters, rather than the continuous cover often formed by *Betula nana* ssp. *exilis* and *Betula glandulosa*, and it often is intermediate between a tree and a shrub in form.

Figure 30. *Betula glandulosa* growing with *Salix* spp. in uplands along the South Fork Kuskokwim River in the Alaska Range (left). *Betula nana* ssp. *exilis* forms the dominant low shrub layer in a tundra community on a hill slope near the Nushagak River in Bristol Bay (right).

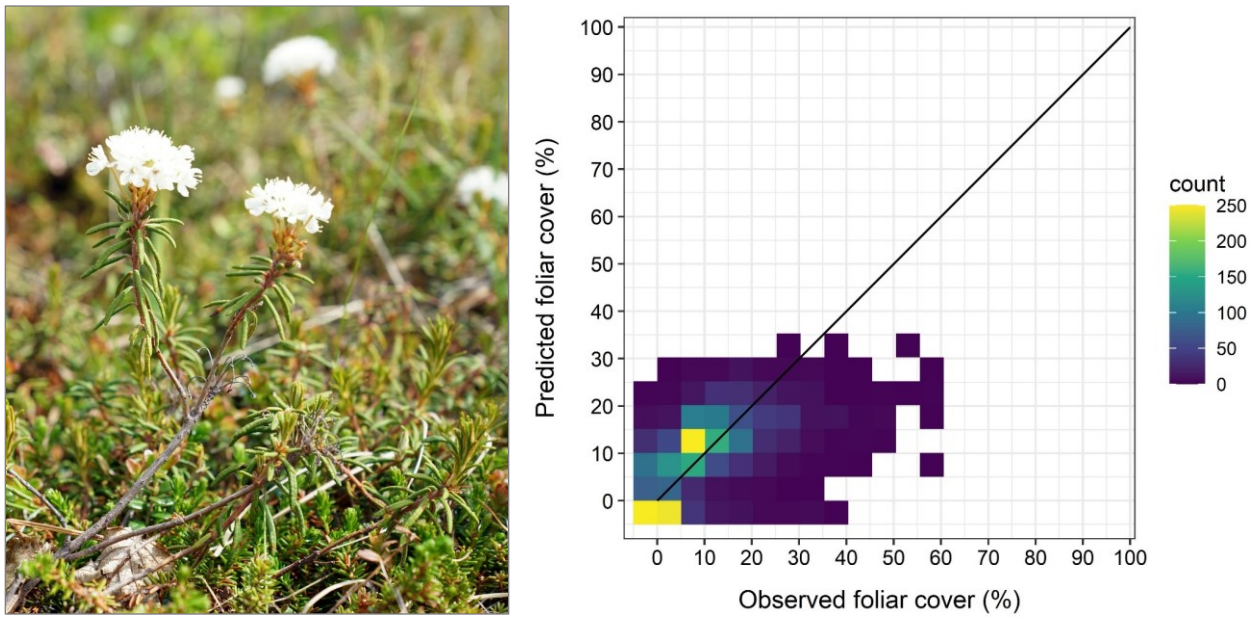

Figure 31. Observed foliar cover compared to predicted foliar cover for *Rhododendron* Shrubs from the merged test partitions of 10-fold cross-validation, wherein each observation was predicted exactly once. R^2 values were calculated relative to the theoretical 1:1 ratio between observed and predicted foliar cover (solid black line). *Rhododendron tomentosum* ssp. *decumbens* shown at left.

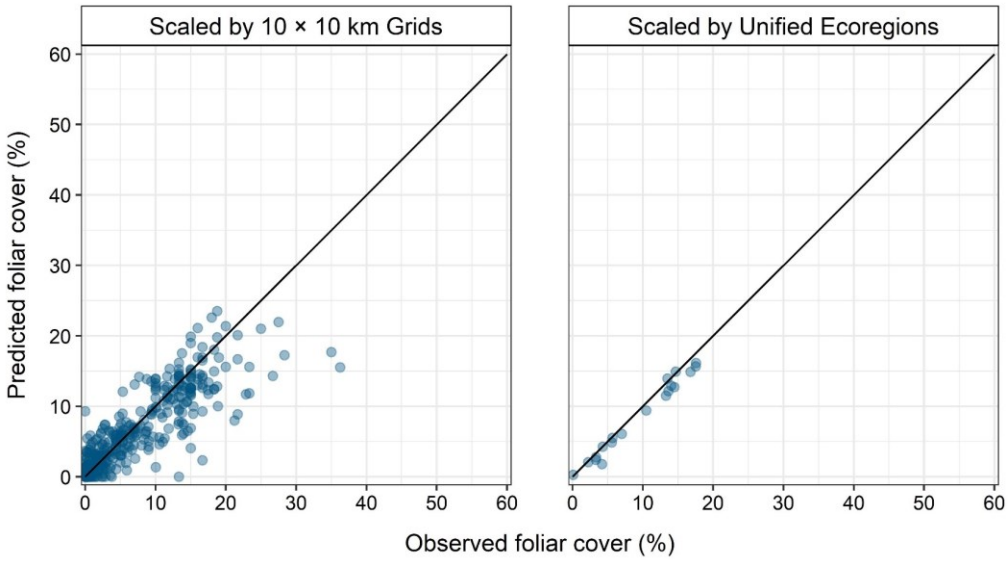

Figure 32. Mean observed foliar cover compared to mean predicted foliar cover for *Rhododendron* Shrubs summarized by 10 × 10 km grids (right) and by ecoregions (left) from the merged test partitions of 10-fold cross-validation.

Table 15. Accuracy of *Rhododendron* Shrubs by region and subregion at the site scale.

Subregion	Continuous Foliar Cover Performance					Cover	
	R^2	MAE	RMSE	AUC	% ACC	Mean	Median
All	0.55	3.4	6.3	0.95	88	13.5	10.0
Northern	0.44	3.0	6.1	0.90	82	10.5	8.0
Western	0.57	3.2	6.4	0.97	91	14.5	10.0
Interior	0.52	4.3	6.6	0.97	92	15.3	15.0

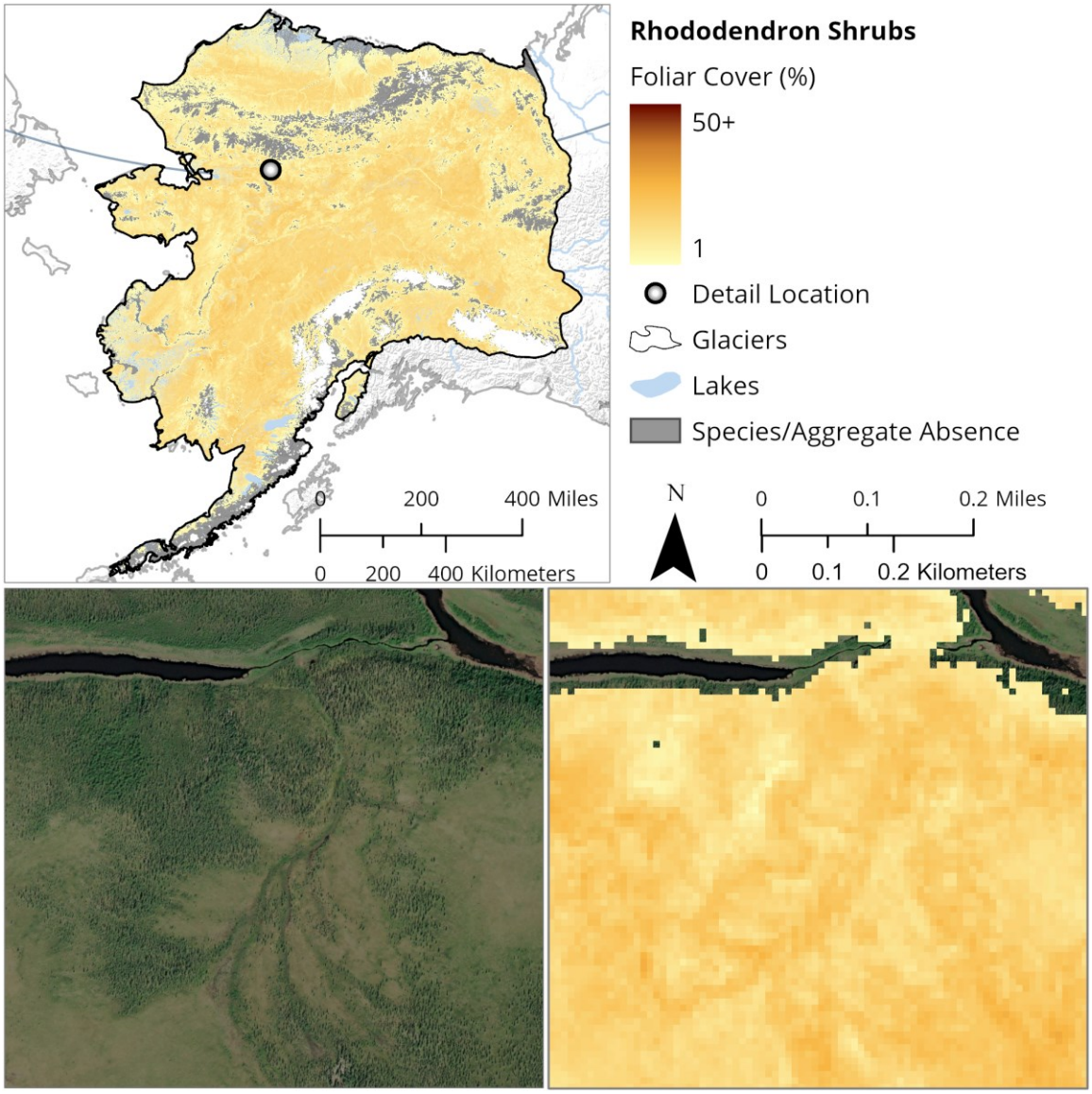

Figure 33. Map of *Rhododendron* Shrubs in North American Beringia (top) and comparison between high resolution Maxar satellite imagery (bottom left) and predicted map (bottom right) at 1:10,000 scale.

Components

The *Rhododendron* Shrubs map group consists of *Rhododendron tomentosum* ssp. *decumbens* (Aiton) Elven & D.F. Murray, *Rhododendron groenlandicum* (Oeder) K.A. Kron & W.S. Judd, and *Rhododendron lapponicum* ssp. *alpinum* (Glehn) A.P. Khokhr. In the past, *Rhododendron tomentosum* ssp. *decumbens* and *Rhododendron groenlandicum* have commonly been known within a *Ledum* genus as *Ledum palustre* ssp. *decumbens* (Aiton) Hultén and *Ledum groenlandicum* Oeder, respectively. A fourth *Rhododendron* shrub, *Rhododendron menziesii* Craven (synonym = *Menziesia ferruginea* Sm.), occurs in the southern portion of the study area in Southwest Alaska, the Cook Inlet Lowlands, and the western Kenai Peninsula. We excluded *Rhododendron menziesii* from the *Rhododendron* Shrubs map group because it is uncommon the study area.

Figure 34. *Rhododendron tomentosum* ssp. *decumbens* growing with *Cladonia* and *Stereocaulon* lichens in a *Picea mariana* dominated community in the southern Brooks Range (left). *Rhododendron lapponicum* ssp. *alpinum* growing with *Dryas integrifolia* ssp. *integrifolia* on a well-drained slope in the vicinity of the Ribdon River (right).

Vaccinium uliginosum

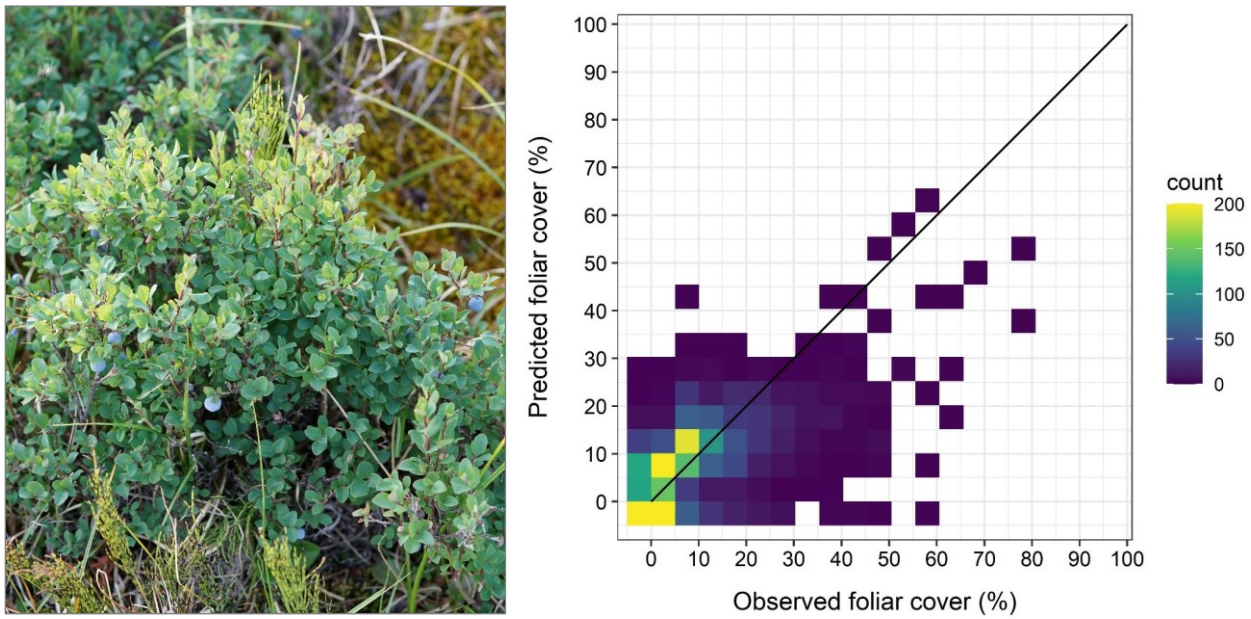

Figure 35. Observed foliar cover compared to predicted foliar cover for *Vaccinium uliginosum* from the merged test partitions of 10-fold cross-validation, wherein each observation was predicted exactly once. R^2 values were calculated relative to the theoretical 1:1 ratio between observed and predicted foliar cover (solid black line). *Vaccinium uliginosum* shown at left.

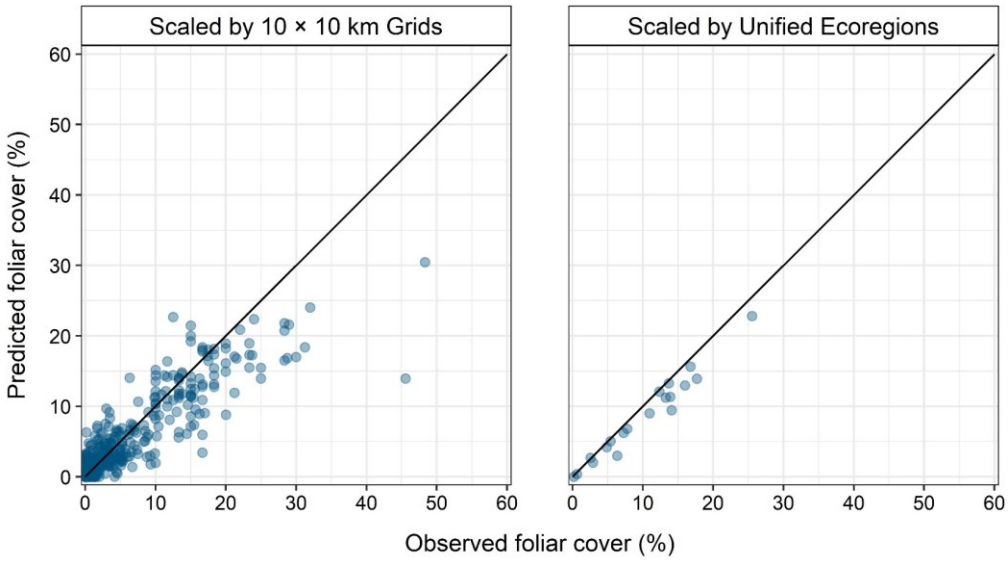

Figure 36. Mean observed foliar cover compared to mean predicted foliar cover for *Vaccinium uliginosum* summarized by 10 × 10 km grids (right) and by ecoregions (left) from the merged test partitions of 10-fold cross-validation.

Table 16. Accuracy of *Vaccinium uliginosum* by region and subregion at the site scale.

Subregion	Continuous Foliar Cover Performance					Cover	
	R^2	MAE	RMSE	AUC	% ACC	Mean	Median
All	0.49	3.8	7.1	0.91	83	12.8	10.0
Northern	0.29	2.8	5.9	0.87	80	8.7	5.0
Western	0.42	4.1	7.5	0.91	83	13.6	10.0
Interior	0.53	5.3	8.5	0.95	89	15.9	10.0

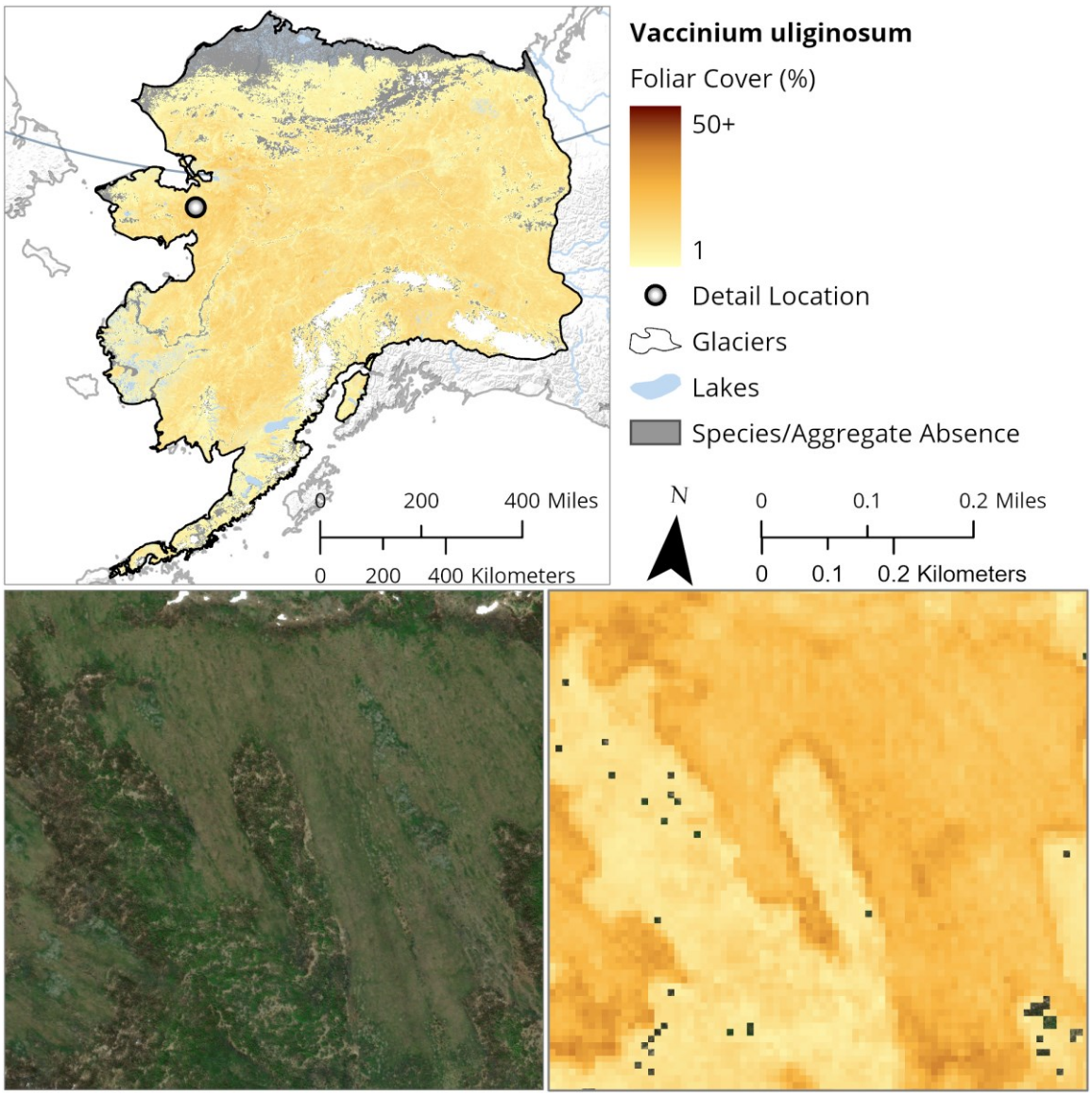

Figure 37. Map of *Vaccinium uliginosum* in North American Beringia (top) and comparison between high resolution Maxar satellite imagery (bottom left) and predicted map (bottom right) at 1:10,000 scale.

Components

The *Vaccinium uliginosum* map group includes only *Vaccinium uliginosum* L.

Figure 38. *Vaccinium uliginosum* commonly grows under *Picea mariana* canopies in the Copper River Basin (left). A *Vaccinium uliginosum*-dominated community on a mesic hill slope near Tikchik Lake in Bristol Bay (right).

Vaccinium vitis-idaea

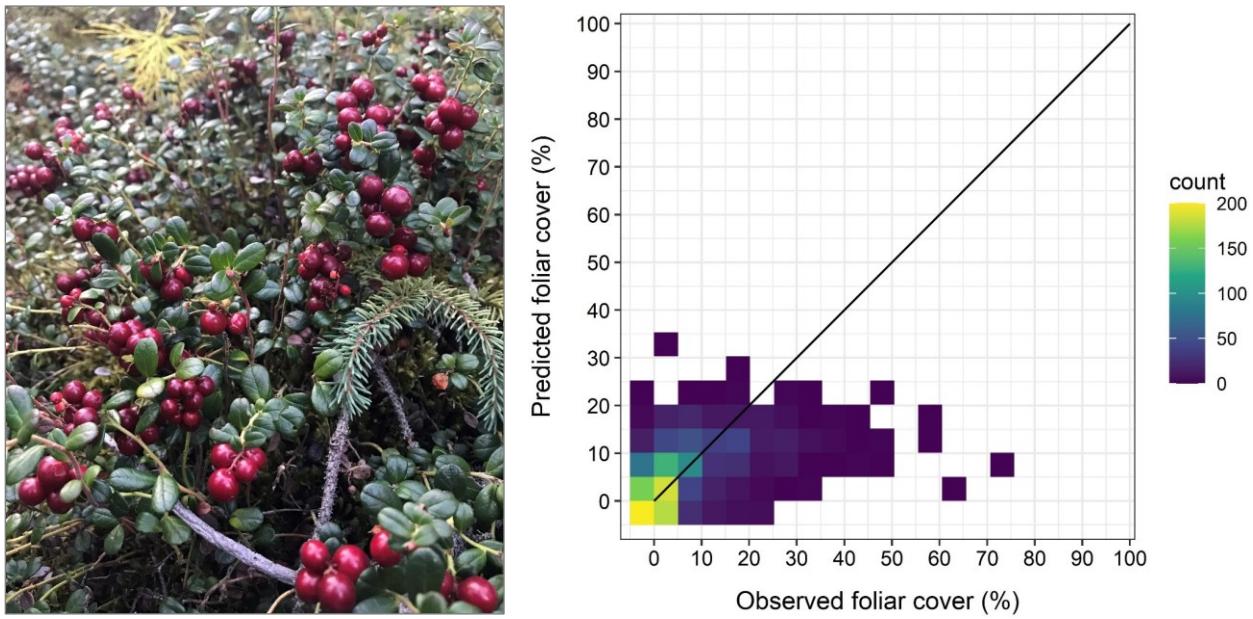

Figure 39. Observed foliar cover compared to predicted foliar cover for *Vaccinium vitis-idaea* from the merged test partitions of 10-fold cross-validation, wherein each observation was predicted exactly once. R^2 values were calculated relative to the theoretical 1:1 ratio between observed and predicted foliar cover (solid black line). *Vaccinium vitis-idaea* shown at left.

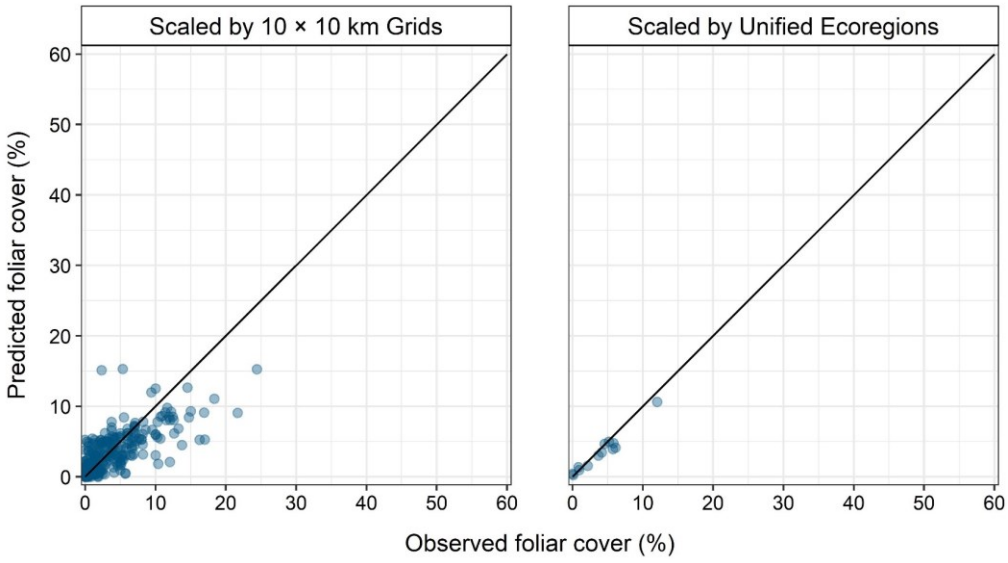

Figure 40. Mean observed foliar cover compared to mean predicted foliar cover for *Vaccinium vitis-idaea* ssp. *minus* summarized by 10 × 10 km grids (right) and by ecoregions (left) from the merged test partitions of 10-fold cross-validation.

Table 17. Accuracy of *Vaccinium vitis-idaea* by region and subregion at the site scale.

Subregion	Continuous Foliar Cover Performance					Cover	
	R^2	MAE	RMSE	AUC	% ACC	Mean	Median
All	0.40	2.5	5.7	0.93	85	10.1	7.0
Northern	0.43	2.8	5.8	0.92	84	10.3	7.0
Western	0.27	1.9	5.4	0.92	87	8.8	5.0
Interior	0.44	2.9	5.8	0.94	85	11.1	10.0

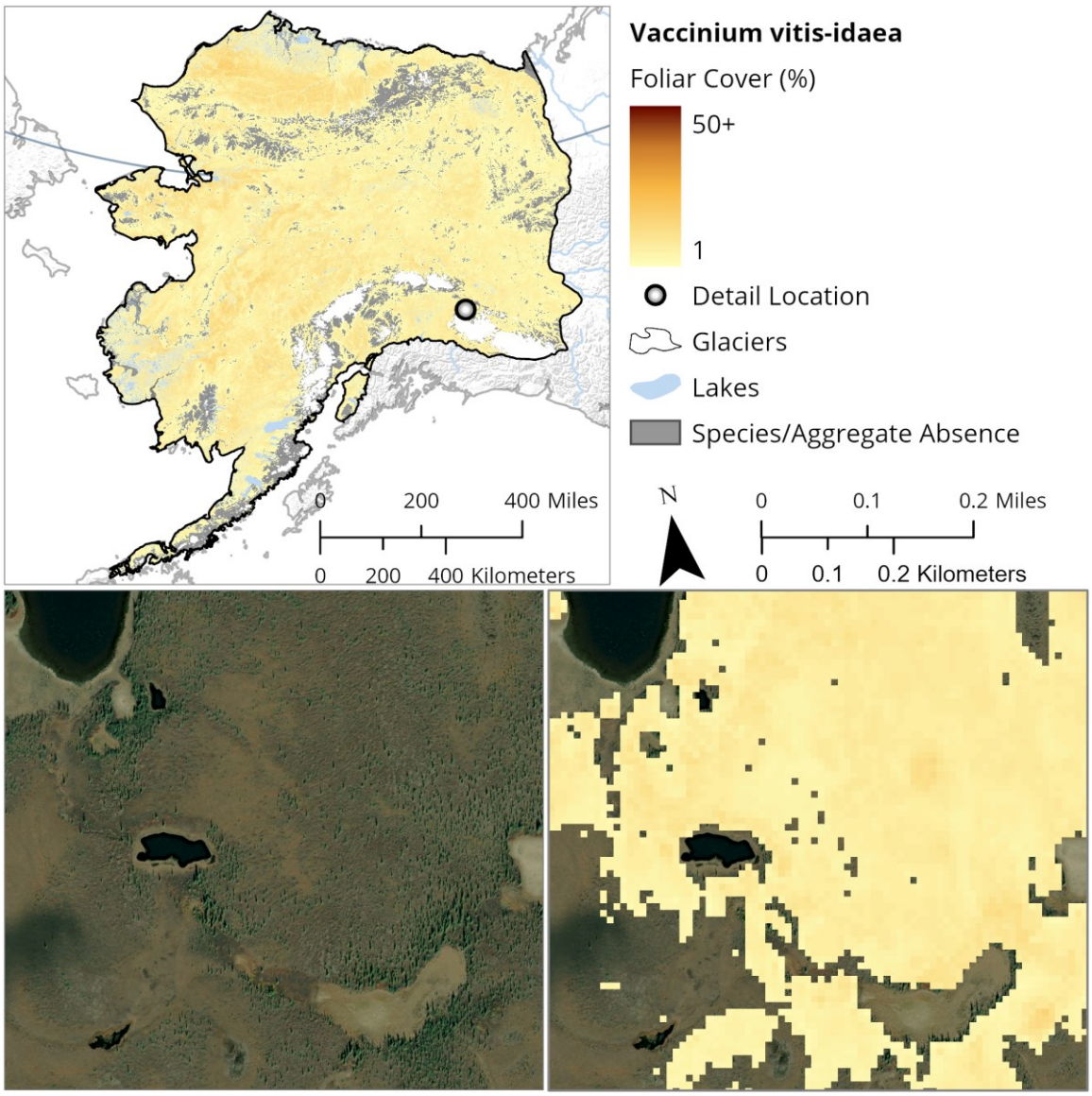

Figure 41. Map of *Vaccinium vitis-idaea* in North American Beringia (top) and comparison between high resolution Maxar satellite imagery (bottom left) and predicted map (bottom right) at 1:10,000 scale.

Components

The V*accinium vitis-idaea* map group includes only V*accinium vitis-idaea* L.

Figure 42. V*accinium vitis-idaea* is common under *Picea* and/or *Betula* canopies in mesic sites, such as shown from the vicinity of the Nuyakuk River in Bristol Bay.

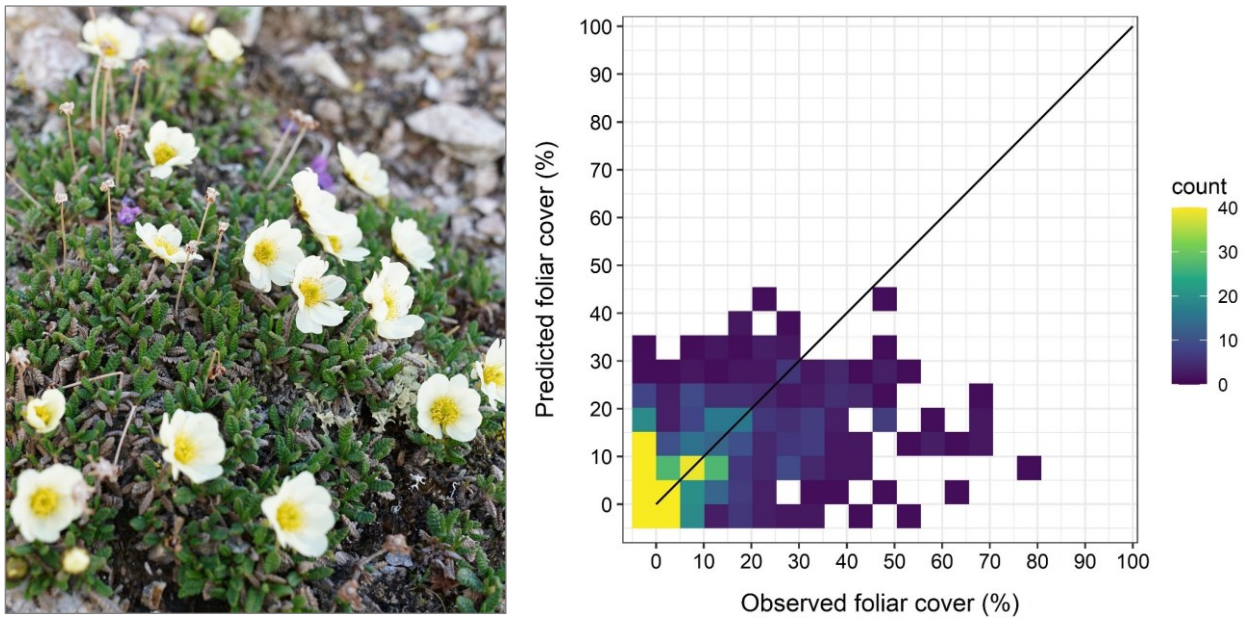

Figure 43. Observed foliar cover compared to predicted foliar cover for *Dryas* Dwarf Shrubs from the merged test partitions of 10-fold cross-validation, wherein each observation was predicted exactly once. R^2 values were calculated relative to the theoretical 1:1 ratio between observed and predicted foliar cover (solid black line). *Dryas ajanensis* ssp. *beringensis* shown at left.

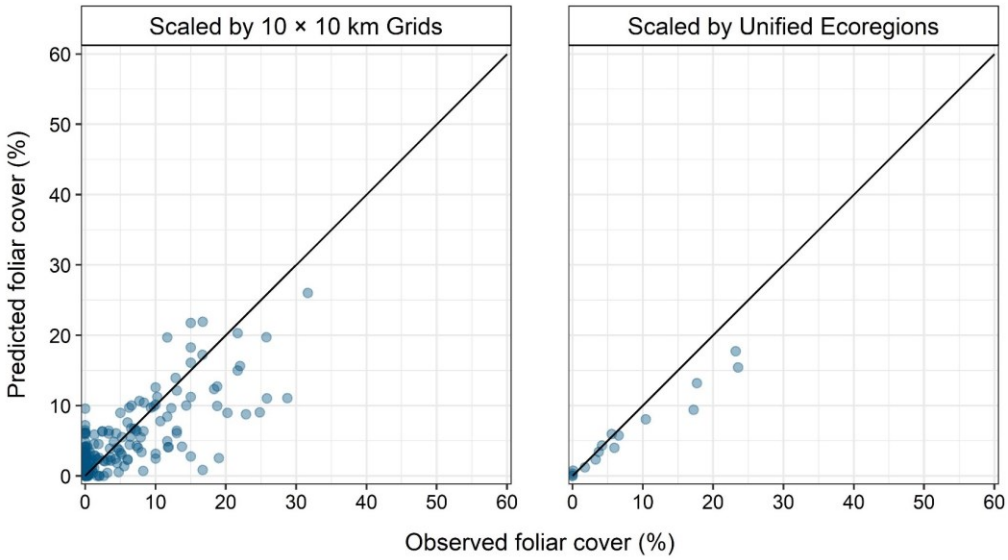

Figure 44. Mean observed foliar cover compared to mean predicted foliar cover for *Dryas* Dwarf Shrubs summarized by 10 × 10 km grids (right) and by ecoregions (left) from the merged test partitions of 10-fold cross-validation.

Table 18. Accuracy of *Dryas* Dwarf Shrubs by region and subregion at the site scale.

Subregion	Continuous Foliar Cover Performance					Cover	
	R^2	MAE	RMSE	AUC	% ACC	Mean	Median
All	0.41	2.6	6.9	0.90	83	16.5	12.0
Northern	0.40	3.0	7.3	0.87	77	15.2	10.0
Western	0.54	1.4	4.2	0.93	89	16.9	15.0
Interior	0.34	3.8	9.4	0.92	86	19.4	15.0

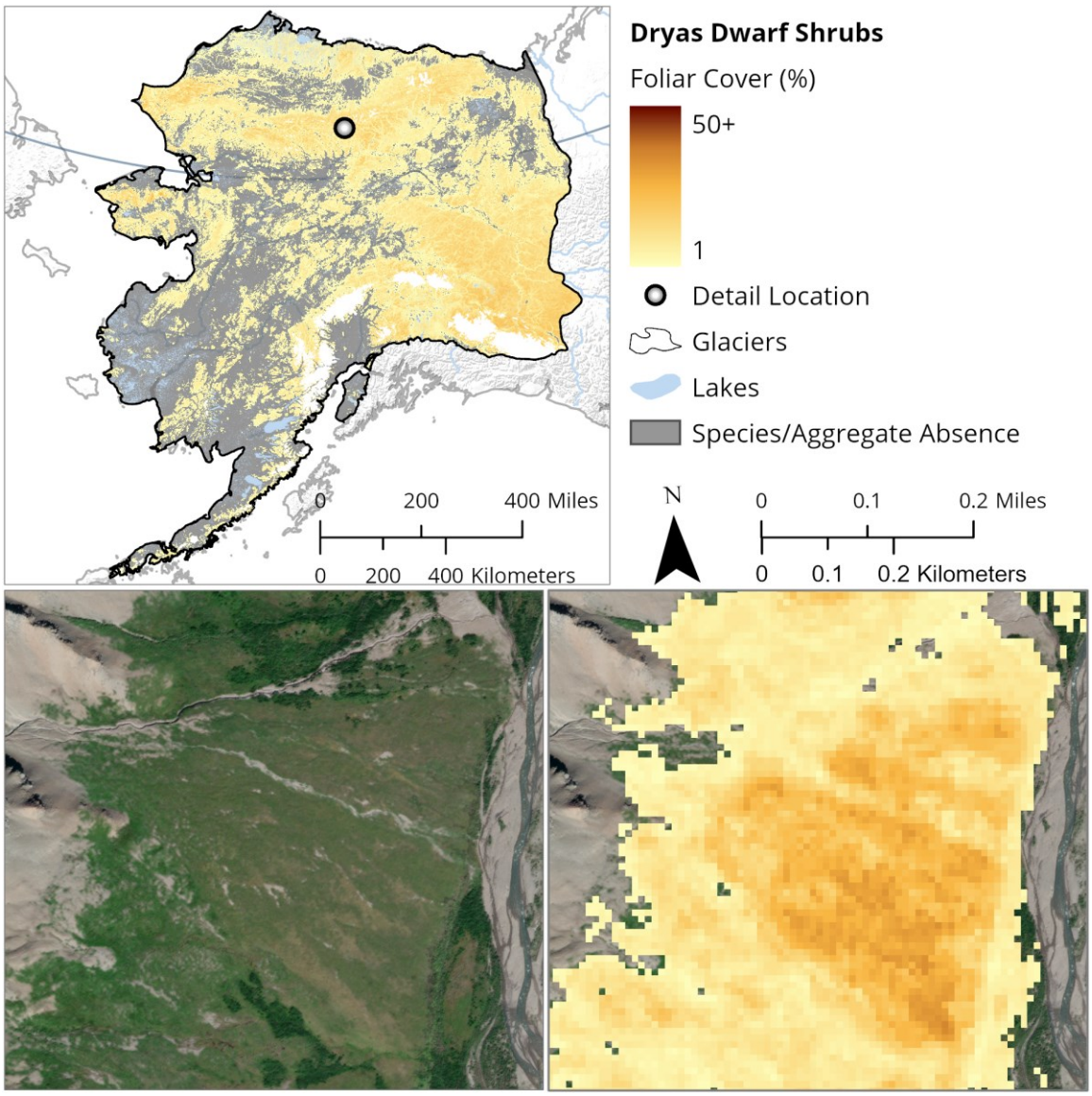

Figure 45. Map of *Dryas* Dwarf Shrubs in North American Beringia (top) and comparison between high resolution Maxar satellite imagery (bottom left) and predicted map (bottom right) at 1:10,000 scale.

Components

The *Dryas* Dwarf Shrubs map group consists of *Dryas ajanensis* ssp. *beringensis* Jurtz., *Dryas alaskensis* A.E. Porsild, *Dryas hookeriana* Juz., *Dryas integrifolia* ssp. *integrifolia* Vahl, and *Dryas integrifolia* ssp. *sylvatica* (Hultén) Hultén. In the past, *Dryas ajanensis* ssp. *beringensis*, *Dryas alaskensis*, and *Dryas hookeriana* have commonly been considered as belonging within a broad *Dryas octopetala* L. However, *Dryas octopetala* is better supported in a narrower taxon concept that is restricted to Greenland and Eurasia (Elven et al. 2011). Thus, all material identified in the study area as *Dryas octopetala* should belong to *Dryas ajanensis* ssp. *beringensis*, *Dryas alaskensis*, or *Dryas hookeriana*. In many cases, it is not possible to determine from past data which *Dryas* species occurred at particular sites. *Dryas hookeriana* has been overlooked in the study area and is likely more common than the several voucher specimens for Alaska indicate.

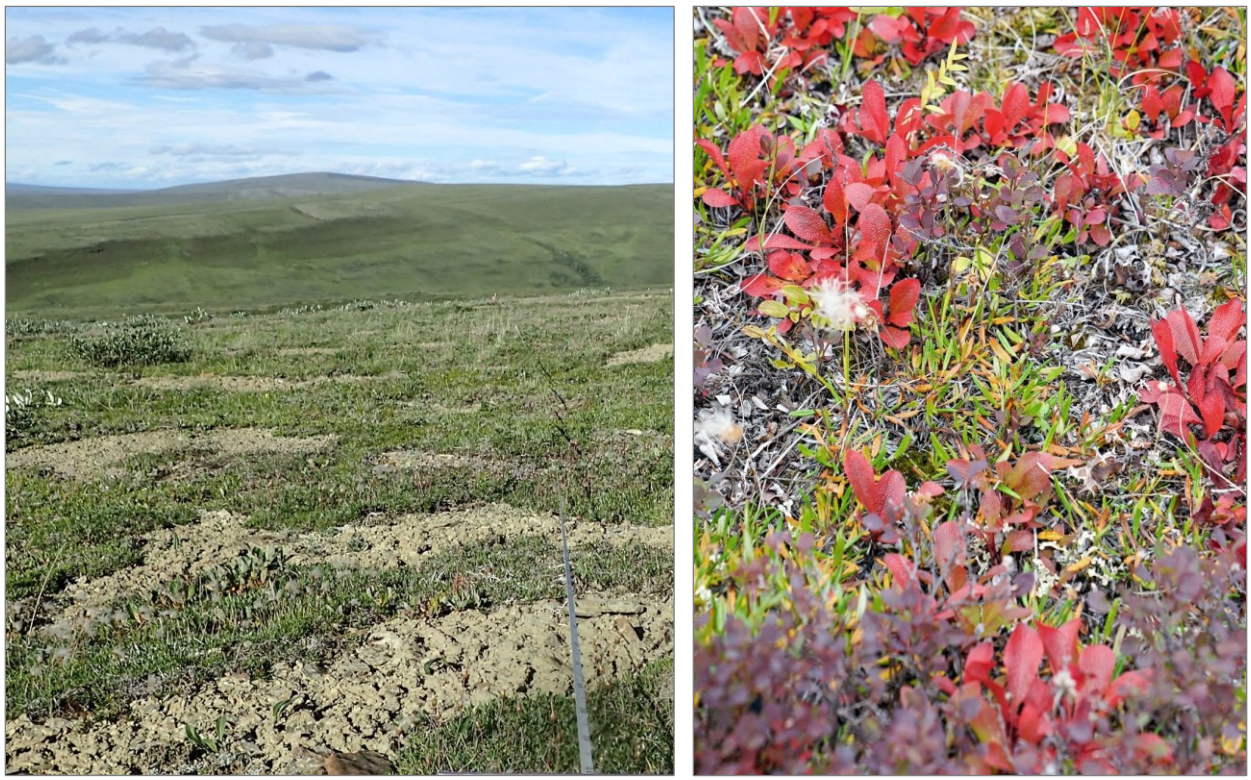

Figure 46. *Dryas ajanensis* ssp. *beringensis*-dominated community on a rocky mesic ridge in the Brooks Foothills (left). Low abundance of *Dryas integrifolia* ssp. *integrifolia* growing on a well-drained floodplain in the eastern Brooks Range (right).

Empetrum nigrum

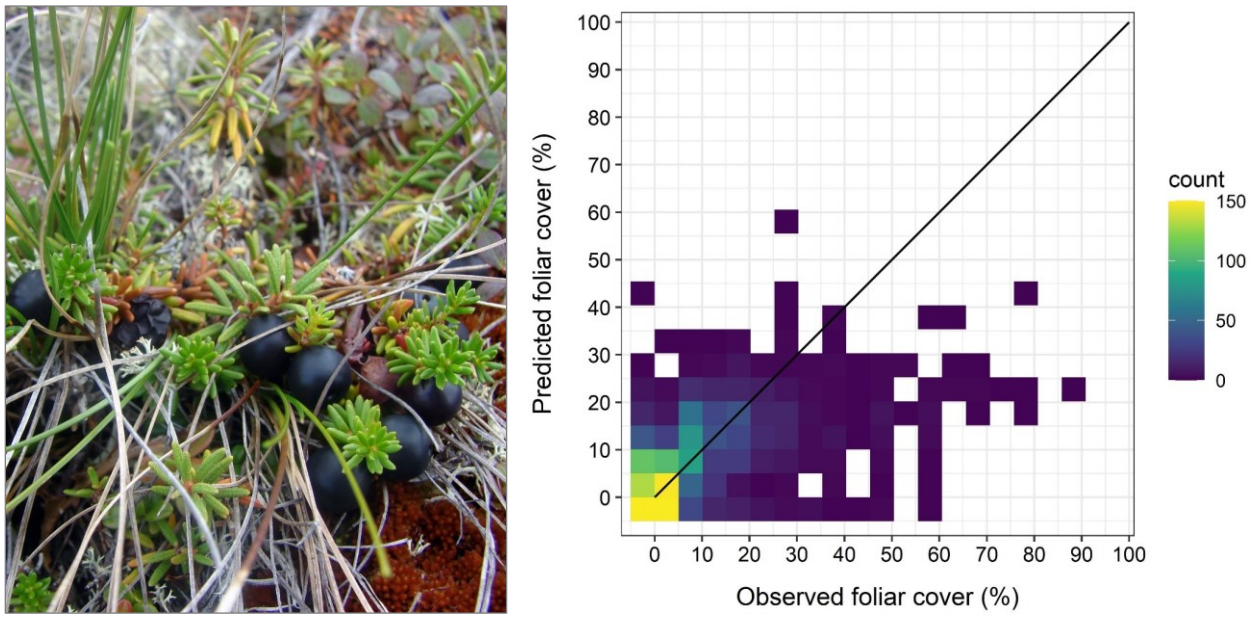

Figure 47. Observed foliar cover compared to predicted foliar cover for *Empetrum nigrum* from the merged test partitions of 10-fold cross-validation, wherein each observation was predicted exactly once. R^2 values were calculated relative to the theoretical 1:1 ratio between observed and predicted foliar cover (solid black line). *Empetrum nigrum* shown at left.

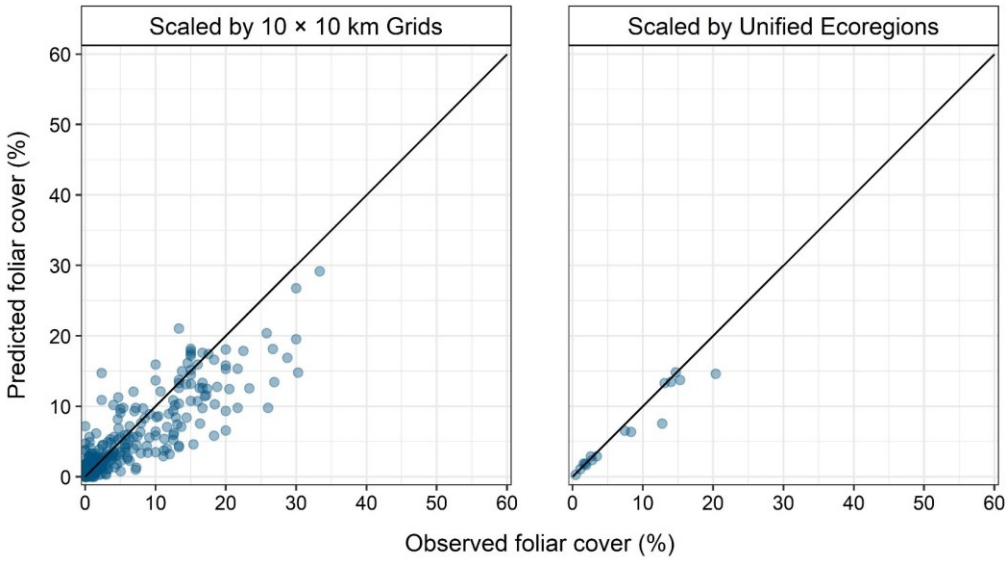

Figure 48. Mean observed foliar cover compared to mean predicted foliar cover for *Empetrum nigrum* summarized by 10 × 10 km grids (right) and by ecoregions (left) from the merged test partitions of 10-fold cross-validation.

Table 19. Accuracy of *Empetrum nigrum* by region and subregion at the site scale.

Subregion	Continuous Foliar Cover Performance					Cover	
	R^2	MAE	RMSE	AUC	% ACC	Mean	Median
All	0.43	3.6	7.9	0.91	83	13.7	10.0
Northern	0.22	1.5	3.8	0.89	83	6.0	3.0
Western	0.36	6.2	11.5	0.90	81	18.8	15.0
Interior	0.41	3.5	6.3	0.93	85	12.5	10.0

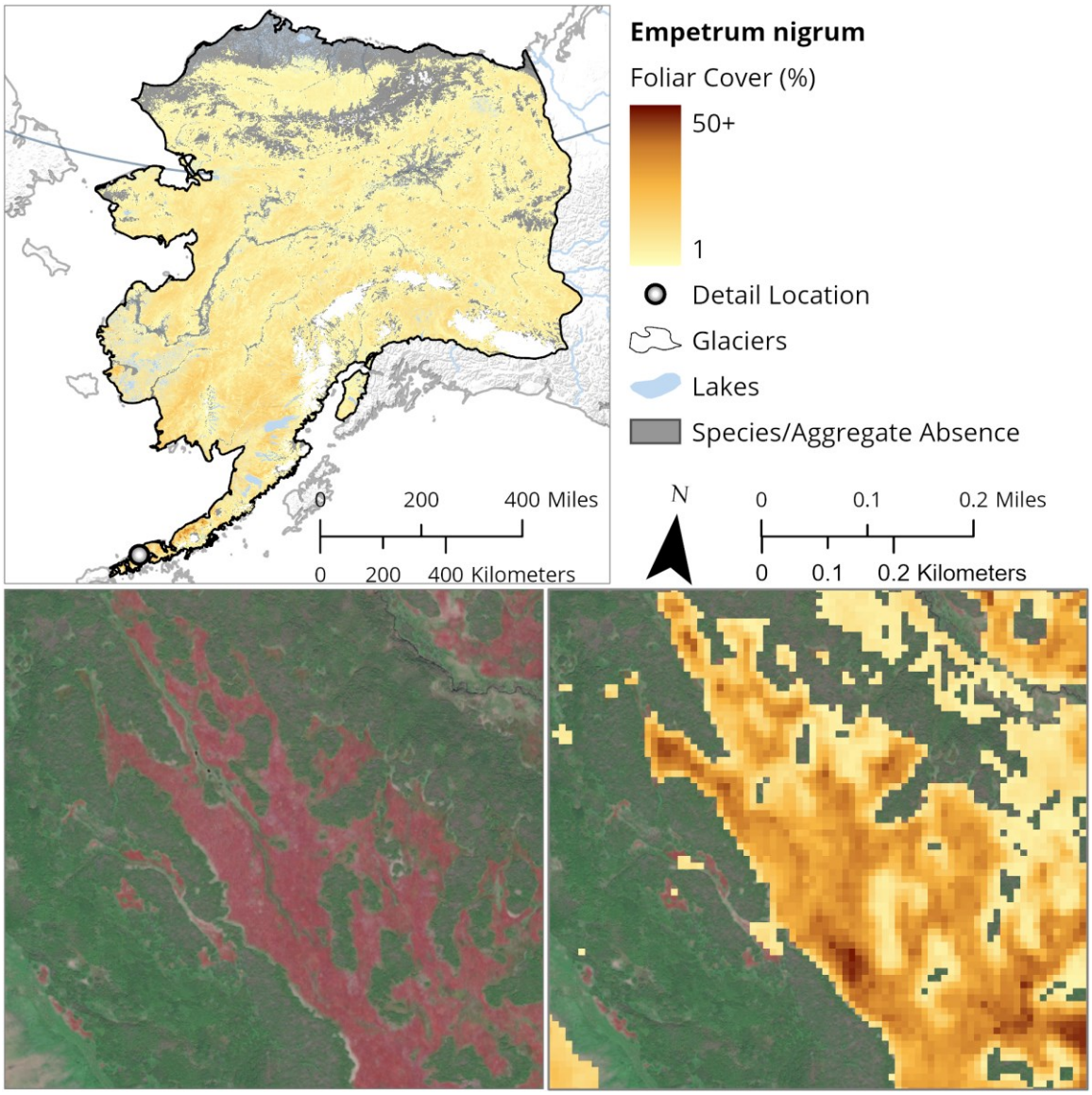

Figure 49. Map of *Empetrum nigrum* in North American Beringia (top) and comparison between high resolution Maxar satellite imagery (bottom left) and predicted map (bottom right) at 1:10,000 scale. The imagery shows winter-killed *Empetrum nigrum* as brown-red patches.

Components

The *Empetrum nigrum* map group includes only *Empetrum nigrum* L.

Figure 50. *Empetrum nigrum* grows in low to moderate abundances in a variety of mesic communities, such as shown on the hill top in the vicinity of the Nushagak River in Bristol Bay.

Eriophorum vaginatum

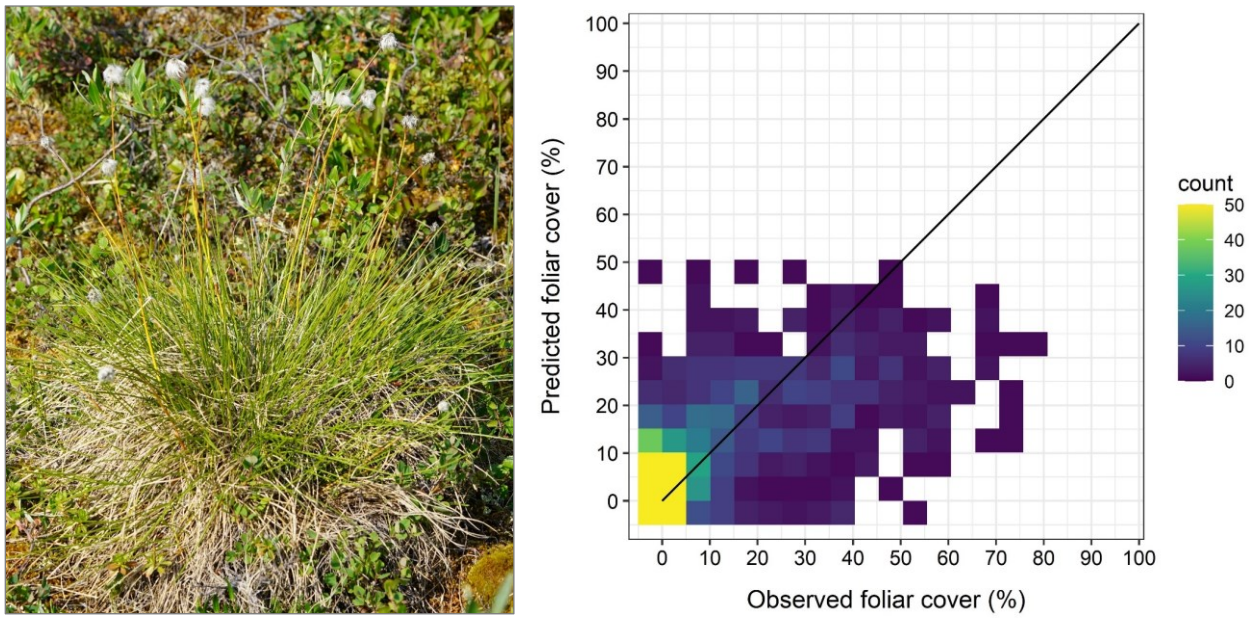

Figure 51. Observed foliar cover compared to predicted foliar cover for *Eriophorum vaginatum* from the merged test partitions of 10-fold cross-validation, wherein each observation was predicted exactly once. R^2 values were calculated relative to the theoretical 1:1 ratio between observed and predicted foliar cover (solid black line). *Eriophorum vaginatum* shown at left.

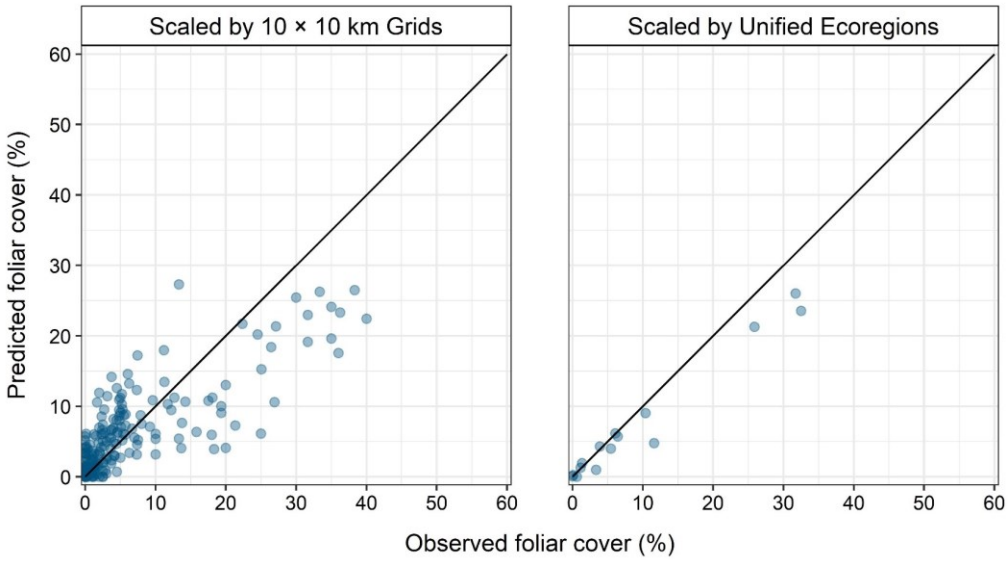

Figure 52. Mean observed foliar cover compared to mean predicted foliar cover for *Eriophorum vagiantum* summarized by 10 × 10 km grids (right) and by ecoregions (left) from the merged test partitions of 10-fold cross-validation.

Table 20. Accuracy of *Eriophorum vaginatum* by region and subregion at the site scale.

Subregion	Continuous Foliar Cover Performance					Cover	
	R^2	MAE	RMSE	AUC	% ACC	Mean	Median
All	0.53	3.3	8.2	0.95	88	19.5	15.0
Northern	0.45	3.6	8.3	0.93	84	14.9	8.0
Western	0.57	2.0	6.4	0.97	95	26.9	25.0
Interior	0.58	4.9	10.5	0.97	89	26.3	25.0

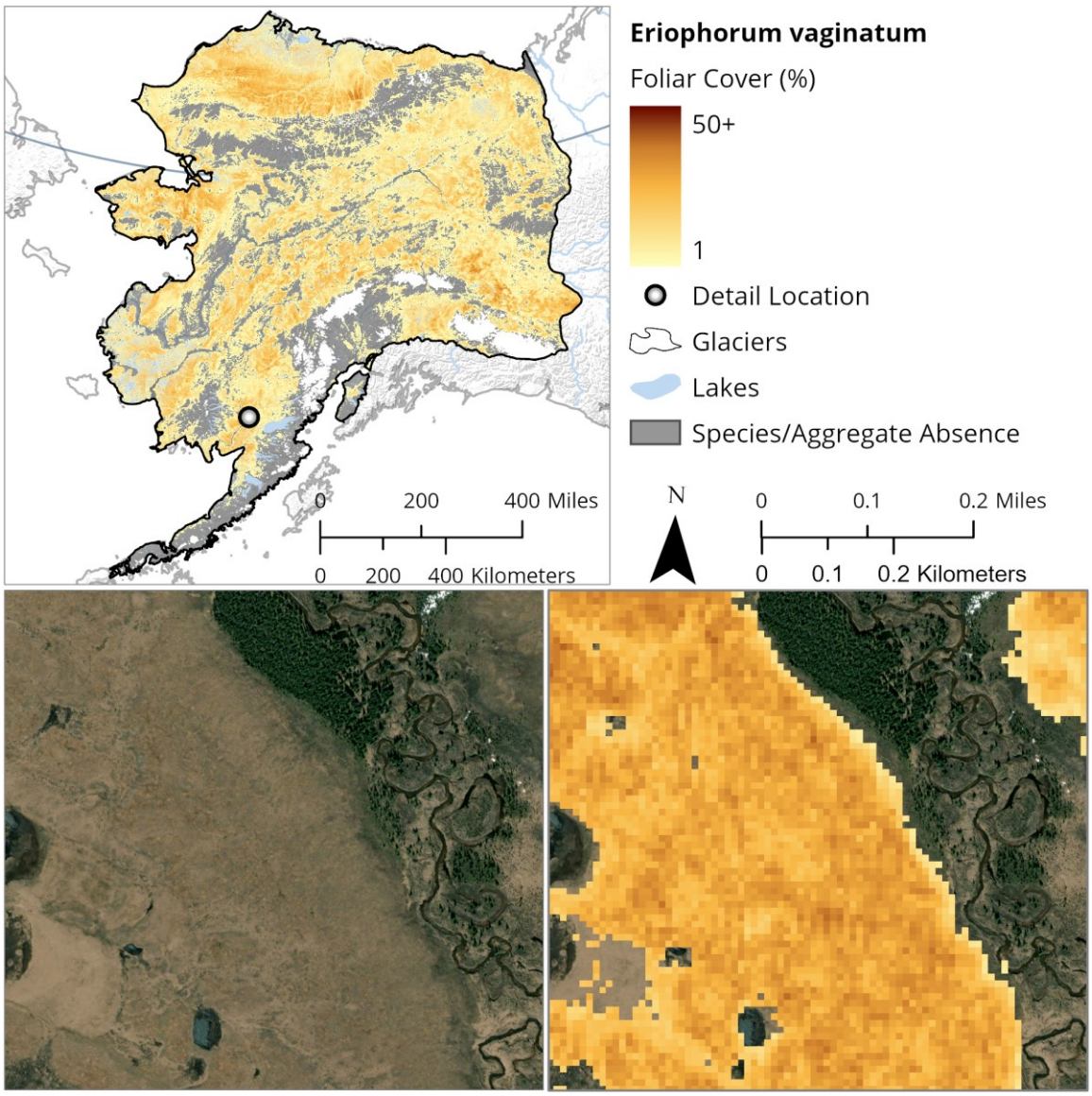

Figure 53. Map of *Eriophorum vaginatum* in North American Beringia (top) and comparison between high resolution Maxar satellite imagery (bottom left) and predicted map (bottom right) at 1:10,000 scale.

Components

The *Eriophorum vaginatum* map group includes only *Eriophorum vaginatum* L. In the study area, only *Eriophorum vaginatum* ssp. *vaginatum* is known.

Figure 54. High abundance of *Eriophorum vaginatum* and correspondingly high tussock coverage in the vicinity of the Colville River in the Brooks Foothills (left) and the vicinity of the Nushagak River in Bristol Bay (right).

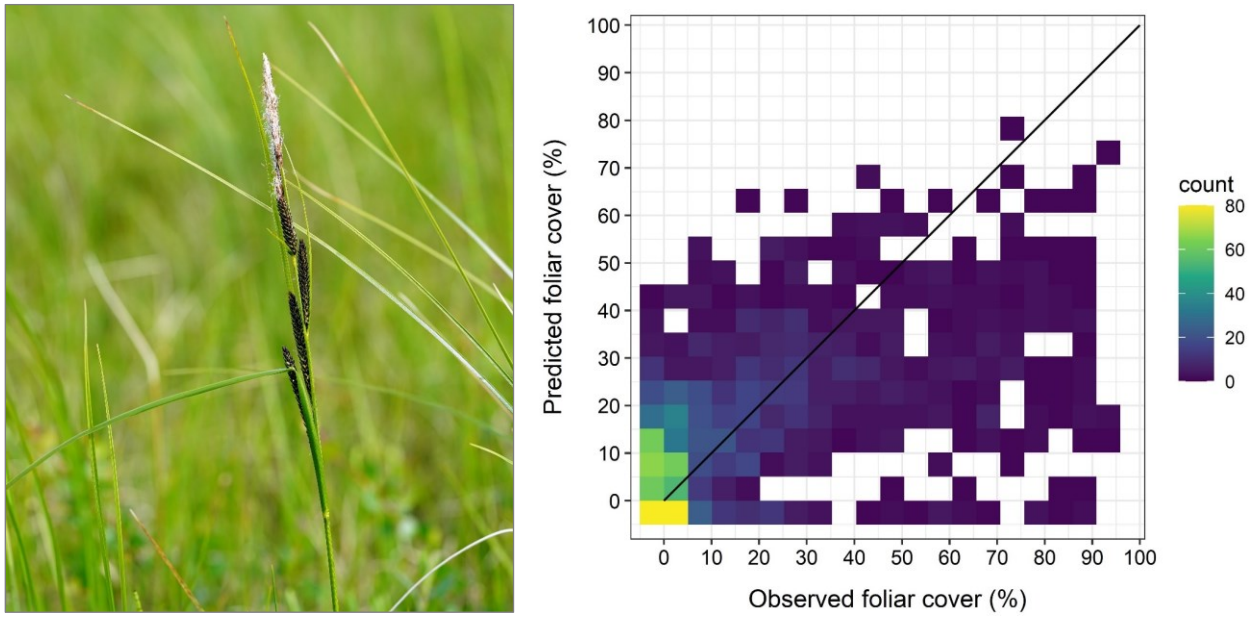

Figure 55. Observed foliar cover compared to predicted foliar cover for Wetland Sedges from the merged test partitions of 10-fold cross-validation, wherein each observation was predicted exactly once. R^2 values were calculated relative to the theoretical 1:1 ratio between observed and predicted foliar cover (solid black line). *Carex aquatilis* shown at left.

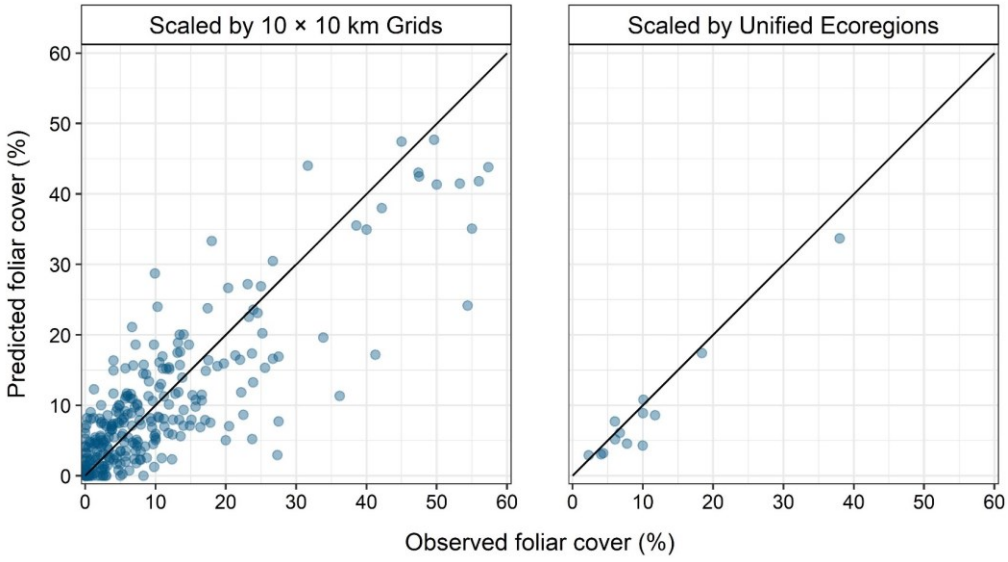

Figure 56. Mean observed foliar cover compared to mean predicted foliar cover for Wetland Sedges summarized by 10 × 10 km grids (right) and by ecoregions (left) from the merged test partitions of 10-fold cross-validation.

Table 21. Accuracy of Wetland Sedges by region and subregion at the site scale.

Subregion	Continuous Foliar Cover Performance					Cover	
	R^2	MAE	RMSE	AUC	% ACC	Mean	Median
All	0.45	7.1	14.9	0.91	83	25.6	17.7
Northern	0.49	7.6	14.9	0.89	81	24.5	17.0
Western	0.39	6.7	15.3	0.92	86	29.1	20.0
Interior	0.40	6.3	14.0	0.89	83	22.6	14.7

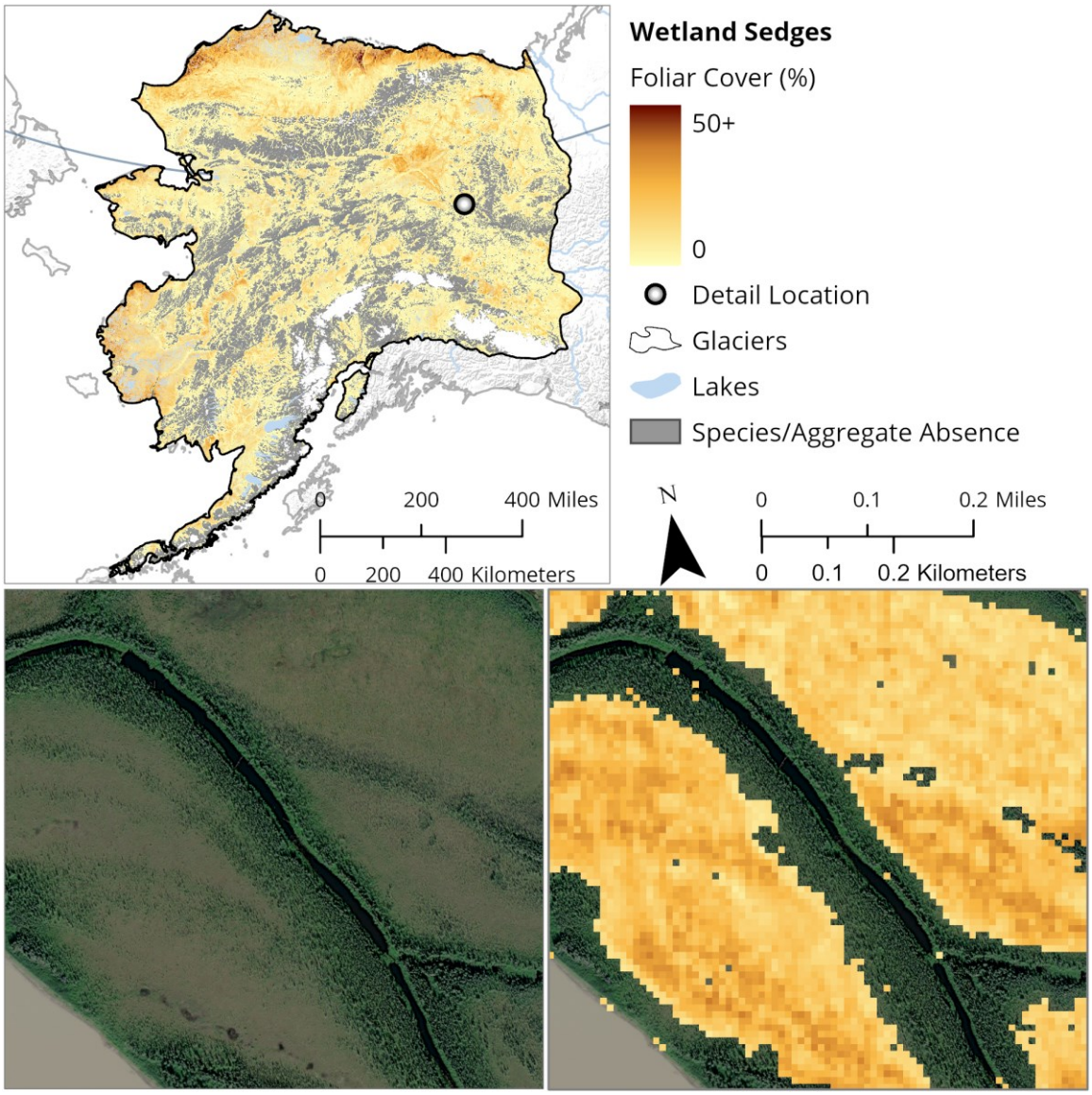

Figure 57. Map of Wetland Sedges in North American Beringia (top) and comparison between high resolution Maxar satellite imagery (bottom left) and predicted map (bottom right) at 1:10,000 scale.

Components

The Wetland Sedges map group includes the *Eriophorum* and *Carex* species listed in Table 22, which are typically restricted to hygric, hydric, seasonally inundated, or shallow aquatic moisture regimes. Most of the species are considered as obligate wetland species by the U.S. Army Corps of Engineers; however, they can also occasionally grow in mesic sites at low abundances, especially where moisture regime is variable or drying.

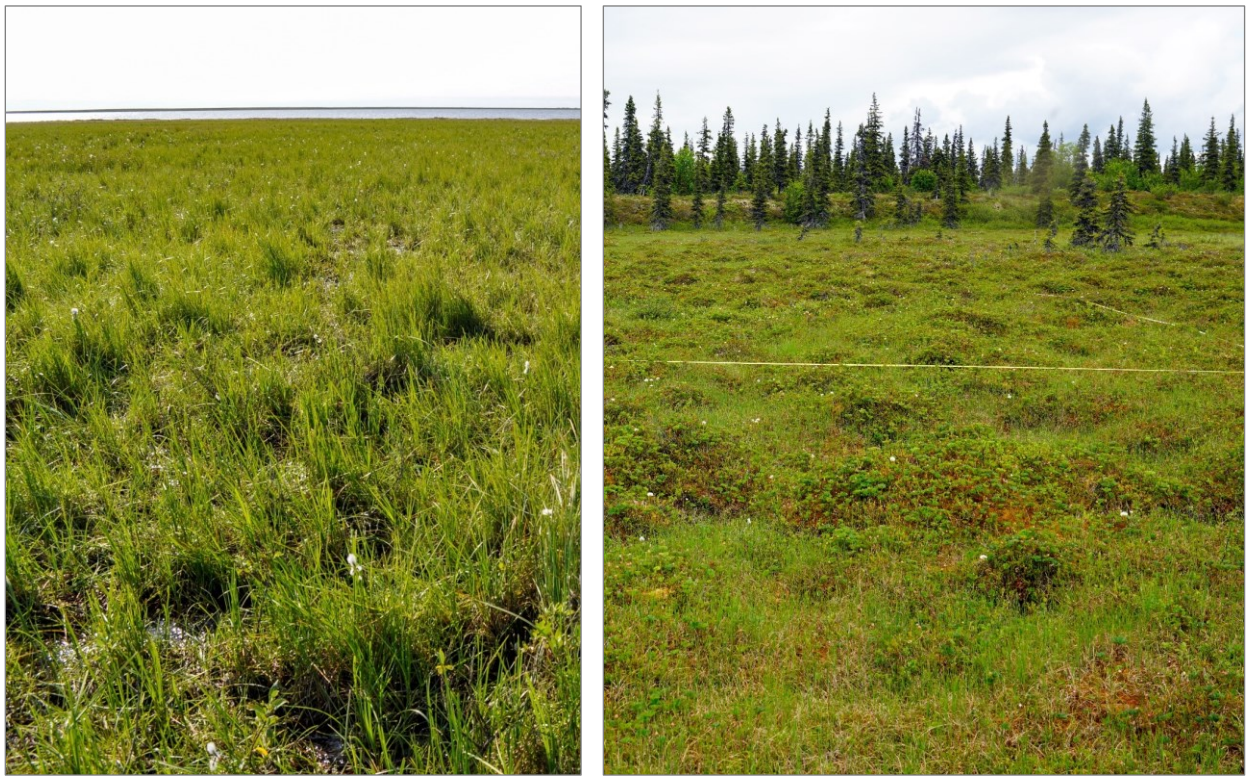

Figure 58. *Carex aquatilis*-dominated community in hydric soil near a lake on the Arctic Coastal Plain (left). High abundance of *Carex rariflora* in hygric soil near the Nuyakuk River in Bristol Bay (right).

Table 22. Species included in the Wetland Sedges aggregate.

Typically obligate wetland sedges (family Cyperaceae)
Carex adelostoma Krecz.
Carex aquatilis Wahlenb.
Carex arcta Boott
Carex bicolor Bellardi ex All.
Carex chordorrhiza Ehrh. ex L. f.
Carex diandra Schrank
Carex echinata ssp. *echinata* Murray
Carex echinata ssp. *phyllomanica* (W. Boott) Reznicek
Carex enanderi Holm
Carex glareosa ssp. *glareosa* Schkuhr ex Wahlenb.

Typically obligate wetland sedges (family Cyperaceae)
Carex glareosa ssp. *pribylovensis* (Macoun) Halliday & Chater
Carex gynocrates Wormsk. ex Drejer
Carex holostoma Drejer
Carex interior L.H. Bailey
Carex kellogii W. Boott
Carex lachenalii Schkuhr
Carex lasiocarpa Ehrh.
Carex laxa Wahlenb.
Carex leptalea ssp. *leptalea* Wahlenb.
Carex limosa L.
Carex livida (Wahlenb.) Willd.
Carex lyngbyei Hornem.
Carex marina ssp. *marina* Dewey
Carex membranacea Hook.
Carex microglochin Wahlenb.
Carex pauciflora Lightf.
Carex paupercula Michx.
Carex pluriflora Hultén
Carex rariflora (Wahlenb.) Sm.
Carex rostrata Stokes
Carex rotundata Wahlenb.
Carex saxatilis ssp. *laxa* L.
Carex sitchensis Prescott ex Bong.
Carex utriculata Boott
Carex vaginata Tausch
Carex viridula ssp. *viridula* Michx.
Eriophorum ×medium ssp. *album* J. Cay
Eriophorum angustifolium Honck.
Eriophorum chamissonis C.A. Mey.
Eriophorum gracile ssp. *gracile* W.D.J. Koch
Eriophorum komarovii V.N. Vassil.
Eriophorum russeolum ssp. *leiocarpum* M.S. Novos.
Eriophorum scheuchzeri ssp. *arcticum* M.S. Novos.
Eriophorum scheuchzeri ssp. *scheuchzeri* Hoppe
Eriophorum triste (Th. Fr.) Hadac & Á. Löve
Eriophorum viridicarinatum (Engelm.) Fernald

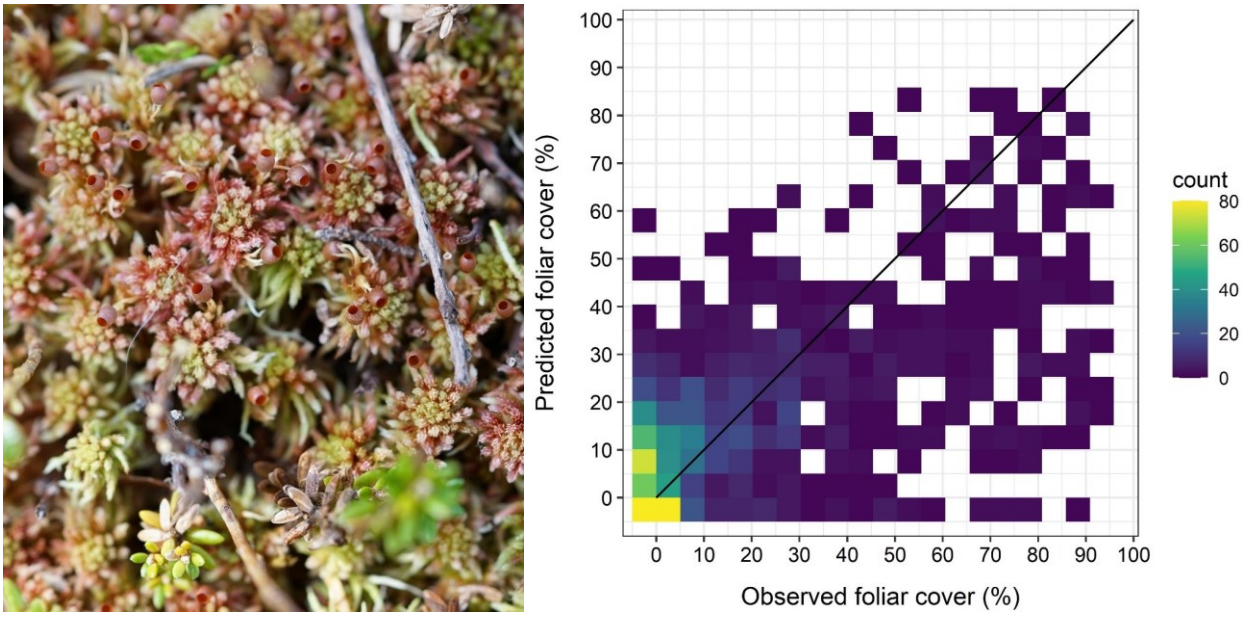

Figure 59. Observed foliar cover compared to predicted foliar cover for *Sphagnum* from the merged test partitions of 10-fold cross-validation, wherein each observation was predicted exactly once. R^2 values were calculated relative to the theoretical 1:1 ratio between observed and predicted foliar cover (solid black line). *Sphagnum* sp. (sect. *Acutifolia*) shown at left.

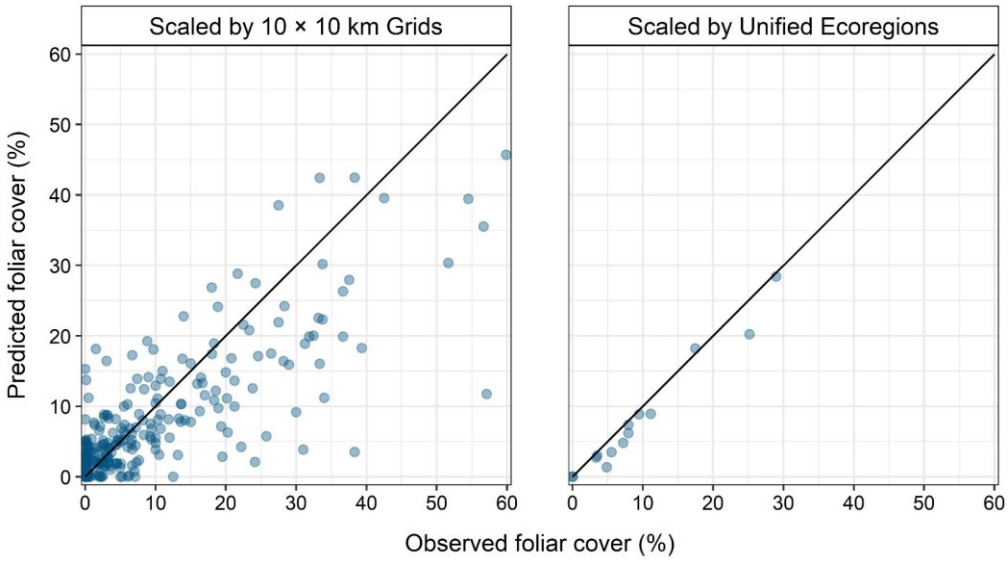

Figure 60. Mean observed foliar cover compared to mean predicted foliar cover for *Sphagnum* summarized by 10 × 10 km grids (right) and by ecoregions (left) from the merged test partitions of 10-fold cross-validation.

Table 23. Accuracy of *Sphagnum* by region and subregion at the site scale.

Subregion	Continuous Foliar Cover Performance					Cover	
	R^2	MAE	RMSE	AUC	% ACC	Mean	Median
All	0.52	6.3	13.6	0.92	83	25.5	16.0
Northern	0.53	5.7	12.4	0.90	81	21.4	10.0
Western	0.50	7.0	14.5	0.94	87	28.7	20.0
Interior	0.48	6.3	14.8	0.90	83	32.5	19.5

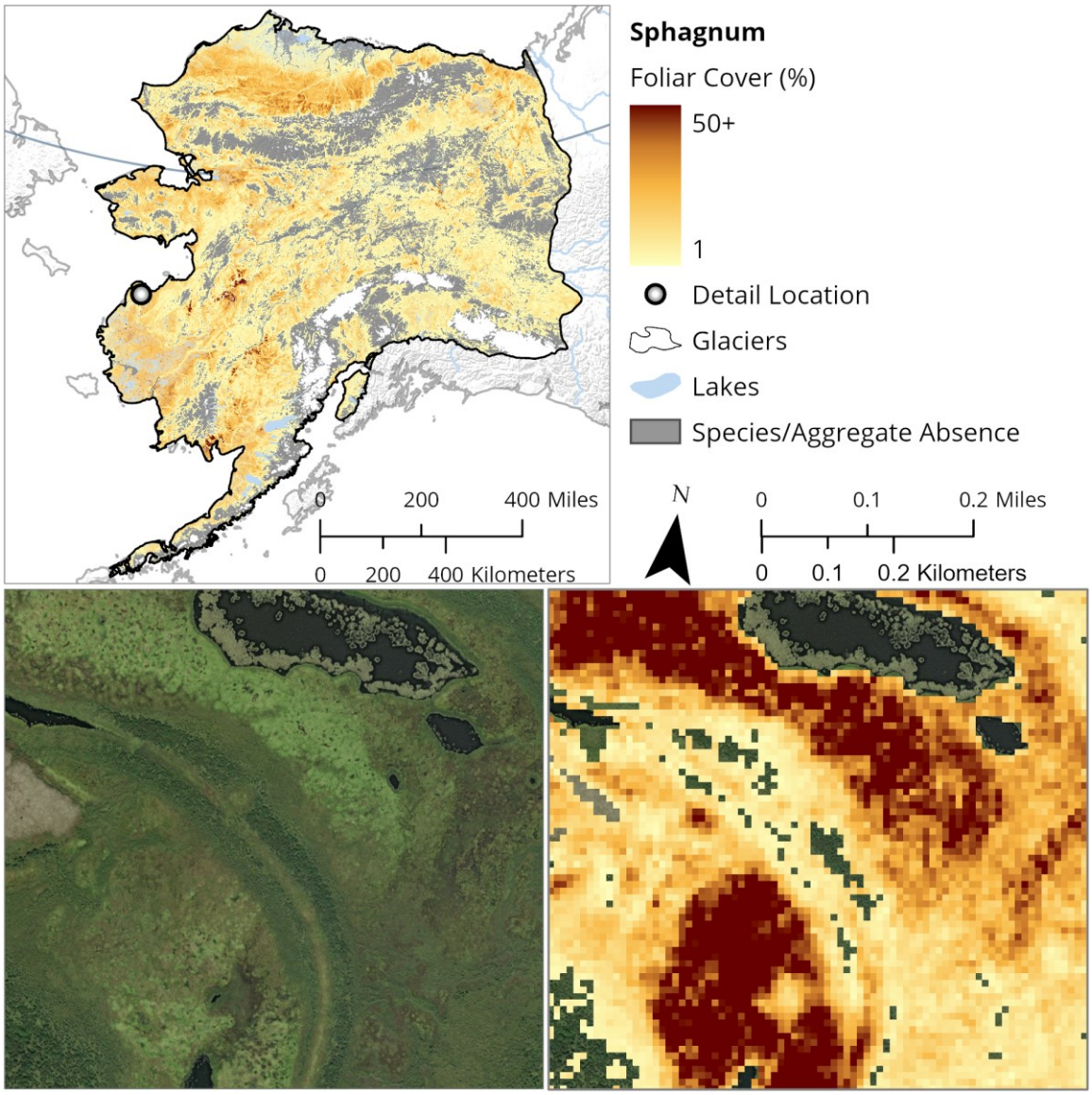

Figure 61. Map of *Sphagnum* in North American Beringia (top) and comparison between high resolution Maxar satellite imagery (bottom left) and predicted map (bottom right) at 1:10,000 scale.

Components

The *Sphagnum* map group includes all *Sphagnum* species known to occur in the study area, which are listed in Table 24.

Figure 62. *Sphagnum* mosses can form nearly continuous cover in poorly drained, hygric or hydric sites, such as shown from the vicinity of the Nushagak River in Bristol Bay (left). Some *Sphagnum* species, such as *Sphagnum girgensohnii*, occur in hygric microsites under forest canopies (right).

Table 24. Species included in the *Sphagnum* aggregate.

Sphagnum
Sphagnum alaskense R.E. Andrus & Janssens
Sphagnum andersonianum R.E. Andrus
Sphagnum angustifolium (C.E.O. Jensen ex Russow) C.E.O. Jensen
Sphagnum annulatum Warnst.
Sphagnum aongstroemii Hartm.
Sphagnum arcticum Flatberg & Frisvoll
Sphagnum austinii Sull.
Sphagnum balticum (Russow) C.E.O. Jensen
Sphagnum bergianum R.E. Andrus
Sphagnum beringiense A.J. Shaw, R.E. Andrus, & B. Shaw
Sphagnum brevifolium (Lindb.) Röll

Sphagnum
Sphagnum capillifolium (Ehrh.) Hedw.
Sphagnum compactum Lam. & DC.
Sphagnum contortum Schultz
Sphagnum cuspidatum Ehrh. ex Hoffm.
Sphagnum fimbriatum ssp. *concinnum* (Berggr.) Flatberg & Frisvoll
Sphagnum fimbriatum ssp. *fimbriatum* Wilson
Sphagnum fuscum (Schimp.) Klinggr.
Sphagnum girgensohnii Russow
Sphagnum henryense Warnst.
Sphagnum imbricatum Russow
Sphagnum inexspectatum Flatberg
Sphagnum inundatum Russow
Sphagnum jensenii H. Lindb.
Sphagnum kenaiense R.E. Andrus
Sphagnum lenense H. Lindb.
Sphagnum lindbergii Schimp.
Sphagnum magellanicum Brid.
Sphagnum majus ssp. *majus* (Russow) C.E.O. Jensen
Sphagnum majus ssp. *norvegicum* Flatberg
Sphagnum mendocinum Sull. & Lesq.
Sphagnum mirum Flatberg & Thingsgaard
Sphagnum obtusum Warnst.
Sphagnum orientale L.I. Savicz
Sphagnum pacificum Flatberg
Sphagnum papillosum Lindb.
Sphagnum perfoliatum L.I. Savicz
Sphagnum platyphyllum (Lindb.) Warnst.
Sphagnum pulchrum (Lindb.) Warnst.
Sphagnum quinquefarium (Lindb. ex Braithw.) Warnst.
Sphagnum riparium Ångstr.
Sphagnum rubellum Wilson
Sphagnum rubiginosum Flatberg
Sphagnum russowii Warnst.
Sphagnum squarrosum Crome
Sphagnum steerei R.E. Andrus
Sphagnum subfulvum Sjörs

Sphagnum
Sphagnum subnitens Russow & Warnst.
Sphagnum subsecundum Nees
Sphagnum talbotianum R.E. Andrus
Sphagnum tenellum (Brid.) Bory
Sphagnum teres (Schimp.) Ångstr.
Sphagnum tescorum Flatberg
Sphagnum tundrae Flatberg
Sphagnum warnstorfii Russow
Sphagnum wilfii H.A. Crum

Literature Cited

Argus, G.W. 2004. A guide to the identification of *Salix* (willows) in Alaska, the Yukon Territory, and adjacent regions. Unpublished from workshop on willow identification.

Berry, J.K. 2002. Use surface area for realistic calculations. Geoworld. 15: 20-1.

Bivand, R.S., T. Keitt, and B. Rowlingson. 2018. Rgdal: Bindings for the 'Geospatial' Data Abstraction Library. R package version 1.4-7. https://CRAN.R-project.org/package=rgdal

Blaszczynski, J.S. 1997. Landform characterization with geographic information systems. Photogrammetric Engineering & Remote Sensing. 63:183–191.

Boggs, K., S.C. Klein, J. Grunblatt, and B. Koltun. 2003. Landcover Classes, Ecoregions, and Plant Associations of Katmai National Park and Preserve. Natural Resource Technical Report. NPS/KATM/NRTR—2003/001. National Park Service, U.S. Department of the Interior. Fort Collins, Colorado. 273 pp.

Boucher, T.V., and L.A. Flagstad. 2014. Alagnak Wild River: Landcover Classes and Plant Associations. Natural Resource Technical Report. NPS/ALAG/NRTR—2014/927. National Park Service, U.S. Department of the Interior. Fort Collins, Colorado. 136 pp.

Boucher, T.V., K. Boggs, T.T. Kuo, B. Koltun, J. McGrath, and C. Lindsay. 2012. Plant Associations, Vegetation Succession, and Earth Cover Classes: Aniakchak National Monument and Preserve. Natural Resource Technical Report. NPS/ANIA/NRTR—2012/557. National Park Service, U.S. Department of the Interior. Fort Collins, Colorado. 241 pp.

Breen, A.L. 2014. Balsam poplar (*Populus balsamifera* L.) communities on the Arctic slope of Alaska. Phytocoenologia. 44:1–24.

Carlson, M.L., E.J. Trammell, T.W. Nawrocki, and E. Noongwook. 2018. Additions to the Vascular Plant Flora of St. Lawrence Island, Alaska: New Records, Rare Species, and Phytogeographic Patterns. Rhodora. 120:1-41.

Cawley, G.C., and N.L.C. Talbot. 2010. On Over-fitting in Model Selection and Subsequent Selection Bias in Performance Evaluation. Journal of Machine Learning Research. 11:2079–2107.

Cushman, S.A., K. Gutzweiler, J.S. Evans, and K. McGarigal. 2010. The gradient paradigm: a conceptual and analytical framework for landscape ecology. In: Cushman, S.A., and F. Huettmann (eds.). Spatial complexity, informatics, and wildlife conservation. Springer. New York, New York. 83–108.

Ducks Unlimited. 2013. North Slope Science Initiative Land Cover Mapping Summary Report. Ducks Unlimited, Inc. Rancho Cordova, California.

Elvabakk, A. 1999. Bioclimate delimitation and subdivisions of the Arctic. In: Nordal, I., and V.Y. Razzhivin (eds.). The Species Concept in the High North - A Panarctic Flora Initiative. The Norwegian Academy of Science and Letters. Oslo, Norway. 81–112.

Elven, R., D.F. Murray, V.Y. Razzhivin, and B.A. Yurtsev. 2011. Annotated Checklist of the Panarctic Flora (PAF) Vascular Plants. Available: http://panarcticflora.org/

Evans, J.S., J. Oakleaf, S.A. Cushman, and D. Theobald. 2014. An ArcGIS toolbox for surface gradient and geomorphometric modeling, version 2.0-0. Available: http://evansmurphy.wixsite.com/evansspatial/arcgis-gradient-metrics-toolbox

Feilhauer, H., A. Zlinszky, A. Kania, G.M. Foody, D. Doktor, A. Lausch, and S. Schmidtlein. 2020. Let your maps be fuzzy! – Class probabilities and floristic gradients as alternative to crisp mapping for remote sensing of vegetation. Remote Sensing in Ecology and Conservation. https://doi.org/10.1002/rse2.188

Friedman, J.H. 2002. Stochastic gradient boosting. Computational Statistics & Data Analysis. 38:367–378.

Furlow, J.J. 1997. *Betulacaceae*. In: Flora of North America Editorial Committee (eds.). 1993+. Flora of North America North of Mexico [Online]. 21+ volumes. New York and Oxford. Volume 3. Available: http://floranorthamerica.org/Betulaceae

Gao, B. 1996. NDWI - A Normalized Difference Water Index for Remote Sensing of Vegetation Liquid Water from Space. Remote Sensing of the Environment. 58:257–266.

Gessler, P.E., I.D. Moore, N.J. McKenzie, and P.J. Ryan. 1995. Soil-landscape modeling and spatial prediction of soil attributes. International Journal of Geographical Information Systems. 9:421–432.

Gleason, H.A. 1926. The individualistic concept of the plant association. Bulletin of the Torrey Botanical Club. 53:7–26.

González, J., J. Longworth, D. James, and N.D. Lawrence. 2014. Bayesian optimization for synthetic gene design. The Neural Information Processing Systems (NIPS'14) Workshop in Bayesian Optimization.

Gorelick, N., M. Hancher, M. Dixon, S. Ilyushchenko, D. Thau, and R. Moore. Google Earth Engine: Planetary-scale geospatial analysis for everyone. Remote Sensing of Environment. 202:18–27.

GPy. 2014. A Gaussian Process Framework in Python. Available: https://github.com/SheffieldML/GPy

Greuter, W., and E. von Raab-Straube. 2011. Euro Med Notulae, 5. Willdenowia. 41:129-138.

Hall, D.K., G.A. Riggs, and V.V. Salomonson. 1995. Development of methods for mapping global snow cover using moderate resolution imaging spectroradiometer data. Remote Sensing of Environment. 54:127–140.

Hastie, T., R. Tibshirani, and J. Friedman. 2009. The elements of statistical learning: data mining, inference, and prediction. 2nd edition. Springer. New York, New York.

Hijmans, R.J. 2017. Raster: Geographic Data Analysis and Modeling. R package version 3.0-7. https://CRAN.R-project.org/package=raster

Jiang, Z., A.R. Huete, K. Didan, and T. Miura. 2008. Development of a two-band enhanced vegetation index without a blue band. Remote Sensing of Environment. 112:3833–3845.

Jiménez-Valverde, A., and J. Lobo. 2007. Threshold criteria for conversion of probability of species presence to either-or presence-absence. Acta Oecologica. 31:361–369.

Jin, S., and S.A. Sader. 2005. Comparison of time series tasseled cap wetness and the normalized difference moisture index in detecting forest disturbances. 94:364–372.

Jorgenson, M.T., and D. Meidinger. 2015. The Alaska Yukon Region of the Circumboreal Vegetation Map (CBVM). CAFF Strategies Series Report. Conservation of Arctic Flora and Fauna. Akureyri, Iceland. ISBN: 978-9935-431-48-6. 39 pp.

Jorgenson, M.T., J.E. Roth, P.F. Loomis, E.R. Pullman, T.C. Cater, M.S. Duffy, W.A. Davis, and M.J. Macander. 2008. An Ecological Survey for Landcover Mapping of Wrangell-St. Elias National Park and Preserve. Natural Resource Technical Report NPS/WRST/NRTR—2008/094. National Park Service, U.S. Department of the Interior. Fort Collins, Colorado. 265 pp.

Jorgenson, M.T., J.E. Roth, P.F. Miller, M.J. Macander, M.S. Duffy, A.F. Wells, G.V. Frost, and E.R. Pullman. 2009a. An Ecological Land Survey and Land Cover Map of the Arctic Network. Natural Resource Technical Report NPS/ARCN/NRTR—2009/270. National Park Service, U.S. Department of the Interior. Fort Collins, Colorado. 307 pp.

Jorgenson, M.T., J.E. Roth, P.F. Miller, M.J. Macander, E.R. Pullman, E.A. Miller, L.B. Attanas, A.F. Wells, and S. Talbot. 2009b. An Ecological Land Survey and Land Cover Map of the Selawik National Wildlife Refuge. Fish and Wildlife Service, U.S. Department of the Interior. Fairbanks, Alaska. 238 pp.

Ke, G., Q. Meng, T. Finley, T. Wang, W. Chen, W. Ma, Q. Ye, T. Liu. 2017. LightGBM: a highly efficient gradient boosting decision tree. NIPS'17: Proceedings of the 31st International Conference on Neural Information Processing Systems. 3149-3157.

Key, C.H., and N.C. Benson. 1999. The normalized burn ratio (NBR): a Landsat TM radiometric measure of burn severity. Northern Rocky Mountain Science Center, U.S. Geological Survey, U.S. Department of the Interior. Bozeman, Montana.

Kuhn, M., and K. Johnson. 2013. Applied Predictive Modeling. Springer. New York, New York.

Langford, Z., J. Kumar, F.M. Hoffman, R.J. Norby, S.D. Wullschleger, V.L. Sloan, and C.M. Iversen. 2016. Mapping Arctic plant functional type distributions in the Barrow environmental observatory using Worldview-2 and LiDAR datasets. Remote Sensing. 8:733.

Lortie, C.J., R.W. Brooker, P. Choler, Z. Kikvidze, R. Michalet, F.I. Pugnaire, and R.M. Callaway. 2004. Rethinking Plant Community Theory. Oikos. 107:433–438.

Little, E.L. 1971. Atlas of United States Trees. Volume 1. Conifers and Important Hardwoods. Misc. Publ. 1146. Forest Service, U.S. Department of Agriculture. Washington, D.C. 97 pp.

Liu, C., P.M. Berry, T.P. Dawson, and R.G. Pearson. 2005. Selecting Thresholds of Occurrence in the Prediction of Species Distributions. Ecography. 28:385–393.

Macander, M.J., G.V. Frost, P.R. Nelson, and C.S. Swingley. 2017. Regional quantitative cover mapping of tundra plant functional types in Arctic Alaska. Remote Sensing. 9:1024.

Moore, I.D., P.E. Gessler, G.A. Nielsen, and G.A. Petersen. 1993. Terrain attributes: estimation methods and scale effects. In: Jakeman, A.J., M.B. Beck, and M. McAleer (eds.). Modeling Change in Environmental Systems. Wiley. London, United Kingdom. 189–214.

Murphy, S.M., M.J. Macander, A.F. Wells, G.V. Frost, A.E. Gall, A.K. Prichard, J.C. Seigle, and R.H. Day. 2016. Shell Onshore/Nearshore Environmental Studies, 2010–2015. Expanded Executive Summary. Report for Shell Exploration and Production Company. ABR, Inc. Fairbanks, Alaska.

Nawrocki, T.W. 2018. Sessile Organism Range. Git Repository. Available: https://github.com/accs-uaa/sessile-organism-range

Nawrocki, T.W. 2021. Alaska Vegetation Plots Database. Git Repository. Available: https://github.com/accs-uaa/vegetation-plots-database

Nicholson, M., and R.P. McIntosh. 2002. H.A. Gleason and the Individualistic Hypothesis Revisited. Bulletin of the Ecological Society of America. 83:133-142.

Nowacki, G., P. Spencer, M. Fleming, T. Brock, and T. Jorgenson. 2001. Unified Ecoregions of Alaska. U.S. Geological Survey Open-File Report 02-297 (map).

Pebesma, E.J., and R.S. Bivand. 2005. Classes and methods for spatial data in R. R News. 5:9–13.

Pedregosa, F., G. Varoquaux, A. Gramfort, V. Michel, B. Thirion, O. Grisel, M. Blondel, P. Prettenhofer, R. Weiss, V. Duborg, et al. 2011. Scikit-learn: machine learning in python. Journal of Machine Learning Research. 12:2825–2830.

Pike, R.J., and S.E. Wilson. 1971. Elevation relief ratio, hypsometric integral, and geomorphic area altitude analysis. Bulletin of the Geographic Society of America. 82:1079–1084.

Riemann, R., B.T. Wilson, A. Lister, and S. Parks. 2010. An effective assessment protocol for continuous geospatial datasets of forest characteristics using USFS Forest Inventory and Analysis (FIA) data. Remote Sensing of Environment. 114:2337-2352.

Riley, S.J., S.D. DeGloria, and R. Elliot. 1999. A terrain ruggedness index that quantifies topographic heterogeneity. Intermountain Journal of Sciences. 5:23–27.

SNAP. 2020. SNAP Data. Scenarios Network for Alaska and Arctic Planning, University of Alaska Fairbanks. Fairbanks, Alaska. Available: http://ckan.snap.uaf.edu/dataset

Tucker, C.J. 1979. Red and photographic infrared linear combinations for monitoring vegetation. Remote Sensing of Environment. 8:127–150.

Viereck, L.A., and E.L. Little. 2007. Alaska Trees and Shrubs. Second Edition. University of Alaska Press. Fairbanks, Alaska. 359 pp.

Wan, Z. 2013. Collection-6 MODIS Land Surface Temperature Products Users' Guide. Earth Research Institute, University of California Santa Barbara. Santa Barbara, California. 33 pp. Available: https://lpdaac.usgs.gov/documents/118/MOD11_User_Guide_V6.pdf

Wells, A.F., G.V. Frost, T. Christopherson, M.J. Macander, and E.R. Trainor. 2016a. Ecological Land Survey and Soil Landscapes Map for Aniakchak National Monument and Preserve, Alaska, 2014. Natural Resource Report. NPS/ANIA/NRR—2016/1133. National Park Service, U.S. Department of the Interior. Fort Collins, Colorado. 190 pp.

Wells, A.F., M.J. Macander, M.T. Jorgenson, T. Christopherson, B. Baird, and E.R. Trainor. 2013. Ecological Land Survey and Soil Landscapes Map for Lake Clark National Park and Preserve,

Alaska, 2011. Natural Resource Technical Report. NPS/LACL/NRTR—2013/693. National Park Service, U.S. Department of the Interior. Fort Collins, Colorado. 349 pp.

Wells, A.F., T. Christopherson, J.G. Kidd, and E.K. Johnson. 2016b. Ecological Land Survey and Soil Landscapes Map for Alagnak Wild River, Alaska, 2014. Natural Resource Report. NPS/ALAG/NRR—2016/1359. National Park Service, U.S. Department of the Interior. Fort Collins, Colorado. 109 pp.

Whitley, M.A., G.V. Frost, M.T. Jorgenson, M.J. Macander, C.V. Maio, and S.G. Winder. 2018. Assessment of LiDAR and Spectral Techniques for High-Resolution Mapping of Sporadic Permafrost on the Yukon-Kuskokwim Delta, Alaska. Remote Sensing. 10:258.

Whittaker, R.H. 1967. Gradient analysis of vegetation. Biological Review. 42:207–264.

Zhu, Z., and C.E. Woodcock. 2014. Continuous change detection and classification of land cover using all available Landsat data. Remote Sensing of Environment. 144:152-171.

Appendix 1: Vegetation Survey and Monitoring Projects

Numerous vegetation ecologists, botanists, and field technicians from multiple agencies and organizations collected the data that enabled this map (Table A.1.).

Table A.1. Vegetation observation datasets from the AKVEG, ABR, and NPS Inventory & Monitoring Vegetation Plots Databases that provided data to train and test statistical models for each mapped species or aggregate.

Project (Data Reference)	Years	Methods	Plot Size (m)	Number
GMT-2 Assessment, Inventory, and Monitoring (Steer, M.A., and T.W. Nawrocki. 2019. Unpublished data.)	2019	Line-point Intercept	30 radius	40
Vegetation Survey of the Nuyakuk and Nushagak Rivers (This Study)	2019	Grid-point Intercept	10 × 10	61
Vegetation Survey of the Ribdon River (This Study)	2019	Grid-point Intercept	10 × 10	9
Colville Small Mammal Surveys 2015 (Flagstad, L.A., and T.W. Nawrocki. 2015. Unpublished data.)	2015	Semi-quantitative Visual Estimate	10 × 10	16
Ecological Land Survey and Soil Landscapes Map for Alagnak Wild River (Wells et al. 2016b)	2014	Semi-quantitative Visual Estimate	10 radius	68
Ecological Land Survey and Soil Landscapes Map for Aniakchak National Monument and Preserve (Wells et al. 2016a)	2014	Semi-quantitative Visual Estimate	10 radius	80
NPR-A Assessment, Inventory, and Monitoring (Nawrocki et al. 2020)	2012–2017	Line-point Intercept	30 radius	183
Shell Onshore/Nearshore Environmental Studies (Murphy et al. 2016)	2011-2012	Semi-quantitative Visual Estimate	10 radius, 10 × 10, various	471
Ecological Land Survey of Lake Clark National Park and Preserve (Wells et al. 2013)	2011	Semi-quantitative Visual Estimate	10 radius, 10 × 10, various	44
Alagnak Wild River Land Cover and Plant Associations (Boucher and Flagstad 2014)	2010	Semi-quantitative Visual Estimate	10 × 10, various	89

Project (Data Reference)	Years	Methods	Plot Size (m)	Number
NPS ARCN Inventory & Monitoring (*Picea* species only)	2009-2014	Line-point Intercept	8 radius	444
Plant Associations, Vegetation Succession, and Earth Cover Classes of Aniakchak National Monument and Preserve (Boucher et al. 2012)	2009-2010	Semi-quantitative Visual Estimate	10 × 10, various	188
North Slope Science Initiative Land Cover Map (Ducks Unlimited 2013)	2008-2011	Semi-quantitative Visual Estimate	10 × 10, various	115
Ecological Land Survey of Katmai National Park and Preserve (Wells A.F., et al. 2017. Unpublished Data)	2007-2017	Semi-quantitative Visual Estimate	10 radius, 10 × 10, various	320
An Ecological Land Survey and Land Cover Map of the Selawik National Wildlife Refuge (Jorgenson et al. 2009b)	2007–2008	Semi-quantitative Visual Estimate & Grid-Point Intercept	10 radius, 10 × 10, various	252
Yukon Delta National Wildlife Refuge Earth Cover	2006	Semi-quantitative Visual Estimate (Aerial)	Used as 20 radius	1178
Tetlin National Wildlife Refuge Earth Cover	2005	Semi-quantitative Visual Estimate (Aerial)	Used as 20 radius	361
Ecological Land Survey of Wrangell-St. Elias National Park and Preserve (Jorgenson et al. 2008)	2004-2006	Semi-quantitative Visual Estimate	10 radius, various	11
Seward Peninsula Earth Cover	2003	Semi-quantitative Visual Estimate (Aerial)	Used as 20 radius	218
An Ecological Land Survey and Land Cover Map of the Arctic Network (Jorgenson et al. 2009a)	2002–2008	Semi-quantitative Visual Estimate	10 radius, 10 × 10, various	873
Dalton Highway Corridor Earth Cover	2002	Semi-quantitative Visual Estimate (Aerial)	Used as 20 radius	228

Project (Data Reference)	Years	Methods	Plot Size (m)	Number
NPS CAKN Inventory & Monitoring (*Picea* species only)	2001-2016	Line-point Intercept	8 radius	1988
Goodnews Bay Earth Cover	2001	Semi-quantitative Visual Estimate (Aerial)	Used as 20 radius	218
Kvichak Earth Cover	2001	Semi-quantitative Visual Estimate (Aerial)	Used as 20 radius	294
Melozitna River and Koyukuk National Wildlife Refuge Earth Cover	2001	Semi-quantitative Visual Estimate (Aerial)	Used as 20 radius	450
Galena Military Operations Area and Nowitna National Wildlife Refuge Earth Cover	2000	Semi-quantitative Visual Estimate (Aerial)	Used as 20 radius	571
Landcover Classes, Ecoregions, and Plant Associations of Katmai National Park and Preserve (Boggs et al. 2003)	2000	Semi-quantitative Visual Estimate	10 × 10	80
Naknek Military Operations Area Earth Cover	2000	Semi-quantitative Visual Estimate (Aerial)	Used as 20 radius	621
Northern Yukon Military Operations Area Earth Cover	1999-2000	Semi-quantitative Visual Estimate (Aerial)	Used as 20 radius	284
Southern Yukon Military Operations Area Earth Cover	1999-2000	Semi-quantitative Visual Estimate (Aerial)	Used as 20 radius	205

Appendix 2: Change Log

Version 1.0

Version 1.0 is the initial full release. Future changes will be documented from this release.